1-11-2022

Cell-type Specific Expression of Apolipoprotein E by Astrocytes and Microglia: Implications for the Development of Amyloid-β Pathology in Alzheimer Disease

Thomas Mahan
Washington University in St. Louis

WASHINGTON UNIVERSITY IN ST. LOUIS

Division of Biology and Biomedical Sciences
Neurosciences

Dissertation Examination Committee:
David M. Holtzman, Chair
John R. Cirrito
Marco Colonna
Celeste M. Karch
Jin-Moo Lee
Timothy M. Miller

Cell-type Specific Expression of Apolipoprotein E by Astrocytes and Microglia: Implications for
the Development of Amyloid-β Pathology in Alzheimer Disease

By
Thomas E. Mahan

A dissertation presented to
The Graduate School
of Washington University in
partial fulfillment of the
requirements for the degree
of Doctor of Philosophy

December 2021
St. Louis, Missouri

Table of Contents

List of Figures

List of Tables

__Acknowledgments__

My journey through graduate school has been filled with many wonderful moments with many wonderful people. During the process of writing my dissertation and preparing to defend my thesis I have been able to reflect back on the last seven years and just how fortunate I have been for this experience. When I started graduate school in August of 2014, I knew that I wanted to continue to pursue the Alzheimer disease (AD) research that I had been engaged in for prior three years as a research assistant. However, I did not realize how my time in graduate school would not only solidify my motivation for AD research, but how it would show me what my purpose in life is. I will expand on this purpose towards the end of my acknowledgments.

First and foremost I would like to acknowledge and thank Dr. David M. Holtzman. Prior to starting graduate school, I worked as a research assistant in the Holtzman lab for nearly three years. When I applied for the position, I had very little academic research experience and Dave took a chance hiring me as the primary histologist for his lab. Little did I know back then that ten years later I would be writing and defending my thesis to receive my doctorate. My work as a histologist further ignited my passion for Alzheimer research and to pursue my Ph.D. in Neuroscience. The research opportunities I have had, and will continue to have, would not have been possible if it was not for Dave hiring me and giving me the chance to pursue my childhood dream of performing research science to try to help treat diseases that people suffer from. I would also like to thank Dave's wife, Tracy. Throughout the years Tracy has helped organize many wonderful lab outings and get-togethers, like the annual lab float trip, the annual Holtzman

lab Holiday party, and several Ph.D. thesis defense celebration parties (which includes my party that will take place after I hopefully successfully defend my thesis!)

Next, I would like to thank the members of my thesis committee. First, I would like to thank Dr. John R. Cirrito. I was fortunate enough to get to know John prior to the start of my Ph.D. program when I worked in the Holtzman lab as a research assistant. As a former Holtzman lab member, John would often stop by the lab to say hello (and make sure to harass us at least a little bit while stopping by!). While applying to the Neuroscience program at Wash U, John was able to help provide me with some wisdom and support throughout the process, something I will be forever grateful for. Having been a fan of both John the scientist and John the man, I knew when I first began grad school that he was the first professor whose lab I wanted to rotate in. It was an honor to be able to start my graduate school career with John and it has been an honor to have him serve as my thesis committee chair. To Dr. Timothy Miller, thank you for all the helpful comments on my research and all of the great scientific discussions that have arisen from our joint lab meetings throughout the years. I often think back to when I first worked with Dr. Sarah DeVos on her Tau projects when she was a graduate student in your lab and all of the great connections I have made with the members of your lab. To Dr. Jin-moo Lee, thank you for always having kind words and a genuine interest in how my research was coming along when I would converse with you on the 9th floor of BJCIH. I was incredibly excited when it was announced that you would be the next chair of the department of Neurology to succeed Dave and I cannot think of any else more deserving! To Dr. Marco Colonna, I am so grateful for the collaborations that the Holtzman lab has had with your lab and the knowledge that has been gained from researching how TREM2 and APOE regulate immune system function and the impact on Alzheimer disease. I also want to thank you for the support you gave me when I

discovered the Aldh1l1-Cre mice that I had been generating for my thesis had a major insurmountable issue and that I needed to generate a whole new line of mice for my research. I will never forget how you told me that you had also ran into similar issues when trying to generate a mouse line and how major setbacks are something that all researchers run in to. You may not have realized it at the time, but you really helped me recognize that everything was going to be ok and that I just needed to keep pushing forward to find the answers that I sought in my thesis research. To Dr. Celeste Karch, it has been so wonderful to have you on my committee and to be able to have had many great meetings with you regarding not only my current research, but also my future research plans. I have continually admired the way you have created a wonderfully congenial and easy going lab. I've enjoyed being able to collaborate with your lab and all of the joint lab meetings we have had. I am so glad to have been able to discuss with you my future hopes and dreams for Down syndrome research at WashU and I hope to continue collaborating for years to come!

I also need to recognize all the members of the Holtzman lab both past and present. There have been many research technicians, undergrad students, rotation students, senior scientists, and others who had made the time in the Holtzman lab so fantastic. To Mary Beth Finn, I can't begin to thank you enough for all you have done for me throughout my time in the in the lab. You have given me more kind and supportive words than I could have ever asked for and you have been there for me through the good times and the bad. I am truly grateful for you! To Hong Jiang, I was first amazed by CSF collection skills when I first started in the lab and I have continued to be impressed by your work ethic and skillset. You have impressed me in so many ways and it was so incredibly difficult when your husband and fellow lab mate Aimin Li passed away. I will never forget him and I am so glad I had the opportunity to have known him.

To Cindy Lawrence, the wheels would have fallen off the Holtzman lab without all that you do to keep things going. From the float trips to the Walks to End Alzheimer's, it has been great making so many memories with you. To Qing Fu, thank you for doing the work that is so necessary to keep our lab operating, you are such a kind and thoughtful person and I've truly enjoyed my time in the lab with you. To all members of Dr. Anne Fagan's lab in the biomarker core, it has been great working with all of you! When I first started in the Holtzman lab I was able to meet a great cohort of researchers, some of whom include Drs. Adam Bero, Joe Castellano, Jacob Basak, Philip Verghese, Fan Liao, Kiran Yanamandra, Kaoru Yamada, Jerrah Holth, Chrisitna Ising, and Sarah Fritschi. I also was able to witness the continued career development of Drs. Erik Musiek, Gus Davis, Rafael Galindo, Gilbert Gallardo, Gerry Kress, Jason Ulrich, and Shannon-Macauley Rambach. To Shannon, I will say that your friendship and support that you have given me throughout my grad school career is something that I value more than you know! You helped give me supportive words and hugs when I needed them most and although you have moved on to bigger and better things at Wake Forest, I still view you as one my best scientific and real life friends. It has been wonderful to see your career grow the way it has and you continue to be an inspiration as both a scientist and a parent. I look forward to hopefully collaborating on some scientific projects in the future and to continually running into you at scientific conferences. I also need to acknowledge Dr. Jason Ulrich. You have been a second mentor to me and have provided me with countless tips and help to face all the various challenges that life in and outside the lab has thrown my way. It has been a pleasure to be able to have many discussions about science and life, especially with your perspective as a fellow father of three, and to share in many laughs along the way.

There have also been a number of fellow graduate students who I have shared my time with in the Holtzman lab. Drs. Cheryl Leyns, Courtney Sutphen, Yang Shi, Phat Huynh, Tirth Patel, Monica Xiong, and Molly Stanley. I have enjoyed being able to go through this graduate school experience with all of you and to have each of you know firsthand the trials and tribulations and what it is like to reach this milestone. To Molly, it was an honor to be a part of team HyGly with you and to have had many a wonderful chat about life and all its wonders! To all of the other current and past members of the lab that I may not have mentioned by name, thank you, thank you, thank you for all you have done to make my time in the lab so enjoyable.

I also cannot leave out all of the other Neuro grad students I have met through these last seven years. To my classmates Claire, Brian, Ben A., Ben S., Helen, Cody, Cici, Katherine, Kael, and Alex, who started this journey back in 2014 with me, it has been great to have had the opportunity to have you as classmates and to have enjoyed the Neuro recruiting events, Neuro retreats, SfN conferences, Brain Discovery, Trivia Nights at iTap, and many other events along the way. As we continue on our scientific journeys I hope that we will always keep in touch and look back at our WashU Ph.D. experience and remember the good times!

I would like to acknowledge and thank everyone involved with the Lucille P. Markey Pathway program. It was a great learning experience and helped provide me with knowledge that I know I will continue to use throughout my career. To Sally Vogt, the amazing student coordinator for the Neuroscience program, you have been there in so many ways since the beginning to help steer me through this grad school program. Your smile and easy-going demeanor have helped put so many students' worries at ease, including mine. Your thank you parties at your house for the students who helped with recruiting events were always such a blast. You are one of the first people I have turned to whenever I needed help and when life threw me

few unexpected curveballs. I hope to continue to keep in touch as I go forward in my research career and I promise to keep providing you with pictures of my boys. From the bottom of my heart, THANK YOU!

And last but certainly not least, I need to acknowledge and thank all of my family. To my wife's family, you have all been so supportive of me on this journey and I can't thank you enough for helping watch my boys and for providing so many enjoyable time outside of the lab. To my in-laws Larry and Pat. I could not have done this without all of your help. You have been there for Jessica and me in so many ways. From helping to watch the boys, to providing so many words of wisdom and life advice, you have been such a source of love and support. To my sister Janielle, you have always been there for me since we were little kids and I could not have asked for a better best friend to go through life with. I know it has been tough being so far away these several years, but I love being able to take trips to NY to see you, Steve, Joycelyn, and Micah and I cherish every time we get to FaceTime and catch up. I love you J! To my Mom and Dad, you have been nothing but supportive of everything I have done in my life. You provided me with so many opportunities to explore my interests and to have every chance to be successful in life. I still do not know how you managed to always be there to take me to all of my sports and to help me with homework and do everything you have done for me. I would not be the man I am today without having had such amazing parents as you. I hope I have made you proud. I love you! To my sons Conley, Zackary, and Teddy, I love you more than you may ever know! You have given me more love and joy than I ever thought possible. You bright each one of my days and I am so glad that I get to be your Dad. I am so thankful you came into my life and I look forward to watching you all grow up into wonderful young men. To Teddy in particular, you are a gift I never saw coming. When your mom and I found out about your diagnosis of having

Down syndrome we were very surprised! We had no idea that you would come into our lives and send us on an entirely new journey. You have opened my eyes to my purpose. I will continue to do all that I can to help create a world without Alzheimer disease that is inclusive and that people like you with Down syndrome will get to experience that world. You motivate me every day to be a better dad, a better advocate, a better researcher, and a better person. I love you Teddy bear! And finally, they say you should save the best for last, so I must give my last thank you to my amazing wife Jessica. You have been by my side these last 10 years of marriage and have supported me throughout my journey to my Ph.D. I know it has not always been easy and that you have sacrificed so much for me to pursue my scientific dreams. We have certainly faced our fair share of challenges, from this pandemic to all the difficulties of parenthood. While in grad school you also gave me the gift of becoming a father, something I have always wanted to be. Although our journey into parenthood was not what we expected, you have been a remarkable mother! I look forward to what the future holds for our family and I hope I continue to be the husband and man that you so deserve. There is no one else in this world that I would want to be on this journey with. You are an amazing teacher, mother, and wife. You are my rock. I LOVE YOU!

Thomas E. Mahan

Washington University in St. Louis

December 2021

Dedicated to my parents Edward and Lynn,

my sons Teddy, Zackary, and Conley,

and my wife Jessica.

ABSTRACT OF THE DISSERTATION

Cell-type specific expression of apolipoprotein E by astrocytes and microglia: Implications for

the development of amyloid-β pathology in Alzheimer disease

By

Thomas E. Mahan

Doctor of Philosophy in Biology and Biomedical Sciences

Neurosciences

Washington University in St. Louis, 2021

Professor David M. Holtzman, Chair

Alzheimer disease (AD) is characterized by two main pathological hallmarks,
extracellular amyloid plaques primarily comprised of the amyloid-β (Aβ) peptide, and
intracellular neurofibrillary tangles mainly comprised of the tau protein. Although the
pathologies underlying AD were first described over one hundred years ago, researchers today
are still trying to understand how the development of Aβ pathology is regulated in the hopes of
developing more effective treatments. Advances in genetics over the last several decades have
allowed for several genetic risk factors to be identified that increase or decrease ones likelihood
for developing (AD). Of these genetic risk factors, the strongest one for developing late onset
AD is apolipoprotein E (APOE). The ε2 allele of *APOE* (*APOE2*) is considered to be protective
relative to the more common ε3 allele (*APOE3*), while the ε4 allele (*APOE4*) confers the
strongest increased risk. For those who carry one copy of *APOE4* there is an approximate 3-fold
increase in risk while those with two copies of *APOE4* have a 12-fold increase in risk. APOE4
has been shown to influence the development of Aβ pathology in several ways, including the
ability to indirectly increase Aβ levels by competing for clearance mechanisms with Aβ and to

increase fibrillization of Aβ through direct interactions. These influences of APOE4 on Aβ, as well as more recent findings that APOE4 can influence tau mediated neurodegeneration, likely underlie why APOE4 carriers also have an earlier age of onset of AD.

Many studies, including work done in our lab, have shown potential interventions for improving AD pathology could come from targeting apoE. In particular, reducing the levels of apoE in mice has been shown to significantly reduce the overall level of Aβ plaque burden. While the ability to improve overall Aβ pathology by manipulating apoE levels holds promise as a potential therapeutic intervention, few studies have looked closely at how cells respond to, and are impacted by, changes in apoE levels in the presence of developing Aβ pathology, especially at an individual per plaque basis. To begin to address these questions, we investigated how a complete loss of apoE impacts Aβ plaque formation, and the subsequent microgliosis and neuritic dystrophy, in two mouse models of amyloidosis. Here, I report on how the loss of apoE resulted in the formation of fewer amyloid plaques and how the fibrillar plaques that did form had an altered morphology. These morphologically altered plaques also had a reduction in microgliosis as well as an increase in neuritic dystrophy. With these findings, we hypothesized that the phenotypes we were seeing were due not only to the loss of apoE from astrocytes but were also due in part to the loss of microglial apoE. However, little is known about the characteristics of microglial apoE and raises the question as to whether differences exist between microglial apoE and astrocytic apoE.

The physical characteristics of apoE-containing lipoprotein particles have been previously investigated in an attempt to better understand how structural differences between APOE2, APOE3, and APOE4 may be exerting their impact on AD pathology. However, these studies focused primarily on the apoE particles that are produced by astrocytes with minimal

characterization of the apoE lipoprotein particles that are produced by microglia. We hypothesized that the apoE-containing lipoprotein particles that are produced by microglia differ from the particles that are produced by astrocytes. We investigated these potential differences by using primary cultures enriched for either microglia or astrocytes that expressed either APOE2, APOE3, or APOE4. Serum-free media samples from these cultures were analyzed using gel-electrophoresis and run under non-denaturing conditions to determine the size of the secreted apoE particles. I found that microglia produced a far greater amount of smaller apoE particles (~8nm) compared to astrocytes, which produced more of the larger apoE particles (~10-17nm). Furthermore, by changing the cell culture conditions and shifting the state of the microglia, I found that the level, and to some extent the size, of the apoE particles could also be shifted. These drastic changes in microglial apoE levels provide evidence that microglia apoE expression is highly dynamic and can be altered depending on the activation state of the microglia. These findings provide insight into how microglia may regulate their apoE expression and associated lipid components depending on their environment and whether they encounter pathological conditions.

After finding that astrocytes produce larger apoE particles than microglia, we wanted to further explore how a loss of astrocytic apoE might influence the development of Aβ pathology. To do so, we utilized new APOE knock-in (APOE-KI) mouse models that our lab recently developed. These mice express APOE2, APOE3, or APOE4 under the endogenous mouse APOE promoter and contain loxP sites within the *APOE* gene that allow for a cell-specific removal of *APOE* using Cre-recombinase. By crossing the APOE-KI mice with Aldh1l1-Cre/ERT2 mice, we were able to selectively remove apoE from astrocytes and examine the impact on Aβ pathology in the APPPS1-21 mouse model. I found that, similar to a global removal of apoE, the

overall fibrillar Aβ plaque load was significantly reduced after the loss of astrocytic apoE. The overall levels of GFAP and dystrophic neurites in the cortex were also reduced. The fibrillar plaques that did form with a loss of astrocytic apoE still had apoE present in them, however, the intensity of the plaques was greatly reduced. Interestingly, microglia were less activated and the neuritic dystrophy was increased around plaques. These findings indicate that apoE produced by astrocytes is playing a significant role in regulating overall Aβ pathology and is also influencing how microglia are activated in the presence of Aβ plaques. While further work is needed to address how a reduction in microglial apoE may influence Aβ pathology, I have demonstrated that reducing astrocytic apoE may provide therapeutic opportunities to improve outcomes in AD.

Chapter 1: Introduction

1.1 Alzheimer disease

Mental decline with aging has plagued *homo sapiens* for thousands of years, with ancient Egyptians describing aged individuals experiencing declining memory as early as 2000 B.C. and the term 'dementia' being first used around 600 A.D. (1). Yet despite the long documented history of dementia affecting humans, it was not until 1906 that Dr. Alois Alzheimer first reported on the underlying pathology of the disease that now bears his name (1–3). Dr. Alzheimer met his first patient with dementia, Auguste Deter, in 1901 and was intrigued by her mental decline, which he documented over the next 5 years (4). After the passing of Auguste D. at the age of 55, Dr. Alzheimer was able to perform a histopathological exam of her brain, which led to the discovery of senile plaques and neurofibrillary tangles (5). In 1910, Dr. Alzheimer's colleague, Emil Kraepelin, would be the first to coin the term Alzheimer disease (AD) to describe the early onset of dementia that afflicted Auguste D (1,2,5,6). Now, over one-hundred years later, Alzheimer disease is the leading cause of dementia in the world and one of the greatest maladies mankind has ever had to face (7).

Alzheimer disease currently affects over 6 million Americans and ~50 million people worldwide (7,8). The estimated costs to care for and treat individuals with AD in the United States, excluding unpaid care provided by friends and family, will be $355 billion for 2021 (9). Without further development of treatments or cures to delay or prevent the development of AD, the number of individuals with AD could grow to 13.8 million and cost the United States in excess of $1.1 trillion by the year 2050 (10). In addition to the tremendous financial burden, AD

takes an emotional and physical toll on those with the disease, and on their caregivers and loved ones as well. For these reasons, as well as many others, it is critical that investments in AD research continue in order to further develop new treatments and therapies.

The clinical manifestations of AD, which Dr. Alzheimer described with Auguste D., include memory loss, progressive cognitive impairment, confusion, changes in behavior, sleep disturbances, and changes to physical function, to name a few (11). The symptoms of AD can be varied and exist on a spectrum based on the level and location of pathology within the brain. The pathologies that characterize AD include extracellular plaques, primarily composed of the amyloid-β (Aβ) peptide, and intracellular neurofibrillary tangles, primarily composed of the protein tau (12). The Aβ peptide is produced by the sequential cleavage of the amyloid precursor protein (APP). APP is first cleaved by the β-secretase enzyme, encoded by the *BACE1* gene followed by cleavage from the γ-secretase complex (13). The cleavage of APP can produce Aβ peptides of different lengths, of which Aβ40 and Aβ42 are the most prevalent. Aβ42 is the most amyloidogenic and toxic species of Aβ and is a primary component of Aβ plaques (13,14). The formation of Aβ plaques is one of the first pathologies that is seen in AD and can begin anywhere from 10-20 years before the onset of symptoms (15). The amyloid plaque accumulation is then sequentially followed by glial activation, tau pathology, neuronal dysfunction, neuronal loss, and finally brain atrophy as the clinical symptoms initiate and progress (16,17). While this sequence of events tends to be similar for most cases of AD, the initiation and time course of progression of each event can vary from one individual to the next.

The underlying causes that initiate AD pathology, as well as the age of onset of pathology, can be used to help characterize the disease. Individuals who develop cognitive impairment before the age of 65 have an early onset of AD (EOAD) and account for about 5% of

cases, while those who develop symptoms after the age of 65 have late onset AD (LOAD) (12,18). Furthermore, individuals may carry an underlying genetic mutation that can be passed from one generation to the next, resulting in a family history of AD, known as familial AD (fAD). Those with fAD often present with early onset fAD (EOFAD or eFAD), but may also have a later onset. More than 90% of those with AD have no known underlying genetic cause and have what is known as sporadic AD (sAD), most of whom have LOAD (19). For fAD, there have been several deterministic genetic mutations identified in three genes, presenilin1 (*PSEN1*), presenilin2 (*PSEN2*), and amyloid precursor protein (*APP*). These genetic mutations are inherited in an autosomal dominant manner and result in autosomal dominant AD (ADAD), which accounts for less than 1% of AD cases (20).

In addition to those in the general population with EOAD or LOAD, individuals with Down syndrome (DS) also develop AD pathology that results in a very high rate of dementia. Nearly all individuals with DS develop AD pathology in their brains by the time they reach their 40s, which has consequently resulted in those with DS becoming the largest group of individuals with EOAD (21). Additionally, upwards of 77% of those with DS over the age of 60 develop signs of dementia and all individuals with DS have a lifetime risk of AD dementia that is >90% (22–24). One of the main driving factors for developing AD comes from the fact that individuals with DS have an additional copy of their 21st chromosome, known as Trisomy 21. The *APP* gene is located on the 21st chromosome, which results in an increase in the expression of *APP* (22,25). This increased expression of *APP* ultimately leads to an increase in the production of the Aβ peptide and drives the formation of Aβ plaques. More recent research has also begun to investigate other factors that may influence the development of AD pathology and dementia that results from Trisomy 21. The uniqueness of each individual with DS, and the wide range of

cognitive abilities each possesses, adds to the complexity of trying to address the development of AD pathology and dementia in this population. As research continues to provide more insight into the development of therapeutics and treatments for AD, it will be vital that those with DS are included and that the complexity of Trisomy 21 is considered and accounted for in the treatment strategies that are developed. In order to truly achieve a world without Alzheimer disease, individuals with Down syndrome must be included.

1.2   Amyloid-β and the amyloid cascade hypothesis

One of the greatest challenges in trying to pinpoint the etiology of AD has come from determining what the precise biological underpinnings are that result in the clinical manifestations of the disease. Initial post-mortem brain analyses of those with AD, including those by Dr. Alzheimer, identified plaques and tangles in the brain, glial activation, vascular damage, and neuronal cell loss (3,6,26,27). However, it was not quite fully understood how, and in what order, these pathologies developed and whether the presence of one might influence the development of another. When Aβ and tau were identified as the primary components of extracellular plaques and tau tangles, respectively, researchers began to focus in on how each of these proteins might become aggregated and potentially neurotoxic. Additionally, with advances in genetic sequencing, mutations were identified that are involved in the development of AD and provided further evidence for what might be driving the sequence of events that leads to the clinical manifestations of the disease. In 1992, Hardy and Higgins first proposed the amyloid cascade hypothesis to try to explain how the pathology of AD first begins and progresses to cause dementia (28). This hypothesis centers around the Aβ peptide and how its production,

clearance, and aggregation initiate a 'cascade' of pathological events that spread throughout the brain.

Hardy and Higgins proposed that Aβ is the main perpetrator that initiates AD pathology and subsequently induces the hyperphosphorylation of tau, leading to tau aggregation into neurofibrillary tangles, which ultimately causes the neuronal damage that leads to cell death and brain atrophy. The amyloid cascade begins with the amyloidogenesis of Aβ, which occurs in a concentration dependent manner. Soluble monomers of Aβ first bind to create oligomeric species that then go on to form protofibrils, fibrils, and ultimately plaques (29). Aβ can accumulate into different types of plaques, primarily characterized by the plaque structure, the plaque components, and the plaques impact on the cellular environment (30). Aβ is the primary component of amyloid plaques and in *vitro* studies have shown that Aβ is prone to self-aggregation, however, different proteins and molecules can interact with Aβ to influence the aggregation process, such as APOE, APOJ (aka Clusterin), αl-antichymotrypsin (ACT), adaptor protein apoptosis-associated speck-like protein containing a CARD (ASC) specks, and transthyretin (TTR) (31–37). Some of these molecules, like APOE, can become incorporated into the plaque and impact the type of plaque that forms.

Diffuse plaques are accumulations of dispersed Aβ that lack fibrillar structure and tend to lack a dense concentrated core. Fibrillar amyloid plaques on the other hand contain Aβ that has a β-sheet structure which can be identified by several dyes, such as Thioflavin S or Congo red, which bind to and intercalate into the β-sheet structure (38,39). These fibrillar plaques can be further characterized based on their morphology as well. Dense core plaques contain a concentrated, compact central core while filamentous plaques lack a central core with dispersed fibrils that are wispy-like in appearance (30,40). Furthermore, fibrillar plaques can induce

5

damage to neuronal processes, more so than diffuse plaques, that leads to neuritic dystrophy (30,41). These damage inducing plaques are also referred to as neuritic plaques. Neuritic plaques can be identified by the various proteins, and other materials, that accumulate in the neurites, such as BACE1, Reticulon-3, Lamp1, APP, tau, and neurofilaments, (30,42–45). This damage caused by Aβ plaques is one of the key steps that is likely driving the amyloid cascade.

One of the greatest pieces of evidence for the role of Aβ in the amyloid cascade came from the discovery of the determinant mutations in *PSEN1*, *PSEN2*, and *APP* that cause ADAD. All of these mutations influence the processing of APP and the production of the Aβ peptide. Presenilins are the catalytic component of the γ-secretase complex and are responsible for the cleavage of the C-terminus of APP that produces the final Aβ peptide product (46). *PSEN1* and *PSEN2* mutations, as well as *APP* mutations located near the γ-secretase cleavage site, often drive the relative production of Aβ42 relative to other Aβ species and increase the Aβ42/Aβ40 ratio to induce increased aggregation and toxicity of Aβ (47,48). While other mutations have been identified that do not directly influence the dynamics of Aβ accumulation, these mutations only alter ones risk for developing AD and are not deterministic like *PSEN1*, *PSEN2*, and *APP* mutations.

Further support for the amyloid cascade has come from the *APP* gene being located on the 21st chromosome. Individuals with Down syndrome who have Trisomy 21 have an increased gene copy number of *APP* that results in the inevitable formation of Aβ plaques and the subsequent high rate of dementia in DS. In addition to those with DS, there have been individuals who have a partial duplication of HSA21 that contains the APP gene locus and this increased copy number of APP has been shown to cause fAD (49).

These various findings that support the role of Aβ in the amyloid cascade have led to the development of numerous therapeutic treatments that target Aβ. These include gamma-secretase inhibitors and modulators, BACE1inhibitors, active immunization with Aβ peptides, and passive immunization with monoclonal antibodies directed against different forms and epitopes on Aβ (50). Unfortunately, nearly all of the clinical trials using Aβ-targeted therapies have ultimately failed to improve cognitive outcomes. However, most of the trials did not effectively remove amyloid plaques. Recently, several clinical phase II clinical trials and one phase III clinical trial have used anti-Aβ antibodies in patients with very mild dementia due to AD. Antibodies such as lecanemab and donanemab both remove amyloid plaques robustly in humans and provided evidence of slowing of cognitive decline in phase II trials (51,52). Aducanumab, an anti-Aβ antibody that also was recently shown to effectively remove amyloid plaques at monthly doses of 10 mg/kg was just approved by the FDA as an antibody that effectively removes amyloid plaques a process which will "likely will result in cognitive benefit". One phase III trial did show an ~22% slowing of cognitive decline in very mild dementia due to AD and the other similar trial did not (53). Thus, we still await definitive evidence as to whether removing amyloid in patients with very mild dementia will be effective. However, one caveat to the majority of previous Aβ-targeted clinical trials is that they were conducted in individuals that were already symptomatic and presenting with impaired cognition, a phase of the disease in which the brain already has widespread Aβ plaque formation (54). With this in mind, a number of ongoing clinical trials have begun to focus on treating individuals that are in the pre-symptomatic stage, or very early symptomatic stage, of AD when Aβ levels may still be able to be lowered and prevent and/or delay the subsequent cascade of pathological events that leads to impaired cognition and dementia (55,56).

The failed clinical trials, combined with additional studies that have shown that individuals can have high levels of Aβ plaque load with little to no impairment of cognition, have led many in the AD research field to recognize that Aβ plaques alone may be necessary but not sufficient to cause AD (57,58). This had led many to look at other potential therapeutic targets, such as tau, to try to improve clinical outcomes for those with AD. Despite this, the production, accumulation, and formation of Aβ into amyloid plaques is still a necessary component for one to develop AD. The role of Aβ as a key pathology in AD has continued to warrant further investigation into various factors that influence Aβ pathogenesis, factors like APOE.

1.3   Apolipoprotein E

Apolipoprotein E is a protein that is a component of lipoprotein particles and is involved with the shuttling of cholesterol and lipids throughout the body. In the periphery, apoE is mainly produced by the liver and is a component of VLDL and HDL particles and chylomicron remnants (59). In the central nervous system (CNS), apoE is found in HDL-like particles that are mainly produced by astrocytes (60). However, during brain insult microglia can significantly upregulate their APOE production (61,62). Astrocytic APOE particles act to shuttle cholesterol to neurons to aid in neuronal growth and synapse formation (63,64).

The three human APOE isoforms vary from one another at amino acid residues 112 and 158, which are located in the LDL receptor binding region, and change the charge and structure of the protein. APOE2 has Cys-112 and Cys-158, APOE3 has Cys-112 and Arg-158, while APOE4 has Arg-112 and Arg-158 residues (65). The differences in amino acids between each

isoform results in a defect in APOE2 binding to LDL receptors compared to the other two isoforms (66). This results in an isoform dependent difference in cellular uptake of lipoproteins (APOE2 < APOE3 < APOE4) and is the underlying cause of some of those homozygous for APOE2 developing type III hyperlipoproteinemia (67). Additionally, some isoform dependent differences have been observed in the lipoprotein particles. For instance, in plasma, APOE4 has shown more of an association with triglyceride-rich VLDL particles than APOE3 and APOE2 (68,69). The APOE lipoprotein particles produced by astrocytes have also been well characterized based on their particle size, shape, and lipid content. The APOE particles primarily range in size from 8-17nm and are spherical and disc-shaped (70,71). These particles contain phospholipids, free cholesterol, and triglycerides (72,73). APOE4 particles contain more triglycerides, but contain far less cholesterol than APOE3 containing particles (72,74). This results in APOE4 particles being smaller in size overall than APOE3 and APOE2 containing particles, and has led many to theorize that perhaps increasing the lipidation of APOE4, to be more in like APOE2, might lead to improved outcomes in AD (73). Indeed, many studies have been able to increase lipidation of APOE particles by various means and have shown improvements in Aβ pathology and cognition in Aβ mouse models (73).

1.4 The influence of Apolipoprotein E on Alzheimer disease and β-amyloidogenesis

The association of apoE with AD first came when it was discovered that apoE is a component of Aβ plaques (75,76). Shortly thereafter the ε4 allele of the *APOE* gene was identified as a risk factor for AD (77,78). Subsequent studies found that having one copy of *APOE4* increases the risk for AD ~3 fold while those who carry two copies have a 12-fold

increased risk, making APOE4 the strongest genetic risk factor for developing LOAD (79). In addition, APOE4 carriers have an earlier age of onset of AD (79,80). There are however differences in how APOE4 influences ones risk based on sex and ethnic background. Female *APOE4* carriers are more likely to develop AD, have a faster rate of disease progression, and more severe cognitive decline and memory impairment compared to males who are *APOE4* carriers (81–84). For African-Americans, the level of risk from being an *APOE4* carrier appears to not be as great as the level of risk of non-Hispanic whites and does not appear to have the same impact on different measures of brain function and on AD biomarkers. (85–88). Further research is needed to better understand this variation in the risk of being an *APOE4* carrier amongst females and African-Americans, especially when considering different therapeutic approaches that might be needed based on sex and ethnic background.

The overall increased risk that results from APOE4 has led many to investigate how APOE exerts its influence on the development of AD pathology. Due to APOE being a component of Aβ plaques, a lot of attention has been focused on how APOE influences Aβ pathology. However, more recent work, including work from the our lab, has shown that APOE can influence tau-mediated neurodegeneration and that an isoform-dependent effect exists with APOE4 inducing greater tau pathology (89). While more insight into the mechanisms of how APOE is impacting tau pathology is needed, a large amount of work has been done to better understand the relationship between APOE and Aβ.

One area of interest pertaining to how APOE influences Aβ pathology has focused on the direct interactions of APOE with Aβ and how these interactions influence Aβ fibrillogenesis. Studies have shown isoform dependent differences in the binding of apoE particles to Aβ, however, many of these binding interaction studies used apoE expressed artificially in various

non-astrocytic cell lines, plasma-derived apoE particles, or recombinant apoE that was either

lipidated or non-lipidated (90–93). Additionally, in many studies, recombinant or synthetic Aβ

was used, often at non-physiological concentrations, and whether or not the Aβ was in a native

monomer state or had formed into aggregation prone oligomeric 'seeds' was not controlled for.

(90,94–97). All of the variability in what types of apoE and Aβ are used have caused mixed

results and made it difficult to fully interpret all of the findings. However, previous work from

our lab focused on the interactions between apoE and Aβ using more physiological conditions

and multiple sources of both apoE and Aβ, including reconstituted, cell-secreted, and human

CSF derived apoE and Aβ that was synthetic, cell-secreted, and from CSF (94). The results

showed that minimal direct interaction occurs between soluble/monomeric Aβ and lipidated

APOE particles and that the isoform-dependent impact of apoE on Aβ levels likely comes in part

via apoE and Aβ competing for the same clearance mechanisms. For example, like apoE, Aβ can

bind to and taken up and cleared by LDLR (98). Since APOE4 has a higher affinity for LDLR

than APOE2, it is believed that APOE4 is more capable of outcompeting Aβ for clearance via

LDLR than APOE2, which results in increased concentrations of ISF Aβ in APOE4 mice

compared to APOE2 (94,99,100).

Additionally, many in vitro assays looking at amyloid fibril formation and elongation

have shown apoE isoform-dependent effects on the aggregation of Aβ. However, while some *in

vitro* results have shown apoE increases the fibrillization of Aβ, with APOE4 > APOE3 >

APOE2 (34,95,101), others studies have been contradictory and shown that apoE actually has a

reduced ability to fibrillize Aβ, with APOE4 < APOE3 < APOE2 (102–105). Once again, these

studies used experimental conditions with variable sources and forms of apoE and Aβ, including

using apoE with varying lipidation states (106). The lipidation state of apoE is a critical factor

when it comes to how apoE impacts Aβ plaque development. Several studies have shown that APOE4-containing lipoprotein particles tend to be less lipidated than APOE2 and APOE3 particles and that increasing the lipidation of these APOE4 particles, may hold promise as a therapeutic way to improve AD pathology (73,107–109). Most studies have shown that with an increase in apoE lipidation, the aggregation propensity of Aβ is decreased, and, inversely, if apoE lipidation is decreased, Aβ aggregation increases. One of the primary lipidators of apoE in the CNS is ABCA1 and *in vivo* studies have shown that a loss of ABCA1, and subsequent reduction in apoE lipidation, causes an increase in Aβ deposition (110–114). On the other hand, overexpression of ABCA1 leads to increased lipidation of apoE and a reduction in Aβ plaques (115). The impact of apoE lipidation on Aβ pathology has led many to develop various treatments targeting the level of lipidation of apoE in hopes of reducing Aβ plaques and improving disease outcomes (73). One such treatment that was recently developed by our lab uses an anti-APOE antibody, HAE-4, that specifically targets and binds non-lipidated forms of APOE (116). Use of this antibody showed that a non-lipidated form of apoE is present in Aβ plaques and when HAE-4 is administered in mice it elicits an antibody-mediated microglial Fcγ receptor dependent phagocytosis of Aβ plaques by microglia (116,117).

While targeting non-lipidated apoE, or less-lipidated apoE lipoprotein particles, may hold promise as a therapeutic treatment to improve outcomes in AD, there is still much to be discovered about these forms of apoE. For instance, the source of the non-lipidated apoE that is found in Aβ plaques has yet to be fully determined. While some recent work has suggested that microglia may be the source of apoE that ends up deposited in plaques, it has not definitively been shown (118). Additionally, how apoE ultimately comes to exist in a non-lipidated state is unknown. One possibility is that after the apoE protein is translated from apoE mRNA, it never

becomes lipidated and directly interacts with Aβ in an already non-lipidated state. Another possibility is that after apoE is lipidated and forms apoE-containing lipoprotein particles, apoE, prior to interacting with Aβ, is then somehow delipidated and this delipidated form of apoE is then capable of binding to Aβ and participating in the formation of amyloid plaques. Similarly, apoE-containing lipoprotein particles could be delipidated upon interacting with Aβ and the binding to Aβ, whether it be oligomers or protofibrils/fibrils, could induce the shedding of lipids from apoE and thus allow apoE to become non-lipidated and ultimately incorporated into amyloid plaques (105). In order to determine the source(s) of apoE found in amyloid plaques, and the process by which apoE is deposited, further studies are needed, including additional work to characterize the apoE produced by microglia, in order for cross comparisons to be made against apoE produced by astrocytes. In order to address some of the questions regarding potential differences between apoE produced by astrocytes and apoE produced by microglia, we have further characterized apoE lipoprotein particles produced by microglia, including lipoprotein particles containing APOE2, APOE3, or APOE4. Furthermore, to better understand the cell-type specific roles of apoE on the development of Aβ pathology, we have removed apoE, both globally and in a cell-specific manner from astrocytes, to investigate the impact on Aβ plaque formation and the subsequent gliosis and neuritic dystrophy.

The development of treatments for AD have often focused on impacts on neuronal function and improved cognitive outcome, but more recently there has been a growing appreciation for how glia are impacted by Aβ and the role that glial cells play in regulating the development of pathology. In particular, recent discoveries have been made showing that not only are microglia activated in the presence of Aβ plaques, but that their activation state influences inflammation within the brain and plays a key role in regulating the development of

Aβ pathology. Since microglia are the resident macrophages in the brain, initial characterizations of activated microglia divided them into either an M1 (pro-inflammatory) or M2 (pro-phagocytic/repair) state based upon previous classifications for macrophages (119). Two main factors that have been shown to regulate this polarization are macrophage colony-stimulating factor (M-CSF), which helps prime macrophages toward the M1 state, and granulocyte-macrophage colony-stimulating factor (GM-CSF), which drives the M2 state (120,121). However, these classifications are now viewed as being over-simplified and not truly representative of the very diverse states that microglia can move in and out of depending on the various environments they reside in and conditions they encounter (122).

More recently, activated microglia involved in responding to neurodegenerative conditions have been characterized as being disease-associated microglia (DAM) or as having a microglial neurodegenerative (MGnD) phenotype (61,62). One key molecule that regulates this type of activation is apoE. As microglia shift out of homeostasis and into an activated state during neurodegeneration, they upregulate several genes, of which apoE is one of the most significantly upregulated (61,62,123). Interestingly, when *apoE* is removed from microglia, this activation is suppressed and genes that are normally induced in the face of neurodegenerative conditions are repressed (61). This ability of activated microglia to induce apoE expression, and the role that apoE plays in regulating the activation state of microglia, warrants further investigations into how microglial apoE expression is regulated and whether apoE produced by microglia has distinct characteristics and functions compared to astrocytic apoE.

In addition to microglial activation, astrocytes also become activated in the presence of Aβ. One of the most common markers used for astrocyte activation is GFAP. As astrocytes become activated by Aβ, they upregulate their GFAP production and GFAP+ astrocyte processes

14

surround Aβ plaques (124). More recently, additional genes that are altered during changes to activation of astrocytes have been identified and the activation of astrocytes has been characterized into A1 (neurotoxic) or A2 (neurotrophic) (125). Some studies have suggested that apoE can influence astrocyte activation in the presence of Aβ (126). ApoE isoform dependent differences in astrocyte responses to inflammatory stimuli have also been reported (127). The influence of APOE4 on the inflammatory state of astrocytes has been proposed to be through several potential mechanisms, including altering lipid homeostasis, cholesterol synthesis, lipid droplet formation and glucose metabolism to name a few (128). Additionally, it has been theorized that apoE produced by astrocytes might be a secreted factor that can act as a signal to regulate the activation of microglia, however there have not yet been any reports that have provided evidence of such a role (128). However, some of the greatest evidence for how apoE exerts its influence on astrocyte activation comes via the role that apoE plays in regulating Aβ amyloidogenesis and the development of Aβ pathology.

1.5   Modeling the role of Apolipoprotein E on amyloid-β plaque pathology using mouse models

One of the many challenges when trying to understand the role of apoE in the development of AD is the ability to appropriately model the conditions within the human brain in which apoE is exerting its influence on the development of Aβ pathology. One of the ways this challenge has been addressed is through the use of animal models that have been genetically engineered to develop aspects of AD pathology that are similar to what is seen in the human condition. Mouse models in particular have provided invaluable insights into how Aβ is produced, the mechanisms of Aβ clearance, and how Aβ accumulates into plaques. Furthermore,

mice have also been engineered that express the human forms of *APOE2*, *APOE3*, or *APOE4* (129) and the crossing of these mice with mouse models of amyloidosis have provided opportunities to investigate how each apoE isoform influences Aβ pathology.

Mice contain a murine version of the *APP* gene, however the amino acid sequence of the Aβ peptides that are produced by the processing of murine APP varies from the Aβ produced in humans by three amino acids and is non-amyloidogenic during the ~ 2 year lifespan of a mouse (130). As a result, many attempts have been made to engineer mice that are capable of producing Aβ peptides that are similar to those produced in humans and have the ability to aggregate in a manner similar to what is seen in AD. While mice that overexpress wild-type human APP develop neuronal pathology and impairments in cognitive function, the Aβ produced in these mice is essentially non-amyloidogenic (131). In order to drive amyloidosis of Aβ in mice, *APP* or *PSEN1* genes with mutations that cause ADAD, many of which increase the Aβ42/Aβ40 ratio, have been introduced into mice (20,132). One mouse model frequently used by our lab, and for the results I report here, is the APPPS1-21 model, which has the KM670/671NL (Swedish) mutation in *APP* and the L166P mutation in *PSEN1* under the control of a neuron-specific Thy1 promoter (133). This model begins to develop Aβ plaques around 6-8 weeks of age. Another model I report on here is the APPPS1ΔE9, which also has *APP* with Swedish mutation, but carries the ΔE9 mutation in *PSEN1* instead of the L166P mutation and both genes are driven by the mouse prion promoter (134). This model develops Aβ plaques at a slower rate with initial deposition occurring around 6 months of age.

The majority of transgenic models of amyloidosis use various promoters to drive increased *APP* expression, which aids in driving more Aβ production and the formation of Aβ plaques. Many behavioral studies in these mice demonstrated cognitive deficits, including

memory impairment (135). However, given the role that APP plays in neurodevelopment and overall neuronal function, the overexpression of *APP* in and of itself may actually be driving some of the cognitive deficits that are seen in these mice (136). In light of this issue, new *APP* knock-in mouse models were recently created with the expression of the *APP* transgene controlled by the endogenous *APP* mouse promoter (137). Three separate strains were created expressing a combination of different *APP* mutations, the Swedish (NL), Iberian (F), Arctic (G) mutations. While the NL mice developed little to no Aβ pathology, the NLF mice showed the first signs of Aβ plaques around 6 months of age and the NLGF mice had initial Aβ plaque deposition starting around 2 months of age. While these mice help address some of the issues surrounding *APP* overexpression and the interpretation of behavioral experiment results, the NLF mice have a relatively slow plaque development and the NLGF mice carry the Arctic mutation, which is located in the Aβ peptide sequence and alters the properties of the Aβ peptide. The issues surrounding these knock-in mice underscores how each mouse model of amyloidosis has its own unique characteristics and challenges and further highlights the importance of comprehending the limitations of each model when trying to interpret results. Further precautions need to be taken with AD mouse models when trying to understand how apoE influences Aβ pathology.

In order to try to understand how apoE was affecting Aβ levels in mice, apoE knock-out mice were crossed with various *APP* mouse models. The complete removal of apoE resulted in a reduction in the amount of total Aβ, in particular fibrillar Aβ, that accumulated in the brains of mice (138,139). However, murine apoE is only 70% homologous to the human apoE isoforms (140). The differences between mouse apoE and human apoE can lead to varying impacts on Aβ and potential complications when trying to translate findings from mice to humans (141).

Therefore, to better understand how human apoE isoforms might be impacting various types of physiology, knock-in models were generated with either *APOE2*, *APOE3*, or *APOE4* expressed under the endogenous mouse apoE promoter (129). These mice were then further crossed with amyloidosis mouse models and revealed isoform dependent differences on Aβ plaque development. Mice expressing APOE4 had an earlier and more rapid accumulation of Aβ plaques compared to mice carrying APOE3 (142). Furthermore, gene dose dependent effects were revealed when mice heterozygous for APOE3 or APOE4 were shown to have significantly less Aβ plaques than mice that carried two copies of APOE3 or APOE4 (143). Additionally, experiments using anti-sense oligonucleotides (ASO's) to reduce APOE3 or APOE4 revealed that a reduction of apoE prior to Aβ plaque formation had a greater effect at lowering Aβ plaque levels compared to ASO treatments given after the onset of Aβ plaque deposition (144). The reduction in Aβ plaques that is seen with a reduction in apoE levels has helped bolster efforts to try to reduce apoE as a therapeutic intervention. However, given the many functions apoE plays in the brain, it is important to understand how targeting apoE for reduction might impact cellular responses to changes in apoE levels. Furthermore, given the continued development of ways to manipulate genes and proteins of interest in a cell-specific manner, understanding how specifically reducing astrocytic or microglial apoE might influence pathological outcomes will be vitally important for the development of therapeutic interventions.

Chapter 2: ApoE facilitates the microglial response to amyloid plaque pathology

This chapter is adapted from the following manuscript:

Ulrich JD*, Ulland TK*, **Mahan TE***, Nyström S, Nilsson KP, Song WM, Zhou Y, Reinartz M, Choi S, Jiang H, Stewart FR, Anderson E, Wang Y, Colonna M, Holtzman DM. ApoE facilitates the microglial response to amyloid plaque pathology. J Exp Med. 2018 Apr 2;215(4):1047-1058.

* Equal contribution

T.E.M. helped design the experiments, perform the research, and compile the figures

2.1 Introduction

One of the hallmark pathologies of Alzheimer's disease (AD) is the presence of extracellular deposits of diffuse and fibrillar amyloid plaques predominantly consisting of the amyloid-β (Aβ) peptide. Aβ-related pathology is accompanied by the clustering of microglia around fibrillar plaques, although the molecular mechanisms facilitating microglial clustering are still poorly understood (145). The formation of Aβ plaques within the brain parenchyma is influenced by the concentration of monomeric forms of Aβ in the interstitial fluid and by other proteins in the brain, perhaps most notably apolipoprotein E (apoE) (146). ApoE has previously been shown to influence the rate of monomeric Aβ clearance from the brain interstitial fluid in an isoform-dependent manner and to influence the kinetics of amyloid formation in vitro (106,147,148). Both of these characteristics likely contribute to apoE-dependent effects on Aβ plaque formation in vivo.

In addition to influencing Aβ metabolism, increasing evidence suggests that apoE may influence the microglial response in different ways in the context of neurodegenerative disease. ApoE is predominantly expressed by astrocytes but it is strongly up-regulated by microglia in the context of Aβ pathology and can influence the activation state of microglia (61,149,150). The role of microglia in the course of AD remains ambiguous. Recent genetic evidence strongly implicates microglial function in playing a critical role in the disease. Variants in microglial-expressed genes, such as TREM2 and CD33 alter the risk of developing AD, implicating the importance of microglia in the onset and progression of AD (151–154). Although chronic microglial activation is hypothesized to result in neurotoxic inflammatory signaling, recent

studies have shown that plaque-associated microgliosis was negatively correlated with the degree of neuritic dystrophy around plaques, suggesting a potential protective role for microglia in response to amyloid plaque formation (155,156). Mouse models of Aβ deposition that are haploinsufficient or completely deficient in Trem2 exhibit reduced plaque-associated microgliosis, and Trem2-deficient mice exhibit altered plaque morphology and increased neuritic dystrophy, suggestive of a role for microglia in shaping the gross structure of plaques and reducing plaque-associated toxicity (40,157–162).

Previous studies found that genetic deletion of Apoe in amyloid-depositing mouse models overexpressing human amyloid precursor protein (APP), but not PS1, resulted in a dramatic decrease in diffuse plaques and an absence of fibrillar plaque formation (139,163,164). However, more recently developed aggressive mouse models of amyloid deposition exhibit modest fibrillar amyloid deposition in the absence of apoE (165). The effect of the lack of Apoe expression in these mouse models on the tissue response to amyloid pathology is not currently understood and provides an opportunity to understand the role of apoE in this process. In this study, we characterize the impact that apoE has on amyloid pathology and the innate immune response in both the APPPS1ΔE9 and APPPS1-21 amyloid-developing mouse models. We found that Apoe-deficient mice exhibited reduced fibrillar plaque deposition and altered regional distribution of plaque pathology within the hippocampus, consistent with previous studies (164,166,167). However, fibrillar plaques in Apoe-deficient mice exhibited a striking reduction in plaque compaction, and hyperspectral fluorescent imaging using luminescent conjugated oligothiophenes (LCOs) identified distinct Aβ morphotypes in Apoe-deficient mice. We also observed a significant reduction in plaque-associated microgliosis and activated microglial gene expression in Apoe-deficient mice, along with significant increases in dystrophic neurites. Our

results suggest that apart from influencing Aβ plaque formation, apoE facilitates plaque-associated microgliosis and limits plaque-associated neuronal toxicity.

2.2 Experimental Methods

Mice. APPPS1-21 (APPPS1) transgenic mice on a C57BL6 background containing the APP KM670/671NL Swedish mutations and PSEN1 L166P mutation (gift from M. Jucker, University of Tübingen, Tübingen, Germany; (133)) were crossed with Apoe−/− mice on a C57BL6 background (Jackson Labs) to produce Apoe+/−;APPPS1 mice. Apoe+/−;APPPS1 mice were then bred with Apoe+/+ or Apoe−/− mice to produce APPPS1 or APOE−/−;APPPS1 mice. APPPS1ΔE9 (APPPS1;ΔE9) transgenic mice on a C3B6 background (Jackson Labs) containing the APP KM670/671NL Swedish mutations and PSEN1 exon 9 deletion were similarly crossed with Apoe−/− mice to produce Apoe+/−;APPPS1ΔE9 mice. Apoe+/−;APPPS1ΔE9 mice were then bred to either Apoe−/− or C57BL6 mice to produce Apoe−/−;APPPS1ΔE9 or APPPS1ΔE9 mice on a mixed C57BL6;C3B6 background. APPPS1 mice were analyzed at 6 mo of age and APPPS1ΔE9 mice were analyzed at 10 mo of age. All experimental procedures relating to animal use were approved by the Washington University Institutional Animal Care and Use Committee.

Brain sample collection. Mice were anesthetized with intraperitoneal 200-mg/kg injections of pentobarbital and perfused with ice-cold PBS containing 0.3% Heparin. One hemibrain was fixed in 4% paraformaldehyde overnight at 4°C followed by storage in a 30% sucrose in PBS (pH 7.4) solution at 4°C. The other hemibrain was dissected and flash frozen for further analysis and stored at −80°C.

Histological analysis. Fixed hemibrains were frozen and serial 50-μm coronal sections were obtained from the rostral to caudal end using a sliding microtome. Sections were stored in a cryoprotectant solution (30% ethylene glycol, 15% sucrose, and 30 mM phosphate) and stored at −20°C. Three 50-μm sections spaced 300 μm apart were used for each staining procedure.

Amyloid plaque staining and morphology. To visualize Aβ plaques, APPPS1 and Apoe−/−;APPPS1 mice were immunostained using the anti-Aβ1-5 antibody 3D6 (gift from Eli Lilly, Lilly Corporate Center, Indianapolis, IN), whereas immunostaining for APPPS1ΔE9 and Apoe−/−;APPPS1ΔE9 mice was performed with the anti-Aβ1-13 antibody HJ3.4. All sections were free-floating and were first treated with 0.3% hydrogen peroxide, blocked in 3% milk + 0.25% Triton X-100 in Tris-buffered saline (TBS), and then incubated overnight in biotinylated 3D6 or HJ3.4 accordingly at 4°C. Sections were then developed using a Vectastain ABC Elite kit (1:400; Vector Labs), followed by incubation in a 0.025% 3,3′-diaminobenzidine (DAB; Sigma-Aldrich) + 0.01% NiCl + 0.015% hydrogen peroxide solution. Images of the stained sections were obtained using a slide scanner (NanoZoomer; Hamamatsu Photonics), exported using NDP Viewer (Hamamatsu Photonics), and analyzed using ImageJ software (National Institutes of Health). To identify fibrillar plaques, free-floating sections from the APPPS1, Apoe−/−;APPPS1, APPPS1ΔE9, and Apoe−/−;APPPS1ΔE9 mice were all permeabilized with 0.25% Triton X-100 in PBS and stained with 10 μM X-34 in 40% ethanol + 0.02M NaOH in PBS. X-34 images were obtained with an Eclipse 80i microscope (Nikon) equipped with a digital complementary metal-oxide semiconductor camera (ORCA-Flash4.0 V2; Hamamatsu Photonics) and analyzed using ImageJ software to determine fibrillar plaque levels.

To determine fibrillar plaque morphology, z-stacked images were taken every 0.75 µm from X-34–stained sections. Images were acquired on a confocal microscope (A1R+; Nikon) at 40× magnification with 1.5× digital zoom. Max intensity projections of the z-stack images were then used to assess shape compactness, average intensity, and intensity Gini coefficient. A blurring filter was first applied to images to clarify the plaque from background. All pixels >2× background were considered part of the plaque, whereas pixels <1.5× background were considered non-plaque. Pixels between 1.5 and 2× backgrounds were assigned based on edge detection. Average intensity was determined based on plaque pixels. Gini coefficient was based on the distribution of pixel intensity for plaque pixels. Shape compactness was determined as the ratio of plaque area pixels to plaque perimeter pixels after scaling plaques to be the same overall area.

Aβ ELISA. Cortical tissues from 6-mo-old APPPS1 and Apoe−/−;APPPS1 mice were hand-homogenized in 10-fold volume PBS using a Teflon pestle. Brain homogenates were spun at 14,000 g for 30 min, and the supernatant was retained as the soluble fraction. The pellet was resuspended in 10-fold volume 5 M guanidine, hand homogenized, and rotated for 3 h at room temperature. Homogenates were clarified by centrifugation at 14,000 g for 30 min, and the supernatant was retained as the insoluble fraction. Aβ40 and Aβ42 concentrations were measured by sandwich ELISA. Aβ40 concentration was measured using HJ2 as the capture antibody and biotinylated HJ5.1 as the detection antibody. Aβ42 was measured using HJ7.4 as the capture antibody and biotinylated HJ5.1 as the detection antibody. ELISAs were developed using streptavidin-PolyHRP40 (Fitzgerald) and TMB Superslow reagent (Sigma Aldrich). Aβ40 and Aβ42 values were normalized to wet weight of brain tissue.

Western blotting. Hippocampal tissue was homogenized in 10-fold volume lysis buffer (10 mM Tris-HCl, pH 8.0, 1 mM EDTA, 1% Triton X-100, 0.1% SDS, and 150 mM NaCl), and lysate was clarified by centrifugation at 15,000 g at 4°C. Total protein concentrations in lysate were quantified using a BCA assay, and 50 µg of protein were loaded onto a 4–20% Bis-Tris SDS-PAGE gel followed by transfer to nitrocellulose. Full-length APP was detected using 6E10 (1:1,000; Biolegend), and C99 fragment was detected using 82E1 (1:1,000; IBL America). Protein detection was visualized using an HRP-coupled anti–mouse secondary antibody (1:5,000) and ECL reagent. Images of the blot were captured using a G Box (SynGene) and analyzed in ImageJ.

Cytokine assessment. Levels of IL1β, IL-10, TNF-α, CCL3, CCL2, and CCL4 were assessed using a Milliplex multianalyte profiling kit (Millipore) per the manufacturer's instructions. Assays were run on a FlexMAP 3D (Luminex) at the Andrew M. and Jane M. Bursky Center for Human Immunology & Immunotherapy Programs at Washington University, St. Louis, MO. Cytokine levels were normalized for total protein content in lysate as calculated by BCA assay.

LCO staining and fluorescence microscopy. The synthesis of the LCOs, q-FTAA, and h-FTAA have been reported previously (168), and the LCOs were dissolved in deionized water to a final concentration of 1.5 mM. Floating sections from 6-mo-old APPPS1 or Apoe−/−;APPPS1 mice were equilibrated in PBS and stained with a mixture of 2.4 µM q-FTAA and 0.77 µM h-FTAA in PBS or 0.77 µM h-FTAA in PBS for 30 min (169). After washing in incubation buffer the sections were transferred to glass slides and mounted with mounting media (DAKO; Agilent). The mounting medium was allowed to solidify overnight before the rims were sealed with nail polish. The LCO-stained sections were analyzed with a confocal laser scanning

microscope (LSM 780; Zeiss) equipped with a 32-channel spectral array detector (QUASAR GaAsP; Zeiss) and a tunable In Tune laser (488–640 nm; Zeiss), as well as a modular FLIM system (Becker and Hickl). In spectral mode, q-FTAA and h-FTAA were excited with a 458-nm laser, and the emitted light was detected in steps of 8.7 nm from 488 to 686 nm. Z-stacks were recorded with the dimension of x = 250 μm, y = 250 μm, and z = 90 μm using a Plan-Apochromat 20×/0.8 M27, and three-dimensional images were generated by spectral mixing using the ZEN2010 software. Three-dimensional images were rendered by spectral unmixing using the ZEN2010 software. For the FLIM, the emitted photons were routed through the direct coupling confocal port of a scanning unit (LSM 780; Zeiss) and detected by a hybrid detector (HPM-100-40; Becker and Hickl). Data were recorded by a Simple-Tau 152 system (SPC-150 TCSPC FLIM module; Becker and Hickl) with the instrument recording software SPCM version 9.42 (Becker and Hickl) in the FIFO image mode, 256 × 256 pixels, using 256 time channels (Becker and Hickl). For all acquisitions, a main beam splitter (T80/R20; Zeiss) was used and the pinhole was set to 20.2 μm. Scanning area was set to 235.7 × 235.7 μm, with a scanning resolution of 512 × 512 pixels. Furthermore, a Plan-Apochromat 40×/1.3 Oil DIC objective lens was used, and a 510-nm long pass filter was positioned in front of the hybrid PMT. Excitation used the 490-nm laser line from the pulsed tunable In Tune laser with a repetition rate of 40 MHz. Data were subsequently analyzed in SPCImage version 3.9.4 (Becker and Hickl), fitting each of the acquired decay curves to a triexponential function, and color-coded images showing the intensity-weighted mean lifetimes were generated with the same software. Fluorescence decays were collected from 5–10 different plaques in tissue sections from five individual 6-mo-old APPPS1 or Apoe−/−;APPPS1 mice.

Microglia, dystrophic neurites, and fibrillar plaque staining. To assess microglial colocalization with fibrillar plaques, sections from each group of mice were costained with X-34 and Iba-1. Free-floating sections were first stained with X-34 followed by blocking, using 3% normal donkey serum in TBS and then incubation with rabbit anti–Iba-1 (1:10,000; Wako) + 1% donkey serum in TBS overnight at 4°C. Iba-1–stained sections were then incubated in secondary donkey anti–rabbit Alexa Fluor 647 (1:1000; Thermo Fisher) in PBS. Neuritic dystrophy around fibrillar plaques was assessed in each group of mice using 22C11, an antibody to the N terminus of APP, and the X-34 dye. Free-floating sections were blocked in confocal buffer (0.5% BSA, 2% goat serum, and 0.15% Triton X-100 in PBS) and then incubated with 22C11 (1:2,000; Millipore) in confocal buffer overnight at 4°C. Sections were then incubated in confocal buffer with biotinylated goat anti–mouse IgG1 (1:2,000; Thermo Fisher) followed by Streptavidin-488 (1:2,000; Thermo Fisher) + To-Pro3 (nuclear stain, 1:1,000; Thermo Fisher) in PBS.

Confocal analysis. Confocal images were taken in the cortical regions of the Iba-1/X-34– and APP/X-34–stained sections using a confocal microscope (A1R+; Nikon). Z-stacked images were acquired every 1.25 µm at a 20× magnification. Images were then analyzed using Imaris software (Bitplane) or ImageJ. For all Imaris analyses, the Spots and Surfaces functions were used. The coordinates of microglia and the location and volume of Aβ plaques were identified using the Spots and Surfaces functions, respectively, and imported into Matlab (Mathworks). The number of microglia within a 15- and 30-µm radius were then determined using an automated script. The level of APP accumulation in neuritic processes surrounding X-34 plaques for APPPS1 and Apoe−/−;APPPS1 mice was determined by creating Spots for APP and Surfaces for X-34. The volume and number of APP-NT+ neuritic processes was determined within 30 µm using an automated script. For APPPS1ΔE9 and Apoe−/−;APPPS1ΔE9 mice the level of APP

27

around X-34 plaques was determined by creating surfaces for both APP and X-34. The Dilate Xtension was used to dilate out the X-34 plaque surface 15 μm and create a second dilated surface. To determine the volume of APP surface within 15 μm of X-34 plaque, surface–surface colocalization Xtension was run using the dilated surface and APP surface as the two surfaces for comparison. The number and volume of APP-NT+ neurites per plaque was found and determined based on overall X-34 plaque volume.

RNAseq analysis. RNA was extracted from frozen cortex tissue of 6-mo-old APPPS1 and Apoe−/−;APPPS1 mice using TRIzol per the manufacturer's instructions. Isolated RNA was then treated with DNase to remove any contaminating genomic DNA and RNA integrity assessed using a Bioanalyzer 2100 (Agilent) to ensure an RNA integrity number >7. Library preparation was performed using the SMARTer RNA kit (Clontech), and libraries were sequenced on a HiSeq2500. Sequence data were aligned to the mouse reference genome mm10 using STAR. Gene-level differential expression analysis was performed in Partek Genomic Suite. Gene ontology enrichment analysis was performed in Partek Genomic Suite by comparing the list of differentially expressed genes with the gene ontology database using a Fisher's exact test. All data have been deposited at GEO (accession no. GSE109906).

Statistical analysis. Statistical significance between two groups was assessed by two-tailed, unpaired Student's t test with significance assigned for $P < 0.05$. Statistical analysis of differential gene expression from RNAseq data were assessed using Partek Genomic Suite. A corrected p-value of 0.05 following Benjamini-Hochberg correction for multiple comparisons was considered statistically significant.

2.3 Results

2.3.1 ApoE modifies Aβ deposition

Previous studies in human APP transgenic mice, PDAPP and Tg2576, found that Apoe deficiency significantly reduced both total and fibrillar Aβ deposition (138,139,163,166). Therefore, we first assessed total Aβ deposition in the cortex and hippocampus of 6-mo-old APPPS1 and Apoe−/−;APPPS1 mice using an N-terminal Aβ antibody. Surprisingly, we observed significantly more Aβ deposition in the cortex of Apoe−/−;APPPS1 compared with APPPS1 mice, which was attributable to a significant increase in both the number and size of cortical Aβ immunostained plaques in the absence of Apoe expression (Fig. 1, A–D). Marked cortical Aβ deposition was also observed in 10-mo-old Apoe−/−;APPPS1ΔE9 mice (Fig. 1 E). The overall cortical plaque burden did not significantly differ between APPPS1ΔE9 and Apoe−/−;APPPS1ΔE9 mice; however, there was a significant decrease in the number of Aβ plaques (Fig. 1, F and G). Interestingly, the average size of Aβ plaques was significantly larger in Apoe−/−;APPPS1ΔE9 mice than in APPPS1ΔE9 mice, consistent with the effect of apoE on plaque size in the APPPS1 model (Fig. 1 H). In agreement with previous studies (139,163), we observed a marked shift in the regional distribution of Aβ plaques within the hippocampus from the molecular layer of the dentate gyrus to the hilus (Fig. 1, A and E).

In previous studies, Tg2576 and PDAPP mice deficient in Apoe exhibited virtually no true fibrillar amyloid, suggesting that apoE is necessary for Aβ to form Aβ containing a β-sheet structure, i.e., amyloid (139,163). Given that we observed significant levels of Aβ plaque pathology in both APPPS1 and APPPS1ΔE9 mice in the absence of Apoe, we decided to assess whether the fibrillar amyloid burden was significantly altered by Apoe deficiency using X-34, which labels amyloid structures (170). The cortical and hippocampal amyloid burden in both 6-

mo-old Apoe−/−;APPPS1 and Apoe−/−;APPPS1ΔE9 mice was strongly reduced in the absence

of apoE compared with mice expressing ApoE; however, fibrillar plaques were detectable in the

absence of Apoe expression in both strains (Fig. 1, I–N). Biochemical analysis of cortical tissue

from 6-mo-old APPPS1 and Apoe−/−;APPPS1 mice revealed decreased levels of insoluble Aβ40

and Aβ42, consistent with the observed decrease in X-34+ plaque pathology (Fig. S1 A).

Interestingly, although soluble Aβ40 levels were decreased in Apoe−/−;APPPS1 mice, soluble

Aβ42 levels were slightly but statistically significantly elevated (Fig. S1 B). This might reflect

the increase in diffuse Aβ pathology observed by N-terminal Aβ antibody staining (Fig. 1 A).

Western blot analysis of APP and the APP C99 cleavage fragment did not reveal a significant

difference in the ratio of C99 to APP, suggesting that apoE did not significantly affect APP

processing by β-secretase (Fig. S1, C and D).

Recent studies indicate that apoE expression influences the initiation of fibrillar plaque

deposition, but not the subsequent growth of amyloid plaques once plaque formation has

occurred (171,172). This would suggest that apoE serves as a catalyst for the folding of Aβ

peptides into higher-order amyloid/β-sheet conformations. Aβ42 exhibits a greater propensity to

form amyloid fibrils, and variants in APP, PSEN1, or PSEN2 that increase the production of

Aβ42 relative to shorter Aβ species result in autosomal dominant AD (146). We speculate that

the differences we report here in Apoe-deficient APPPS1 models compared with earlier APP

overexpression models stems largely from differences in the relative production of Aβ42:Aβ40

in these different strains. Tg2576 mice exhibited a roughly 1:5 ratio of Aβ42/Aβ40 in young

animals, compared with an ∼1:1 ratio in APPPS1 and APPPS1ΔE9 mice, which likely results in

the accelerated development of Aβ-deposition in APPPS1 and APPPS1ΔE9 mice and the

formation of amyloid (133,134). Thus, although apoE may catalyze the conversion of Aβ into a

fibrillar state, high relative generation of Aβ42 may be sufficient for the development of some true amyloid even in the absence of apoE.

2.3.2 ApoE regulates amyloid morphology and conformation

We noted that the amyloid plaques in Apoe−/− mice appeared to not stain as intensely with X-34 as in Apoe+/+ mice. Given that the plaques in Apoe−/−;APPPS1 plaques were larger than plaques in APPPS1 mice, we decided to assess the effect of Apoe on plaque morphology. High-resolution confocal imaging of amyloid plaques revealed that the gross morphology of the plaque was strikingly different in the presence and absence of apoE (Fig. 2 A). Amyloid plaques in 6-mo-old APPPS1 and 10-mo-old APPPS1ΔE9 mice had a distinct, dense core that was intensely stained with X-34 (Fig. 2 A). In contrast, plaques in Apoe−/−;APPPS1 and Apoe−/−;APPPS1ΔE9 mice contained numerous wispy fibrils, projecting out from a loosely defined core (Fig. 2 A). We quantitatively assessed these qualitative observations using a shape compactness index that takes into account the perimeter and two-dimensional area of the plaque and found that Apoe−/−;APPPS1 and Apoe−/−;APPPS1ΔE9 mice exhibited a significantly less compact morphology (Fig. 2, B and C). We further quantitatively compared plaques by assessing the Gini coefficient of pixel intensity for X-34 staining (Fig. 2, D–F). We found that plaques from Apoe−/−;APPPS1 and Apoe−/−;APPPS1ΔE9 mice exhibited a significant decrease in the Gini coefficient, consistent with the observed decrease in intensity of the dense X-34+ core of amyloid plaques compared with APPPS1 and APPPS1ΔE9 mice (Fig. 2, E and F).

A previous study demonstrated that a combination of two LCOs, q-FTAA and h-FTAA, can be used for spectral assignment of distinct aggregated Aβ morphotypes (169). q-FTAA stains only mature fibrillar Aβ deposits that are also recognized by conventional amyloid ligands, such

as Thioflavin T and X-34, whereas h-FTAA detects a broader subset of disease-associated protein aggregates (168,169,173,174). Given the stark contrast in amyloid plaque morphology in Apoe−/− mice, we stained tissue sections from 6-mo-old Apoe−/−;APPPS1 and APPPS1 mice with a mixture of q-FTAA and h-FTAA. Hyperspectral fluorescence imaging revealed distinct staining patterns using q-FTAA and h-FTAA dependent on the Apoe genotype. For all mice, minor q-FTAA fluorescence was only observed in the core of some plaques. In contrast, h-FTAA staining was much more abundant in the Apoe−/−;APPPS1 mice compared with APPPS1 mice (Fig. 2 G). Hence, in accordance with anti-Aβ antibody staining, h-FTAA fluorescence displayed a greater amount of Aβ deposition in mice lacking Apoe, and these deposits are most likely composed of an Aβ morphotype that is only detected by h-FTAA.

To examine the difference in Aβ morphotypes further, we performed fluorescence-lifetime imaging (FLIM) analysis of h-FTAA–stained Aβ deposits. FLIM is a powerful technique that can be used to determine both differential states of binding and to observe minute variations in ligand–aggregate interactions, and differences in fluorescence decays from h-FTAA have previously been observed from the ligand bound to prion aggregates associated with specific prion strains (174). For APPPS1 mice, h-FTAA–stained Aβ deposits displayed fluorescence decays between 350–600 ps, whereas the decays from h-FTAA bound to Aβ deposits in Apoe−/−;APPPS1 mice were considerably longer at 400–800 ps (Fig. 2, H and I). Hence, a distinct distribution of fluorescence decays was observed for h-FTAA depending on the Apoe genotype, suggesting that the lack of apoE induces an enrichment of a specific Aβ morphotype.

2.3.3 Decreased plaque-associated microgliosis and activated microglial gene expression in Apoe−/−;APPPS1 and Apoe−/−;APPPS1ΔE9 mice

Apoe expression is up-regulated in response to amyloid pathology and is thought to play a role in the innate immune response in the central nervous system. Interestingly, lipidated apoE binds to TREM2 in vitro and may be a potential physiological ligand mediating TREM2 activation (175,176). Given that a lack of Trem2 expression impairs plaque-associated microgliosis, we decided to test whether a lack of Apoe expression affected the microglial response to amyloid plaques. As expected, both 6-mo-old APPPS1 and 10-mo-old APPPS1ΔE9 mice exhibited pronounced microglial clustering around amyloid plaques (Fig. 3, A and C). However, the number of microglia located within 15 or 30 µm of a plaque was significantly decreased in both Apoe−/−;APPPS1 and Apoe−/−;APPPS1ΔE9 mice (Fig. 3, A–D). The number of microglia located farther than 30 µm from a plaque were unaffected by Apoe genotype, suggesting that the effect of apoE on microglial function was specific to activated microglia around amyloid plaques (Fig. 3, B and D).

To further assess the effect of Apoe deficiency in the context of amyloid pathology, we performed RNA sequencing (RNAseq) analysis on cortical tissue from 6-mo-old APPPS1 and Apoe−/−;APPPS1 mice. Gene-level analysis revealed that 115 genes were differentially expressed in APPPS1 and Apoe−/−;APPPS1 mice (Fig. 3 E; Table S1). Changes in microglial gene expression in amyloid models detected using whole tissue methods may result from either the up-regulation of a given transcript at the cellular level or an increase in microglial abundance, which, in general, positively correlates with amyloid burden (177). Evidence from single-cell RNAseq studies indicates that activated microglia around plaques, termed disease-associated microglia, exhibit up-regulation of several genes associated with lipid metabolism and

phagocytosis, including Itgax and Cst7, which are significantly down-regulated in

Apoe−/−;APPPS1 mice, consistent with a decrease in plaque-associated microgliosis (Fig. 3 G;

Table S1; (62)). Gene ontology analysis of differentially expressed genes found a significant

enrichment in genes related to the immune system (Table S2), of which the vast majority were

down-regulated (Fig. 3 E; Table S1). We further analyzed cytokine levels at the protein level in

the hippocampus of 6-mo-old APPPS1 and Apoe−/−;APPPS1 mice and observed reduced levels

of CCL3, consistent with the reduction in CCL3 transcript observed by RNAseq (Fig. 3 F).

Interestingly there was a trend toward elevated TNFα in Apoe−/−;APPPS1 mice (Fig. 3 F). This

may be attributable to increases in peripheral TNF-α expression in Apoe−/− mice, since TNF-α

is transported across the blood–brain barrier (BBB; (178,179)). Collectively, these data suggest

an overall impairment in the microglial response to amyloid pathology in Apoe−/− mice.

2.3.4 Increased neuritic dystrophy in Apoe−/−;APPPS1 mice

Emerging data suggest that reductions in plaque-associated microgliosis are associated

with increases in dystrophic neurites around plaques (40,155,159). Previous studies reported a

lack of dystrophic neurites in Apoe−/− mice crossed with either the PDAPP or Tg2576 models

(139). However, as noted above, PDAPP and Tg2576 mice developed minimal, if any, fibrillar

plaques in the absence of apoE. Moreover, accumulations of protofibrillar Aβ species within

amyloid plaques are spatially associated with increases in dystrophic neurites (155). Since the

Apoe−/−;APPPS1 and Apoe−/−;APPPS1ΔE9 mice developed significant fibrillar and diffuse

plaques, and exhibit significant reductions in microgliosis, we tested whether these mice

exhibited any differences in plaque-associated neuronal toxicity. We labeled dystrophic neurites

with an N-terminal APP antibody (NT-APP) and quantified the abundance of NT-APP staining

within 30 µm of a plaque. (Fig. 4, A and C). The number of dystrophic neurites around plaques

was significantly increased in both 6-mo-old Apoe−/−;APPPS1 and 10-mo-old Apoe−/−;APPPS1ΔE9 (Fig. 4, B and D). This observation is consistent with a role for apoE in facilitating plaque-associated microgliosis and reducing plaque-associated neuronal damage.

2.4 Discussion

Considerable evidence suggests that apoE influences the propensity of Aβ to aggregate into fibrillar plaques through several potential mechanisms, including affecting the rate of Aβ clearance from the brain and the rate of conversion of Aβ monomers and oligomers to mature fibrils (106). However, beyond its effect on amyloid, apoE also influences diverse processes in the brain, such as synaptogenesis, phagocytosis, BBB function, and microglial activation (61,63,89,150,180,181). The histological and gene expression data presented in this study suggest that apoE not only affects the structure and level of amyloid pathology, but also the innate immune response to amyloid plaques, which in turn may protect against plaque-associated neurotoxicity. This observation supports a role for apoE downstream of plaque-deposition in regulating the toxicity and immune response to amyloid pathology. The influence of apoE on microglial activation may have important implications for apoE-modulating therapies in AD.

One limitation of the current study is that we did not examine the potential contribution of apoE-dependent vascular BBB changes on plaque deposition or the immune response. Previous studies indicate that Apoe−/− mice have age-dependent BBB dysfunction, which leads to extravasation of peripheral proteins with neurotoxic consequences (180,182). Moreover, a compromised BBB could lead to increased infiltration of peripheral macrophages and neutrophils into the brain, which may also be neurotoxic (183). Conceivably, the increase in dystrophic neurites we observe in Apoe−/− could be promoted in part by infiltrating neutrophils

or a compromised BBB. In addition, we cannot exclude the possibility that overexpression of APP and PS1 may also influence the phenotypes we report here. Future studies using APP knock-in mice that test whether Apoe-dependent alterations in the BBB affect microgliosis, plaque burden, and neuritic dystrophy could provide additional insight into potential mechanisms underlying our observations (137).

In addition to BBB dysfunction, Apoe−/− mice develop hypercholesterolemia and atherosclerosis, which are accompanied by immune responses to atherosclerotic plaques (184). Interestingly, the background strain can strongly influence the degree of atherosclerosis that develops in Apoe−/− mice; C57BL/6 mice exhibit more robust atherosclerosis pathology than C3H mice (185). We observed an increase in the number of Aβ-immunoreactive plaques in Apoe−/−;APPPS1 mice, which are on a C57BL/6 background, and a decrease in the number of Aβ-immunoreactive plaques in Apoe−/−;APPPS1ΔE9 mice, which are on a mixed C57BL/6C3H background. Whether the degree of vascular pathology contributed to this dichotomous result is unknown, and it is important to note that in addition to background strain and PSEN1 mutations, the APPPS1 and APPPS1ΔE9 mice also differ in the promoter used for transgene expression (Thy1 vs. Prp, respectively). Overall, the different effects of Apoe−/− on Aβ burden we describe in APPPS1 and APPPS1ΔE9 suggest that the choice of Aβ-deposition model can strongly influence the effect of gene KO on Aβ pathology. It is important to note that despite the differing effects on Aβ pathology, we observed consistent effects of Apoe-deficiency on fibrillar Aβ deposition, microgliosis, and neuritic dystrophy in both APPPS1 and APPPS1ΔE9 models.

Apoe expression is up-regulated in AD, which is generally attributed to a proinflammatory response to Aβ pathology. Within the brain, apoE is predominantly expressed

by astrocytes, although microglia, particularly in an activated state, also produce apoE (100). The relative contribution of microglial and astrocyte-derived apoE to the regulation of Aβ deposition and microgliosis is unclear. Microglia immunoreactive for apoE were noted to be intimately associated with senile plaques, in contrast to astrocytes, which were localized more distally to plaques. The proximity of microglia versus astrocytes to plaques could indicate a unique role for microglial expressed apoE in the immune response to AD pathology (149). Investigations into the effects of apoE on plaque-associated microgliosis have focused largely on apoE isoform–dependent effects. ApoE4 and apoE2 exhibited increased numbers of plaque-associated microglia within certain cortical regions of 5xFAD mice compared with apoE3 (186). However, the APOE4 allele did not appear to affect the magnitude of plaque-associated microgliosis in human AD patients (187). Apoe expression in general has been shown to have pleiotropic effects on microglia and the broader immune response. Apoe expression is low in microglia in a homeostatic activation state, but is strongly up-regulated by neurodegenerative insults (61,150,188). Moreover, application of recombinant apoE to cultured microglia is sufficient to polarize gene expression away from a resting state toward a more activated phenotype (150). This suggests that apoE is a powerful modulator of microglial phenotype, in agreement with our current findings. In addition, the influence of apoE on microglial physiology does not appear to be specific to amyloid pathology. Reductions in microgliosis were also observed in the experimental autoimmune encephalomyelitis model of multiple sclerosis and reduced inflammation and neurodegeneration were observed in an Apoe-deficient model of tauopathy (89,189).

The function of plaque-associated microgliosis remains poorly understood. Some recent studies may indicate that microgliosis around plaques may initially have a neuroprotective role.

Plaque-associated dystrophic neurites appear in areas devoid of microglial coverage, suggesting that microglia may limit amyloid toxicity in plaque-adjacent neurons (155). An alternative interpretation is that a reduction in plaque-associated microglia could hamper phagocytic clearance of injured dystrophic neurites, resulting in an apparent increase in neuritic dystrophy. ApoE isoforms can differentially influence the phagocytosis of synapses by astrocytes and the amount of C1q deposition in aging (181). Thus Apoe expression, either by astrocytes or microglia, may promote the clearance of damaged neurites around plaques. Future studies investigating cell type–specific expression of apoE or inhibition of apoE expression following plaque deposition could provide insight into the mechanistic basis by which apoE influences the innate immune response in the context of amyloid pathology.

2.5 Figures
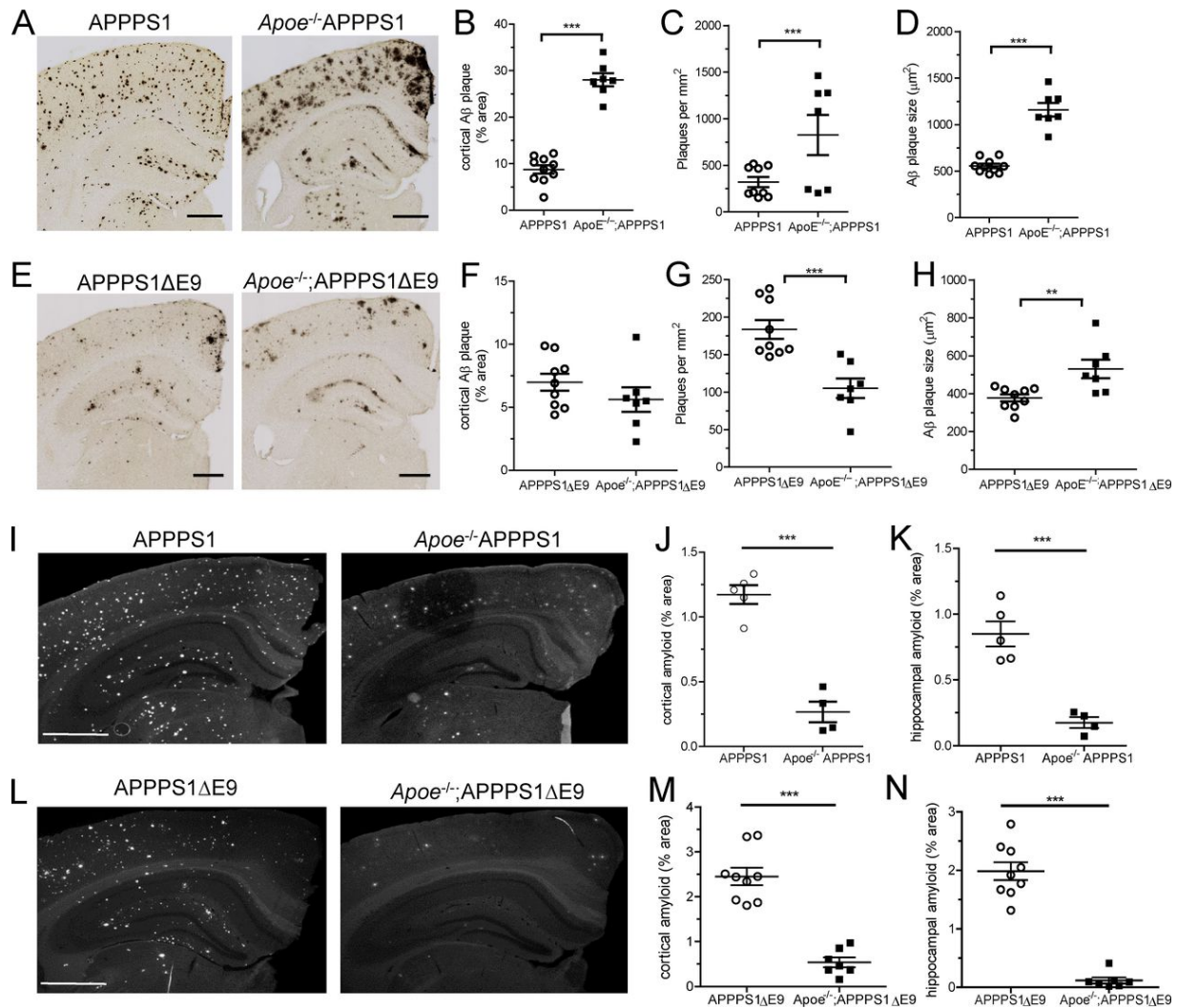
Figure 2.1: *Apoe* **deficiency increases Aβ plaque size but decreases amyloid burden.**
(A) Representative images of APPPS1 and *Apoe*$^{-/-}$;APPPS1 mice stained with an N-terminal Aβ
antibody. **(B)** The percentage of cortical area immunopositive for Aβ was increased
in *Apoe*$^{-/-}$;APPPS1 mice (28.0 ± 1.4%, *n* = 7 mice) relative to APPPS1 (8.8 ± 0.9%, *n* = 10
mice); t(15) = 12.1, P < 0.0001, Student's *t* test. **(C)** The mean number of plaques was increased
in *Apoe*$^{-/-}$;APPPS1 mice (230.6 ± 6.5, *n* = 7 mice) relative to APPPS1 (172.8 ± 9.6, *n* = 9); t(14)
= 4.7, P = 0.0003. **(D)** The mean plaque size was increased in *Apoe*$^{-/-}$;APPPS1 mice (1,159 ±
72.9 μm^2, *n* = 7 mice) relative to APPPS1 (555.1 ± 23.2 μm^2, *n* = 10); t(15) = 9.1, P < 0.0001,
Student's *t* test. **(E)** Representative images of APPPS1ΔE9 and *Apoe*$^{-/-}$;APPPS1ΔE9 mice
stained with an N-terminal Aβ antibody. **(F)** The percentage of cortical area immunopositive for
Aβ was not significantly different between APPPS1ΔE9 (7.0 ± 0.7%, *n* = 9 mice)
and *Apoe*$^{-/-}$;APPPS1ΔE9 (5.6 ± 1.0%, *n* = 7 mice); t(14) = 1.2, P = 0.25,

Student's *t* test. **(G)** The number of cortical plaques was significantly reduced in *Apoe*$^{-/-}$;APPPS1ΔE9 mice (105.2 ± 13.0, *n* = 7 mice) compared with APPPS1ΔE9 mice (183.5 ± 12.4, *n* = 9 mice); t(14) = 4.3, P = 0.0007, Student's *t* test. **(H)** The mean plaque size was increased in *Apoe*$^{-/-}$;APPPS1ΔE9 mice (529.8 ± 48.6 μm^2, *n* = 7 mice) compared with APPPS1ΔE9 mice (377.9 ± 18.5 μm^2, *n* = 9 mice); t(14) = 3.2, P = 0.0064, Student's *t* test. **(I)** Representative images of APPPS1 and *Apoe*$^{-/-}$;APPPS1 mice stained with X-34. **(J)** The percentage of cortical area stained with X-34 was significantly decreased in *Apoe*$^{-/-}$;APPPS1 mice (0.27 ± 0.08, *n* = 5 mice) compared with APPPS1 (1.2 ± 0.07, *n* = 4 mice); t(7) = 8.411, P < 0.0001, Student's *t* test. **(K)** The percentage of hippocampal area stained with X-34 was significantly decreased in *Apoe*$^{-/-}$;APPPS1 mice (0.18 ± 0.04, *n* = 4 mice) compared with APPPS1 (0.85 ± 0.1, *n* = 5 mice); t(7) = 5.9, P = 0.0006, Student's *t* test. **(L)** Representative images of APPPS1ΔE9 and *Apoe*$^{-/-}$;APPPS1ΔE9 mice stained with X-34. **(M)** The percentage of cortical area stained with X-34 was significantly decreased in *Apoe*$^{-/-}$;APPPS1ΔE9 mice (0.54 ± 0.11%, *n* = 7 mice) compared with APPPS1ΔE9 (2.5 ± 0.19%, *n* = 9 mice); t(14) = 8.0, P < 0.0001, Student's *t* test. **(N)** The percentage of hippocampal area stained with X-34 was significantly decreased in *Apoe*$^{-/-}$;APPPS1ΔE9 mice (0.12 ± 0.05%, *n* = 7 mice) compared with APPPS1ΔE9 (2.0 ± 0.15, *n* = 9 mice); t(14) = 10.4, P < 0.0001, Student's *t* test. All values given and plotted as mean ± SEM. Bars, 500 μm. **, P < 0.01; ***, P < 0.001.
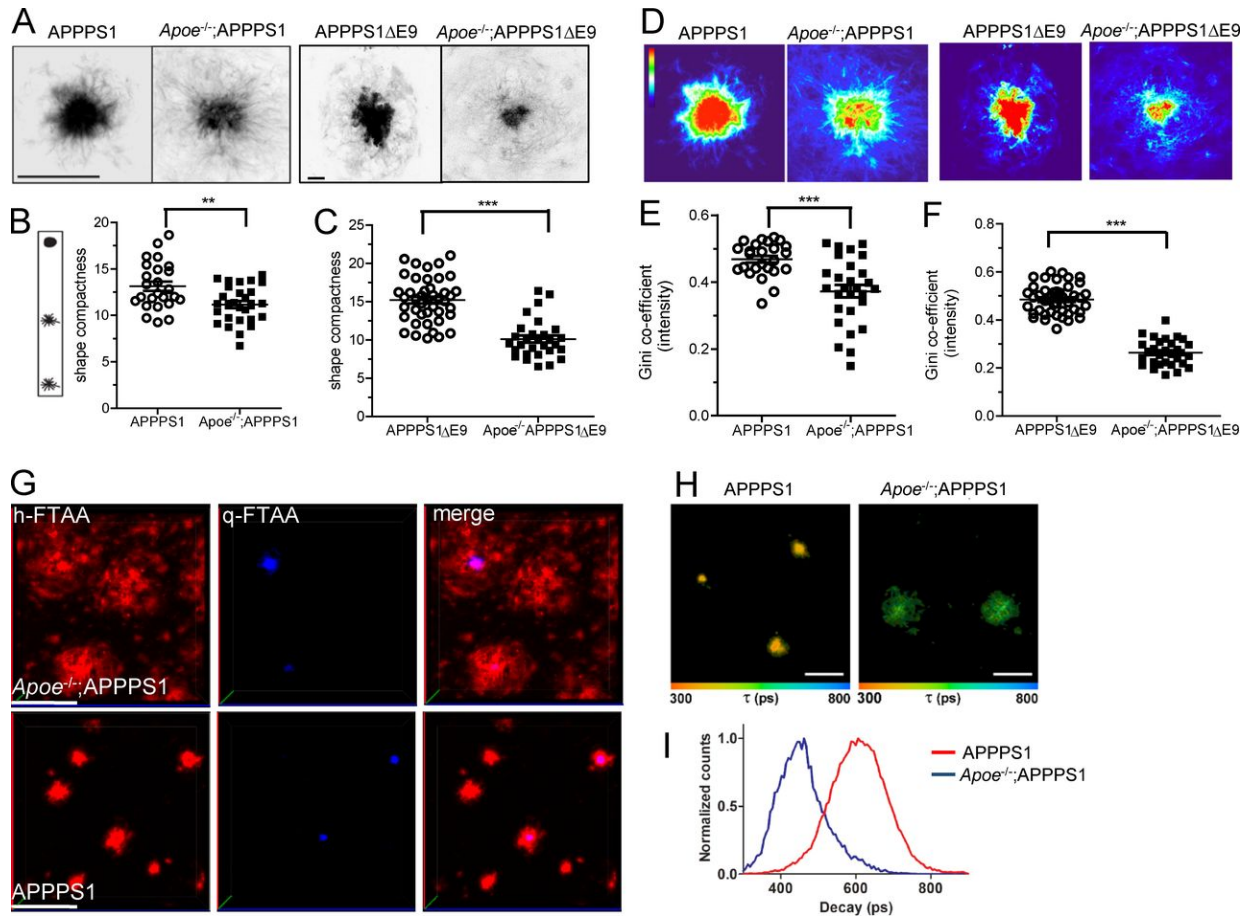
Figure 2.2: *Apoe* deficiency alters amyloid morphology and conformation.

(A) Representative, high-magnification images of X-34[+] plaques from APPPS1 and *Apoe*^{−/−};APPPS1 mice and APPPS1ΔE9 and *Apoe*^{−/−};APPPS1ΔE9 mice. Bars, 10 μm. **(B)** Significant decrease in the shape compactness of *Apoe*^{−/−};APPPS1 mice (11.18 ± 0.38, n = 28 plaques) compared with APPPS1 (13.14 ± 0.50, n = 25 plaques); t(51) = 3.2, P < 0.001, Student's t test. **(C)** Significant decrease in the shape compactness of *Apoe*^{−/−};APPPS1ΔE9 (10.12 ± 0.47, n = 29 plaques) compared with APPPS1ΔE9 (15.19 ± 0.44, n = 43 plaques); t(70) = 7.6, P < 0.001, Student's t test. **(D)** Representative pixel intensity heat maps for APPPS1 and *Apoe*^{−/−};APPPS1. Same scale bars as in A. **(E and F)** The Gini coefficient for pixel intensity was decreased in *Apoe*^{−/−};APPPS1 mice (0.37 ± 0.02, n = 28 plaques) compared with APPPS1 (0.47 ± 0.01, n = 25 plaques); t(51) = 4.3, P < 0.0001, Student's t test (E) and the Gini coeffecient for *Apoe*^{−/−};APPPS1ΔE9 mice (0.26 ± 0.01, n = 29) compared with APPPS1ΔE9 (0.48 ± 0.01, n = 43 plaques); t(70) = 15.53, P < 0.0001, Student's t test (F). Values are given and plotted as mean ± SEM. **(G)** Fluorescence images of Aβ-deposits costained by the tetrameric LCO, q-FTAA (blue), and the heptameric LCO, h-FTAA (red). The images are rendered from z-stacks recorded with the dimensions of x = 250 μm (red line), y = 250 μm (blue line), and z = 90 μm (green line; bar, 75 μm). **(H and I)**

41

Fluorescence lifetime images (H) and lifetime decay curves (I) for h-FTAA stained Aβ-deposits in brain tissue sections. The color bar represents lifetimes from 300 ps (orange) to 800 ps (blue) and the images are color-coded according to the representative lifetime. The fluorescence lifetimes were collected with excitation at 490 nm. Fluorescence decays were collected from 5 to 10 different plaques in tissue sections from five individual APPPS1- or $Apoe^{-/-}$;APPPS1 mice. Bars, 20 μm. **, P < 0.01; ***, P < 0.001.
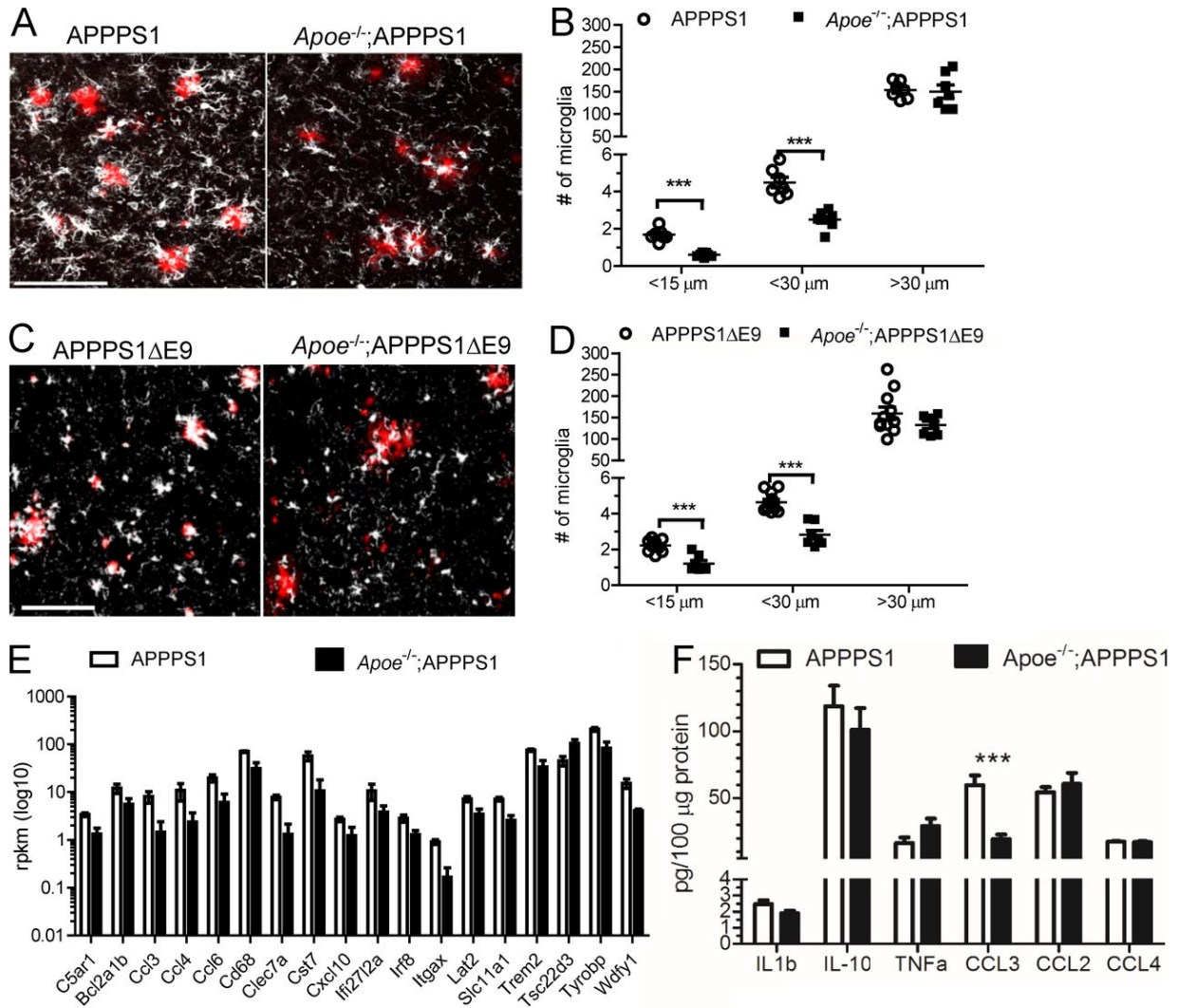
Figure 2.3: Decreased plaque-associated microgliosis in *Apoe*-deficient mice.
(A) Representative images of APPPS1 and $Apoe^{-/-}$;APPPS1 mice stained with Iba1 to label microglia and X-34 to label amyloid plaques. **(B)** Significant reduction in the number of microglia in $Apoe^{-/-}$;APPPS1 (0.60 ± 0.04, n = 7 mice) mice compared with APPPS1 (1.7 ± 0.12, n = 7) within 15 μm (t[12] = 8.3, P < 0.0001) and 30 μm (2.5 ± 0.18, n = 7 mice versus 4.5

42

± 0.28, *n* = 7 mice); t(12) = 5.9, P < 0.0001, Student's *t* test. The number of microglia >30 µm from a plaque in APPPS1 (154.3 ± 7.1, *n* = 7 mice) compared with *Apoe*$^{-/-}$;APPPS1 (150.7 ± 14.9, *n* = 7 mice) was not significantly different; t(12) = 0.22, P = 0.83, Student's *t* test. **(C)** Representative images of APPPS1ΔE9 and *Apoe*$^{-/-}$;APPPS1ΔE9 mice stained with Iba1 and X-34. **(D)** Significant reduction in the number of microglia within 15 µm of *Apoe*$^{-/-}$;APPPS1ΔE9 (1.2 ± 0.17, *n* = 7 mice), compared with APPPS1ΔE9 (2.2 ± 0.1, *n* = 11 mice); t(16) =5.6, P < 0.0001, Student's *t* test, and within 30 µm (2.8 ± 0.24, *n* = 7 mice) compared with (4.6 ± 0.16, *n* = 11 mice); t(16) = 6.5, P < 0.0001, Student's *t* test. The number of microglia >30 µm from a plaque in APPPS1ΔE9 (160.3 ± 14.7, *n* = 11 mice) and *Apoe*$^{-/-}$;APPPS1ΔE9 (133.2 ± 8.5, *n* = 7 mice) were not significantly different; t(16) = 1.4, P = 0.19, Student's *t* test. **(E)** Selected differentially expressed inflammatory gene expression from APPPS1 (*n* = 6 mice) and *Apoe*$^{-/-}$;APPPS1 mice (*n* = 7 mice). See Table S1 for p-values. **(F)** Analysis of cytokine levels in the hippocampus of APPPS1 and *Apoe*$^{-/-}$;APPPS1 mice. *Apoe*$^{-/-}$;APPPS1 mice (*n* = 13 mice) exhibited a significant reduction in CCL3 compared with APPPS1 mice (*n* = 11 mice). P < 0.0001, Student's *t* test. Bars, 100 µm. ***, P < 0.001.
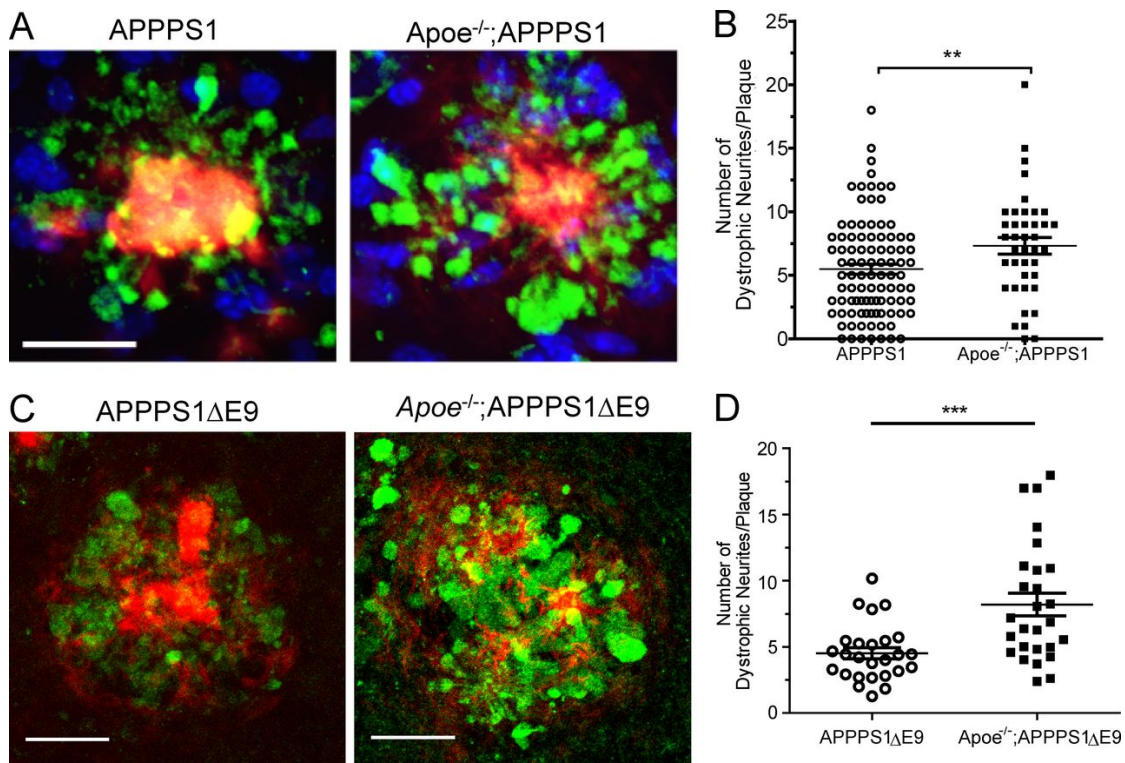
Figure 2.4: Significant increase in plaque-associated neuritic dystrophy in *Apoe*-deficient mice.

(A) Representative image of dystrophic neurites labeled with APP (green) and amyloid labeled with X-34 (red). Nuclei are labeled with Topro-3 (blue). **(B)** Significant increase in the number of dystrophic neurites per plaque in $Apoe^{-/-}$;APPPS1 mice (7.3 ± 0.66, $n = 40$ plaques) compared with APPPS1 (5.5 ± 0.39, $n = 95$ plaques); t(133) = 2.48, P = 0.01, Student's *t* test. **(C)** Representative image of neuritic dystrophy in APPPS1ΔE9 and $Apoe^{-/-}$;APPPS1ΔE9 mice. **(D)** Significant increase in the number of dystrophic neurites per plaque in $Apoe^{-/-}$;APPPS1ΔE9 mice (8.2 ± 0.86, $n = 27$ plaques) compared with APPPS1ΔE9 (4.5 ± 0.42, $n = 26$ plaques); t(51) = 3.8, P = 0.0004, Student's *t* test. All values given and plotted as mean ± SEM. Bars, 20 μm. **, P < 0.01; ***, P < 0.001.

Chapter 3: Differential production of ApoE containing lipoprotein particles by microglia and astrocytes from an apoE knock-in model

This chapter is partially adapted from the following manuscript:

T.E.M. designed the experiment, performed the research, compiled the figure, and wrote the methods and results for the lipoprotein particle analysis (Figure 4 in journal article, Figure 3.4 in this dissertation).

3.1 Introduction

Over the past 20 years, studies on apolipoprotein E (apoE) and its roles in various physiologic processes (atherosclerosis, Alzheimer disease – AD, etc..) have relied heavily on murine models that express the three main human isoforms (ε2, ε3, and ε4) under the control of the endogenous murine *ApoE* regulatory sequences (129,190,191). These *APOE* knock-in mice were generated through targeted replacement strategies (referred to as *APOE*-TR mice from here onward) and have played instrumental roles in elucidating the isoform-specific differences in lipid metabolism and receptor binding affinity. In the context of AD, *APOE* modifies the risk for development of late-onset AD in an isoform-dependent manner (ε2 < ε3 < ε4, where the ε4 allele carries the highest risk) (192). One mechanism through which *APOE* influences AD risk is through its effects on the metabolism of the amyloid-β peptide (Aβ), the main constituent of amyloid plaques found in AD patients. Indeed, crossing of transgenic mice that develop Aβ deposition in the brain (e.g. APP/PS1 or PDAPP mice that develop human-like Aβ plaques) to *APOE*-TR mice led to an isoform-dependent effect on cerebral amyloid plaque accumulation (142,193), which is consistent with observations in humans (194). Intriguingly, the effects of *APOE* on amyloidosis appear to be both isoform- and quantity-dependent, as reduction of apoE3 and apoE4 levels through genetic (143,195) or pharmacologic (144) manipulations results in reduction of cerebral amyloid plaque load. While these studies shed important insights on one aspect of apoE's role in AD pathogenesis, it remains unclear whether the effects resulted from a cell-independent or cell-autonomous mechanism.

Emerging data indicate that *APOE* not only affects AD risk, but also severity of pathology in dementia with Lewy bodies and neurodegeneration in tauopathies (89,196–198). In particular, microglia-derived apoE appears to regulate the inflammatory response (61,62,89,118),

suggesting that the cellular source of apoE in both the brain and periphery has distinct functions in different diseases. In the brain, both astrocytes (199) and microglia (200) contribute to the pool of apoE. ApoE-containing lipoprotein particles produced by astrocytes, including particles containing each of the human apoE isoforms, have been well characterized. However, little work has been done to characterize the apoE-containing lipoprotein particles produced by microglia. Given the recent findings that microglial-derived apoE regulates inflammation in the brain, it is vitally important for microglial apoE particles to be further characterized in order to determine what differences, if any, exist between astrocytic and microglial apoE. Furthermore, a better understanding of how the expression of apoE by microglia and astrocytes is regulated and can be altered will help provide important insight into how each source of apoE is influencing the development of AD-associated pathologies.

ApoE expression in microglia appears to be induced under conditions of injury and insult to the brain (61,62). It is therefore critical to understand how the expression of microglial apoE may be altered in different cellular environments and in the presence of neurodegenerative pathology. Since microglia are the resident macrophages of the brain, some initial classifications for activated microglia were made by applying the M1 and M2 polarization states that are seen in peripheral macrophages (119). Two main factors that help prime and drive the polarization of macrophages into the M1 or M2 state are granulocyte-macrophage colony-stimulating factor (GM-CSF) (M1) and macrophage colony-stimulating factor (M-CSF) (M2) (120,121). In the CNS, astrocytes produce both GM-CSF and M-CSF depending on the types of stimuli they are exposed to (201,202). Studies using both of these factors have shown that they can influence the ability of macrophages to proliferate and impact cell growth and survival (203–206). In addition, culturing macrophages in GM-CSF or M-CSF can also influence the amount of apoE that is

47

secreted by macrophages (207,208). However little is known about how GM-CSF or M-CSF might be influencing the production and secretion of apoE in microglial cells. With more evidence showing that apoE produced by microglia plays a critical role in regulating neuroinflammatory pathways in the brain, it is important to better understand how factors like M-CSF and GM-CSF are influencing the activation state and production of microglial apoE and what effect this might have on impacting overall cellular functions, including neuronal function.

Some early studies in *Apoe*-deficient mice found age-dependent synaptic loss and learning deficits (209). These deficits reflect the potential role of apoE in multiple physiologic processes responsible for maintaining brain homeostasis, including protection from oxidative damage (210,211) , maintenance of the BBB (180,212), and cholesterol transport in the setting of synapse development (213) or neuronal injury (214). These and many other outstanding gaps in knowledge regarding apoE biology necessitate an experimental model where *APOE* expression can be specifically manipulated in different tissues and cell types. Here, we report the generation of an *APOE* knock-in mouse model where the various human *APOE* variants (ε2, ε3, and ε4) replace the endogenous murine *ApoE* locus (termed E2F, E3F, E4F mice individually, and *APOE*-KI mice collectively). Importantly, the human locus (specifically exons 2 to 4) is flanked by loxP sites that allow for the tissue and cell-specific manipulation of *APOE* expression and the potential to better understand how apoE from specific cell sources influences different aspects of pathobiology. We characterized the expression of apoE in the brain and brain cell types and analyzed how apoE lipoprotein particles can differ between microglia and astrocytes. We also show how microglia grown in media containing M-CSF impacts overall microglial apoE production and microglial morphology compared to cells grown in GM-CSF containing media.

3.2 Experimental Methods

Experimental Model

Targeting construct. The targeting strategy allows the generation of a constitutive humanization of the Apoe gene with the various human isoforms (APOE-ε2, APOE-ε3, and APOE-ε4), as well as a conditional knock-out and a constitutive knock-out of the gene. The targeting strategy is based on Ensembl transcripts ENSMUST00000174064 (mouse, corresponding to NCBI transcript NM_009696.3) and ENST00000252486 (human, corresponding to NCBI transcript NM_000041.3). The humanized alleles express the full length human proteins, including its signal peptide. Mouse genomic sequence from the translation initiation codon in exon 2 to the termination codon in exon 4 was replaced with its human counterparts: [Cys130, Cys176] for APOE-ε2, [Cys130, Arg176] for APOE-ε3, and [Arg130, Arg176] for APOE-ε4. Exons 2 to 4 (~ 3.9 kb) have been flanked by LoxP sites. A polyadenylation signal (hGHpA: human Growth Hormone polyadenylation signal) has been inserted to the 3′ of the genes (downstream of the distal loxP sites) in order to prevent transcriptional read-through. Positive selection markers were flanked by FRT (Neomycin resistance – NeoR) and F3 (Puromycin resistance – PuroR) sites and inserted downstream of the proximal loxP site and upstream of the distal loxP site, respectively. The targeting vectors were generated using BAC clones from the mouse C57BL/6 J RPCI-23 and human RPCI-11 BAC libraries.

Generation of knock-in mice homozygous for human APOE isoforms (APOE-KI mice).
Targeting vectors for the various human APOE isoforms were individually transfected into the Taconic Biosciences C57BL/6 N Tac ES cell line. Homologous recombinant clones were isolated using double positive (NeoR and PuroR) and negative (Thymidine kinase – Tk) selections. The constitutive humanized/conditional knockout alleles were obtained after in vivo

49

Flp-mediated removal of the selection markers. The newly introduced human APOE gene is expressed under control of the endogenous Apoe promoter. The resulting strains are referred to by their specific isoform expression (E2F, E3F, and E4F), or collectively as APOE-KI mice. The specific DNA sequence corresponding to each isoform were verified through sequencing of exon 4 by GENEWIZ. DNA was isolated from fresh-frozen brain tissues, and exon 4 was amplified using specific primers (Forward: AACAACTGACCCCG GTGG; and reverse: GCTCGAACCAGCTCTTGAGG).

Methods

Brain extraction and histology. Mice were anesthetized with an intraperitoneal injection of pentobarbital (200 mg kg − 1), and subsequently perfused with 3 U / ml heparin in cold Dulbecco's PBS for 3 min. The brains were then extracted from the skull and fixed in 4% paraformaldehyde for at least 48 h before being transferred to 30% sucrose and stored at 4 °C. Following immersion in sucrose for at least 24 h, serial coronal sections (50 μm thickness) were collected from frontal cortex to caudal hippocampus (right hemisphere) using a freezing sliding microtome (ThermoFisher). Three hippocampal-containing sections (separated by 300 μm) from the right hemisphere of each brain were stained with biotinylated HJ3.4 (anti-Aβ1–13, mouse monoclonal antibody generated in-house, 1:500 dilution) (215), as described previously. Microglia were immunostained using goat anti- IBA1 antibody (Abcam ab5076, 1:500 dilution). Astrocytes were immunostained using mouse anti-GFAP antibody (MAB3402, 1:1000 dilution). ApoE was immunostained with rabbit anti-apoE antibody (Cell signaling D719N, 1:500 dilution. All secondary antibodies were used in appropriate combinations depending on the primary antibody host, including: donkey anti-goat AF-488 (Invitrogen catalog # A-32814), donkey anti-rabbit AF-647 (Invitrogen catalog # A-31573), donkey anti-mouse AF-488 (Invitrogen catalog #

A-21202), donkey anti-rabbit AF-568 (Invitrogen catalog # A-10042). All secondary antibodies were incubated at 1:500 dilution. Quantitative analysis of immunopositive staining was performed as described previously (216). Briefly, images of immunostained sections were exported with NDP viewer (Hamamatsu Photonics). Using ImageJ software, images were converted to 8-bit grayscale, thresholded to highlight Aβ-specific staining and the percent area of a given brain region covered by thresholded staining calculated. For analyses of immunofluorescent staining (including GFAP, IBA1, apoE, X-34, and Aβ), 20X – 40X images were acquired on Nikon A1Rsi confocal microscope. Random z-stacks containing clusters of plaques were imaged, spanning approximately 30 μm of tissue in the z-plane with steps of 1.5 μm. Representative images are generated by projecting maximal intensity of each voxel on the same z-plane (using ImageJ software). All analyses were done blinded to treatment and genotype.

Primary astrocyte and microglia cultures. Mixed glial cultures were prepared from the cortex of E2F, E3F, and E4F neonatal mice (1–3 days old), similar to as previously described (60,71). Cortices were dissected in calcium- and magnesium-free Hanks' Balanced Salt solution (HBSS) with careful removal of meninges. Tissue was digested in HBSS containing 0.25% trypsin and 0.2 mg/ml DNase at 37 °C for 10 min, and was dissociated by trituration in HBSS containing 0.4 mg/ml DNase. Material was filtered through a 70-μm nylon mesh, pelleted at 1000 g for 5 min, and re-suspended in glial media (DMEM + 10% FBS+ 1X Glutamax +1X Penicillin/Streptomyicin). Cells were then plated on a poly-L-lysine (PLL)-coated 10 cm dishes and then switched to glial media containing 10% L929-conditioned media (10% L929 glial media) the next day. 10% L929 glial media changes were performed every 3–4 days until cells were grown to confluence (14–16 days). The top layer of loosely attached microglia were then

harvested by pipetting media over the dish ~ 10–15 times to flush off the microglia. The media

containing the suspended microglia was then collected and spun down at 1000x G for 5 min at

4 °C. Microglia were then re-suspended in 10% L929 glial media and re-plated onto a 12-well

plates coated with PLL. Astrocytes remaining in the 10 cm dish were detached by treating with

3 ml of 0.25% Trypsin-EDTA for 10 min at 37 °C. Seven milliliter of glial media was added to

suspend the astrocytes and material was then collected and spun down at 1000 g for 5 min at

4 °C. Cells were re-suspended in glial media and re-plated onto a T75 flask coated with Geltrex.

Microglia were allowed to grow for 3 days in 10% L929 glial media before being washed 2-

times with sterile PBS and then switched to serum-free glial media (DMEM +1X Glutamax +1X

Penicillin/Streptomyicin) containing 25 ng/ml M-CSF. Astrocytes were allowed to grow for

4 days in glial media before being shaken overnight at 250 RPM at 37 °C to remove loosely

attached cells from the astrocyte layer. The glial media was removed and astrocytes were then

washed 2-times with sterile PBS and switched to serum-free glia media. Serum-free glial media

from microglial and astrocyte cultures was collected after 48 h and stored at 4 °C for non-

denaturing gel electrophoresis.

Primary microglia cultures using 10% L929 and GM-CSF. Primary microglia cultures were

obtained as described above. Mixed glial cultures for each apoE isoform started from the same

pool of dissociated cortical cells that was equally distributed into each starting dish for each of

the culture conditions. For example, the pool of E2F dissociated cortical cells was equally

distributed into one 10cm dish for 5.0 ng/ml GM-CSF, one 10cm dish for 0.05ng/ml GM-CSF,

and one 10cm dish for 10% L929 and this was also done for E3F. However for the dissociated

E4F cells, the starting number of total cortices and, therefore total cortical cells, was lower and

these were distributed into one 6cm dish for 5.0ng/ml GM-CSF, one 10cm dish for 0.05ng/ml

GM-CSF, and one 10cm dish for the 0.05ng/ml GM-CSF. (With the 10cm dish having 2.78-times more surface area than the 6cm dish, the total yield of microglia cells from the 5.0ng/ml GM-CSF was multiplied by 2.78). L929 media obtained from a cultured L929 cell line was aliquoted and stored at -80C and thawed as needed. The day after the mixed glial cells were initially plated on PLL-coated 10cm dishes, the media was switched to just glial media (as a control), glia media containing either 10% L929, 5.0ng/ml GM-CSF or 0.05ng/ml GM-CSF. The cultures were maintained in glia media containing either 10% L929, 5.0ng/ml GM-CSF or 0.05ng/ml GM-CSF until cells were grown to confluence (14–16 days) with media changes performed every 3–4 days. Microglia were then collected from the top layer of the mixed glial cultures as described above. Cell counts were then taken using the Invitrogen Countess II and cells were re-plated with roughly 200,000 cells per well of a 12-well plate. Microglia that started in 10% L929 glial media were re-plated and kept in 10% L929. Microglia that started in 5ng/ml GM-CSF glial media were re-plated and kept in 5ng/ml GM-CSF, re-plated in 5ng/ml GM-CSF with 10% L929 media added, or re-plated and switched to only 10% L929 glial media. Microglia that started in 0.05ng/ml GM-CSF glial media were re-plated and kept in 0.05ng/ml GM-CSF, re-plated in 0.05ng/ml GM-CSF with 10% L929 media added, or re-plated and switched to only 10% L929 glial media. Microglia were allowed to grow for 3 days before being washed 2-times with sterile PBS and then switched to serum-free glial media. Serum-free glial media from the microglia cultures was collected after 48 h and stored at 4 °C for non-denaturing gel electrophoresis. The cells were then washed 1X with sterile DPBS, fixed in 4%PFA for 10 minutes, and then washed 2X and stored in sterile DPBS. The fixed cells were then stored at 4 °C until images of the cells were acquired.

Imaging of microglia cultures. Brightfield images of fixed microglia cultures grown in 10% L929, 5ng/ml GM-CSF, or 0.05ng/ml GM-CSF media were taken using an inverted Nikon Eclipse Ti microscope.

Non-denaturing gradient gel electrophoresis. Microglia-conditioned serum-free media and astrocyte conditioned serum-free media samples were run on a 4– 20% Tris-Glycine native non-denaturing gel at 100 V for 18 h at 4 °C. Gels were transferred to PVDF membrane at 25 V for 90 min at 4 °C and probed with an anti-ApoE antibody (HJ15.7, 1:1000; in house). ApoE immunoreactivity was detected by chemiluminescent development with ECL ultra reagents.

Western blot analysis. PBS-soluble brain lysates from the sequential homogenization step were analyzed for total protein concentration with a micro BCA kit (Thermo Scientific). Thirty microgram of proteins from each sample were loaded onto a NU-PAGE 4–12% Bis-Tris 15 well gel (Thermo Fisher Scientific # NP0336BOX) and the gel was run at 150 V for 1.5 h. The proteins were subsequently dry-transferred onto a PVDF membrane using the iblot2 system (Life Technologies) and blocked with 5% milk in TBS-Tween (0.05%). The membrane was incubated with anti-apoE antibody HJ15.7 (141) (or HJ15.3) and anti-βtubulin antibodies to probe for apoE and a loading control, respectively. Donkey-anti-mouse IgG-HRP was used as secondary antibody (Santa Cruz Biotechnology # sc2096). All blots were developed for ~ 10 s using an enhanced chemiluminescence (ECL) Ultra kit (Lumigen TMA-6) and imaged on the SynGene Imager (BioRad) at the appropriate exposure.

ApoE Sandwich ELISA. The levels of apoE in serum-free cell media samples were measured by sandwich ELISA. For apoE ELISA, HJ6.2 and biotinylated HJ6.1 were used as capture and detection antibodies, respectively, as previously reported (94,98,142,217).

3.3 Results

3.3.1 Design and generation of APOE-KI mice.

In order to investigate the effects of tissue-specific APOE deletion, we set out to create a knock-in model that can allow for promoter-specific deletion of the APOE coding region under the Cre-loxP system. Three separate vector constructs with human sequences corresponding to the ε2, ε3, and ε4 alleles of APOE were generated with loxP sites flanking exons 2 through 4 (Fig. 3.1a – e). The targeting strategy allows for the humanization of the coding region within the murine Apoe gene (Fig. 3.1a) with the various human isoforms (APOE-ε2, APOE-ε3, and APOE-ε4), as well as the opportunity to conditionally knock-out the coding region of the gene. Mouse genomic sequence from the translation initiation codon in exon 2 to the termination codon in exon 4 was replaced with its human counterparts: [Cys130, Cys176] for APOE-ε2, [Cys130, Arg176] for APOE-ε3, and [Arg130, Arg176] for APOE-ε4. Exons 2 to 4 (~3.9 kb) are flanked by LoxP sites to allow for conditional deletion by Cre-recombinase. Homologous recombinant clones were isolated using double positive (NeoR and PuroR) and negative (Thymidine kinase - TK) selections, and the respective resistance genes were included in the targeting vector (Fig. 3.1b, c). The constitutive humanized/conditional knock-out alleles were achieved after in vivo Flp-mediated removal of the selection markers (Fig. 3.1d). In the presence of Cre-recombinase (either through directed genetic crossing with a Cre line or viral vector), constitutive knock-out of the APOE gene is achieved when the loxP-flanked region is removed (Fig. 3.1e). Of note, the chimeric locus retains all normal mouse regulatory sequences in addition to the non-coding exon 1. Exon 2 contains the translation initiation codon. The cleavable signal peptide is encoded within exons 2 and 3 (amino acids 1–18). Due to the non-conserved cleavage

sites of mouse and human signal peptides, the humanized allele expresses the full-length human

APOE protein, including its signal peptide, rather than a fusion protein between the mouse signal

peptide and the human mature protein. To verify accuracy and successful creation of the model,

brain samples from all 3 lines were submitted for sequencing of exon 4 of the APOE locus by

GENEWIZ, which confirmed the presence of human sequence and appropriate single nucleotide

polymorphisms (SNPs) specific for each isoform. Further details on the specific design of the

vector can be found in the methods section.

3.3.2 Human APOE is expressed in astrocytes and microglia in APOE-KI mice

The majority of apoE molecules in the CNS are synthesized by astrocytes (199), with a

small portion coming from microglia (200). We further characterized the expression pattern of

apoE in the brain of APOE-KI mice by co-staining for apoE and traditional markers for

astrocytes as well as microglia. We confirmed the presence of apoE protein in astrocytes by co-

staining for apoE and the astrocytic marker GFAP (Fig. 3.2a). There was some apoE staining in

cells with the morphology of astrocytes that were GFAP-negative. We also assessed microglia

for the presence of apoE protein by co-staining for the microglial marker IBA1, however, we did

not observe significant overlap of apoE and IBA1 signal (Fig. 3.2b). For simplicity, only

representative images from E4F mice are shown, as similar findings were found in E2F and E3F

mice.

ApoE's role in AD pathogenesis was first recognized when apoE was found to co-

localize with amyloid plaques, specifically at the center (i.e. the "core") of mature, fibrillar

amyloid plaques (75,218). ApoE expression is low in microglia under basal, homeostatic

conditions, but is strongly up-regulated in the setting of various neurodegenerative insults

(100,118,150,188). Thus, we investigated whether apoE can be found in microglia in the setting

of amyloidosis, specifically in the APP/PS1–21 model which develops Aβ deposition in amyloid plaques beginning at 6–8 weeks of age (133). APP/PS1–21 mice were crossed with APOE-KI mice for two successive generations and the brain sections from 4-month-old APP/PS1–21 mice homozygous for human APOE alleles (ε2/ε2, ε3/ε3, or ε4/ε4) were subjected to immunohistochemical analysis. Qualitative assessment of the staining pattern showed localization of apoE in the center of plaques, and significant co-localization with IBA1 in surrounding microglia, suggesting microglial expression of apoE (Fig. 3.3a, b). We made similar observations in APP/PS1–21 mice expressing APOE-ε2 and APOE-ε3 (data not shown). These histological observations confirm the presence of apoE in astrocytes and microglia, which is consistent with previous studies, and highlight the validity of our model system.

3.3.3 Qualitative assessment of microglia and astrocyte-derived apoE particles

Most of the biologically active apoE exists in the brain in lipidated HDL-like particles and alterations in the lipidation state of apoE have been shown to drastically affect Aβ accumulation in models of Aβ amyloidosis (111–113,115,219). Thus, we investigated whether apoE particles from astrocytes and microglia are comparable in size, which is associated with the amount of lipidation. Additionally, we examined microglial apoE particles produced from E2F, E3F, and E4F mice in order to understand if isoform dependent differences exist between lipoprotein particles that contain human APOE.

The majority of ApoE-containing lipoprotein particles from astrocyte-conditioned media for all three APOE isoforms were > 12 nm in diameter, consistent with what has been reported previously (Fig. 3.4) (60,71). While the E2F and E3F astrocyte-derived particles showed little to no particles that were < 12 nm in size, E4F astrocytes did appear to produce a small, but notable,

amount of approximately 8 nm-sized particles (Fig. 3.4). Microglia-conditioned media contained apoE particles that were overall much smaller than the astrocyte-derived particles. For E3F and E4F microglia, the majority of particles produced were about 8 nm in size with a small amount of particles 10–17 nm in size (Fig. 3.4). However, for E2F microglia there did appear to be a shift in the relative amount of 10–15 nm-sized particles versus 8-nm-sized particles. While E2F microglia did produce a considerable amount of ~ 8 nm-sized particles, more 10–15-nm-sized particles were present than what was seen for E3F and E4F microglia. As larger particles contain greater amounts of cholesterol and phospholipid, these findings suggest that microglia secrete poorly lipidated apoE relative to the larger HDL-like lipoproteins secreted by astrocytes. These results highlight the need for future studies to more closely examine the properties of these apoE-containing particles and whether they also differ in their normal function as well as in pathological states.

3.3.4 Microglia proliferation and morphology under varying cell culture conditions

The ability of M-CSF and GM-CSF to aid in macrophage proliferation has been reported, however whether or not primary microglia cells expressing human apoE react in a similar fashion is unknown. Therefore, we used primary microglial cells from E2F, E3F, and E4F mice cultured in glia media containing 5.0ng/ml GM-CSF, 0.05ng/ml GM-CSF, or 10% L929 media to assess the effect on microglia proliferation and cellular morphology. For a source of M-CSF, we used media collected from an L929 cell line which secretes M-CSF.

The microglia cells showed a dose-dependent effect of GM-CSF on overall cell proliferation with cells grown in 5.0ng/ml GM-CSF showing a high level of cellular proliferation compared to the cells grown in 0.05ng/ml GM-CSF and 10% L929. A full layer of microglia

cells completely coated the underlying layer of astrocytes at around day 9-10 of the 5.0ng/ml

GM-CSF cultures, a full 3-4 days before the 0.05ng/ml GM-CSF and 10% L929 media had a

well-established layer of microglia. Cell counts performed on the pooled microglia prior to re-

plating in a 12-well plate showed dramatically increased cell numbers for the 5.0ng/ml GM-CSF

condition (Table 3.1). The E2F microglia had 1.98 million cells in 5.0ng/ml GM-CSF compared

to just 780,000 and 653,000 cells for 10% L929 and 0.05ng/ml GM-CSF, respectively. The E3F

microglia had 4.81 million cells in 5.0ng/ml GM-CSF compared to just 1.51 million and 1.28

million cells for 10% L929 and 0.05ng/ml GM-CSF, respectively. The E4F microglia had 3.63

million cells in 5.0ng/ml GM-CSF compared to just 780,000 and 940,000 cells for 10% L929

and 0.05ng/ml GM-CSF, respectively. The E3F cultures had a greater number of cortices and

total number of cortical cells that were initially cultured, which may account for why the total

yield for all three conditions was greater than for the E2F and E4F.

     After the microglia cells were collected and re-plated, the microglia in 5.0ng/ml GM-CSF

microglia maintained a more spherical like shape and appeared to continue to proliferate.

However, for the microglia in the 0.05ng/ml GM-CSF and 10% L929, upon re-plating the cells

appeared to adhere to the plate and send out cellular processes. After the switch to, and collection

of, serum-free media, imaging of the final fixed microglia showed that the vast majority of cells

in 5.0ng/ml GM-CSF continued to have a more rounded spherical-like shape with little to no

cellular processes coming from the cells (Fig. 3.5). In contrast, the microglia in 0.05ng/ml GM-

CSF or 10% L929 had mostly laid flat on the plate and had sent out projections into the cellular

environment (Fig. 3.5). While images for E2F and E3F were obtained, images for E4F were

unfortunately not acquired, however visual inspection of the cells did show similar results as

were seen in the E2F and E3F cultures.

3.3.5 Microglial apoE secretion and apoE particle analysis from varying cell culture conditions

In addition to the ability of M-CSF and GM-CSF to aid in macrophage proliferation, it has also been reported that these same factors alter apoE secretion in macrophages. However, whether or not primary microglia cells expressing human apoE have altered apoE secretion when exposed to these factors is unknown. Therefore, we collected and analyzed serum-free media from primary microglial cells expressing E2F, E3F, or E4F cultured in glia media containing 5.0ng/ml GM-CSF, 0.05ng/ml GM-CSF, or 10% L929 media. Additionally, to analyze whether microglia initially cultured in GM-CSF could alter their secretion of apoE upon being exposed to 10% L929 media, we switched some microglia that started in media containing GM-CSF to media that had 10% L929 combined with the GM-CSF, or to glia media that only had 10% L929 added. We collected serum-free media samples from these microglia for analysis as well. Next, we then analyzed the impact of the varying culture conditions on the level of secretion of apoE-containing lipoprotein particles and assessed whether there were any differences in the size of the particles.

The serum-free media samples that were analyzed for apoE levels by ELISA showed that overall 10% L929 resulted in the highest levels of apoE secretion, while 0.05ng/ml GM-CSF secreted only slightly lower levels of apoE. 5.0ng/ml GM-CSF, however, showed a dramatic reduction in apoE levels compared to the cells grown in 10% L929 media and 0.05ng/ml GM-CSF (Table 3.1). For E2F microglia, the percentage of the amount of apoE secreted for 5.0ng/ml GM-CSF compared to 10% L929 and 0.05ng/ml GM-CSF was 12.0% and 17.0%, respectively. For E3F microglia, the percentage of the amount of apoE secreted for 5.0ng/ml GM-CSF compared to 10% L929 and 0.05ng/ml GM-CSF was 5.3% and 9.9%, respectively. For E4F

microglia, the percentage of the amount of apoE secreted for 5.0ng/ml GM-CSF compared to 10% L929 and 0.05ng/ml GM-CSF was 11.2% and 28.1%, respectively.

For microglia cells that started in media containing GM-CSF, when switched to glia media that had 10% L929 combined with the GM-CSF, or to glia media that only had 10% L929 added, the amount of secreted apoE went up for all apoE isoforms compared to cells that stayed in media that only had GM-CSF (Table 3.1). In particular, the 5.0ng/ml GM-CSF cells switched to 10% L929 media showed increases in apoE levels of 637% for E2F, 353% for E3F, and 1783% for E4F when compared to cells that remained in just 5.0ng/ml GM-CSF (Table 3.1). The 0.05ng/ml GM-CSF cells switched to media containing both 0.05ng/ml GM-CSF and 10% L929 had the greatest amount of apoE secreted of all cell conditions and showed an increase of 196% for E2F, 504% for E3F, and 573% for E4F compared to cells that remained in just 0.05ng/ml GM-CSF (Table 3.1). Overall, these findings showed that culturing in 10% L929 glial media, or switching cultures that started in media with GM-CSF to media that contained 10% L929, results in greater amounts of apoE being secreted.

To assess how GM-CSF and 10%L929 containing media were impacting both the level and the type of apoE-containing lipoprotein particles secreted by microglia, non-denaturing gel electrophoresis followed by Western blotting (WB) for apoE was performed. The lower amount of apoE secreted by microglia grown in 5.0ng/ml GM-CSF that was detected by apoE ELISA was also seen by WB for all three apoE isoforms, as evidenced by the very faint bands that were barely detectable (Fig.3.6A). The microglia in 10%L929 and 0.05ng/ml GM-CSF on the other hand produced bands that were easily detectable from 8nm-17nm, even with some samples being diluted 2-fold. Interestingly, there appeared to be less of the particles around 8nm in size than the particles around 10-17nm, especially around ~14nm, in the E2F and E3F samples. However, the

E4F samples had the greatest amount of particles around 8nm in size for the microglia in 10% L929. Additionally, for the E4F in 0.05ng/ml GM-CSF, the amount of 8nm sized particles was about the same level as particles around 10-17nm (Fig. 3.6A), indicating an apparent shift away from the smaller 8nm size compared to the 10% L929. The effect of GM-CSF and APOE4 on the size of apoE particles was also evident looking at the samples initially in 5.0ng/ml GM-CSF that were switched to media with both 5.0ng/ml GM-CSF and 10% L929 (Fig. 3.6B). These E4F samples had an appreciable amount of particles at 8nm, but far more particles were ~14nm in size (Fig 3.6B), in contrast to E4F cells that continually had 10% L929 which had predominantly 8nm sized particles (Fig 3.6A). However, for the 5.0ng/ml GM-CSF + 10% L929 samples, the proportion of particles 8nm in size compared to particles 10-17nm for the E4F was greater than the proportion of 8nm to 10-17nm sized particles in the E2F mice (Fig 3.6B). These results further support an isoform-dependent effect on the size of apoE-containing lipoprotein particles with E4F mice having a greater amount of the particles they secrete around 8nm in size than the E2F and E3F mice. Additionally, it was intriguing to find that not only can GM-CSF impact the amount of apoE being secreted, but that in E4F mice there are relatively fewer 8nm sized particles secreted in the presence of GM-CSF.

3.4 Discussion

APOE is the strongest genetic risk factor for late-onset AD and intensive research efforts have led to several important insights regarding apoE and its role in AD. Nevertheless, cell-type specific roles for *APOE* isoform expression, secretion, and lipidation in neurodegenerative disease remain poorly understood. We generated three separate lines of *APOE*-KI mice, each carrying one of the three most common variants of the human *APOE* gene. The presence of loxP

site on either side of the human gene sequence allow for cell-type-specific manipulation of *APOE* expression through the Cre-loxP system. Our targeting construct retained the natural genetic context surrounding the human exon sequence, including endogenous regulatory elements such as enhancers. Thus, we expected the tissue-specific expression of the human *APOE* gene to closely parallel that of the endogenous mouse *Apoe* gene. Future studies using floxed allele APOE KI mice can test the temporal and cell-type specific effects of disrupting *APOE* expression on Aβ and tau pathology using a variety of inducible *Cre* mouse strains. We also qualitatively compared apoE particles isolated from astrocytes and microglia, and found the latter to produce significantly smaller lipid-containing particles.

Astrocytic apoE particles had previously been shown to be HDL-like and exist as particles primarily ranging in size from 10-17nm with some particles around 8nm in size (60,71). Initial studies using BV2 cells, a type of immortalized microglia cell line that expresses murine apoE, reported that these cells produce apoE particles that tend to be smaller in size, primarily around 8nm, than those produced by astrocytes (220). However, there had not previously been a characterization of apoE particles produced by primary microglia expressing human apoE isoforms. Our results show that not only do microglia produce more apoE particles that are smaller in size, but that there may also be an apoE isoform dependent influence on the size of apoE particles produced by microglia, with E4F microglia producing the greatest amount of smaller less-lipidated particles. The regulation of apoE secretion by microglia also appears to be dynamic given that microglia upregulate there apoE production when activated.

The characterization of activated microglia has recently become an area of great interest, especially given the role activated microglia play in regulating neuroinflammation and neurodegeneration (221–223). While the polarization of microglia into an M1 (pro-

inflammatory) or M2 (reparative) state is debated and thought to be oversimplified (122,224), it does provide a basis for understanding how microglia can exist in varying states of activation and how these activation states can influence microglial function and inflammatory pathways. The M1 state has been associated with being pro-inflammatory and is thought to be more detrimental and damaging in the context of neurological diseases. On the other hand, microglia activated more toward the M2 state are thought to be pro-phagocytic and more reparative, which allows them to aid in responses to neurological injury. With this in mind, studies have investigated potential ways to target M-CSF signaling pathways in a therapeutic manner to improve disease and CNS injury outcomes (225). One area that has been investigated in regards to the role that GM-CSF may play in neurological disease has been in autoimmune disorders. Astrocytes are the primary producers of GM-CSF in the CNS and it is believed that GM-CSF helps regulate microglial function (226). In particular, EAE mouse models of MS have shown that GM-CSF aids in increasing microglial proliferation and activation, which helps initiate the disease and increase destruction of the myelin sheath (227,228).

In vitro work using M-CSF or L929 cell media, which contains M-CSF, to culture macrophages has been shown to aid in the growth and survival of macrophages (203–205). Furthermore, recent in vitro work looking at how both M-CSF and GM-CSF influence alveolar macrophages showed that GM-CSF induced higher rates of proliferation (206), something that was clearly evident in our primary microglia cultures. Surprisingly, the highly-proliferative microglia in 5.0ng/ml GM-CSF also maintained a rounded shape with a noticeably different morphology where they appeared to not become differentiated and had little to no extending processes. In vivo analysis of microglial activation has shown that microglia morphology can change based upon the activation state of the microglia. Therefore, further work looking into

whether cells exposed to GM-CSF are functionally different than cells in M-CSF (as is found in L929 media) would be warranted.

In addition to the role that GM-CSF may be playing in microglial/macrophage proliferation, GM-CSF has also been shown to influence the secretion of apoE by macrophages. Macrophages cultured in GM-CSF showed a dose dependent reduction in the secretion of apoE over a range of 0.0001ng/ml GM-CSF to 100ng/ml GM-CSF (207). On the other hand, one study has shown that in contrast to GM-CSF, M-CSF is capable of inducing a significant secretion of apoE from macrophages (208). However, up until now, little work has been done investigating how GM-CSF or M-CSF might be influencing the production and secretion of apoE in microglial cells. We show that microglia grown in M-CSF containing L929 media do indeed produce significant amounts of apoE while cells grown in GM-CSF have dramatically reduced amounts of apoE that is secreted. Further understanding of how each of these factors is influencing microglial activation and the production and secretion of apoE particles could prove important for better understanding the role that microglial apoE plays in neurological diseases like AD.

It is our hope that these new APOE-KI mice will facilitate studies into apoE physiology and AD pathogenesis. It is also important, however, to acknowledge their limitations. While the APOE-KI mice harbor the human gene sequence, they retain the regulatory elements found in mice. Considerable species differences between rodents and humans exist and might challenge our ability to generate findings that are all relevant and directly translatable to humans from studies in mice and rats. Apparent differences in physiological function and metabolism, such as lipid metabolism and immune response between humans and rodents might preclude some discoveries that are relevant to disease mechanism. For example, apoB is a ligand for the LDLR along with apoE in humans, albeit with a lower affinity than apoE. Hepatic-derived apoB is

secreted as apoB100 (a full length protein) and contains the LDLR binding domain. However, a large portion of hepatically derived apoB in mice is truncated (apoB48) and does not contain the LDLR domain. Wild-type mouse VLDL and IDL contain roughly equal portions of apoB48 and apoB100, and this leads to a compromised compensatory mechanism in the absence of apoE, leading to severe hypercholesterolemia in ApoE knock-out mice [86, 97]. This latter example highlights the need to address these and other caveats when interpreting rodent studies, especially in those where such physiologic differences might confound some findings.

3.5 Figures and Table
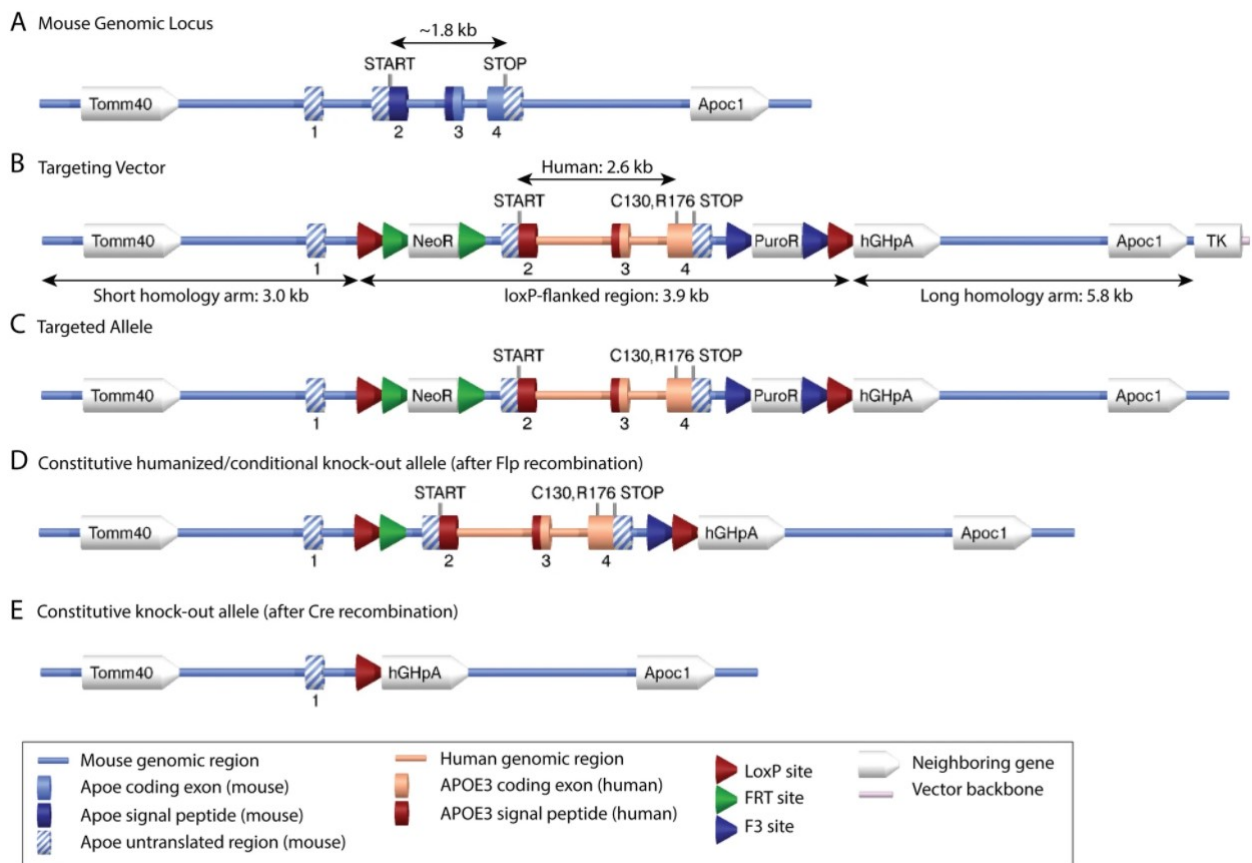
Figure 3.1: Replacement of the mouse Apoe gene with the human APOE gene in APOE-KI mice.

A) Genomic organization of the mouse Apoe gene containing exons 1–4. **B)** The APOE-ε3 targeting construct containing the 5′ and 3′ arms of mouse homology interrupted by the human APOE-ε3 gene sequence. Exons 2 to 4 of the human sequence were flanked with loxP sites. Positive selection markers were flanked by FRT (Neomycin resistance – NeoR) and F3 (Puromycin resistance – PuroR) sites and inserted downstream of the proximal loxP site and upstream of the distal loxP site, respectively. **C)** Homologous recombinant clones were isolated using double positive (NeoR and PuroR) and negative (Thymidine kinase - TK) selections. **D)** The constitutive humanized/conditional knock-out alleles were achieved after in vivo Flp-mediated removal of the selection markers. The newly introduced human APOE gene is expressed under control of the endogenous Apoe promoter. **E)** Constitutive knock-out allele is achieved when the loxP-flanked region is removed by Cre-recombinase. (Figure modified from (229))
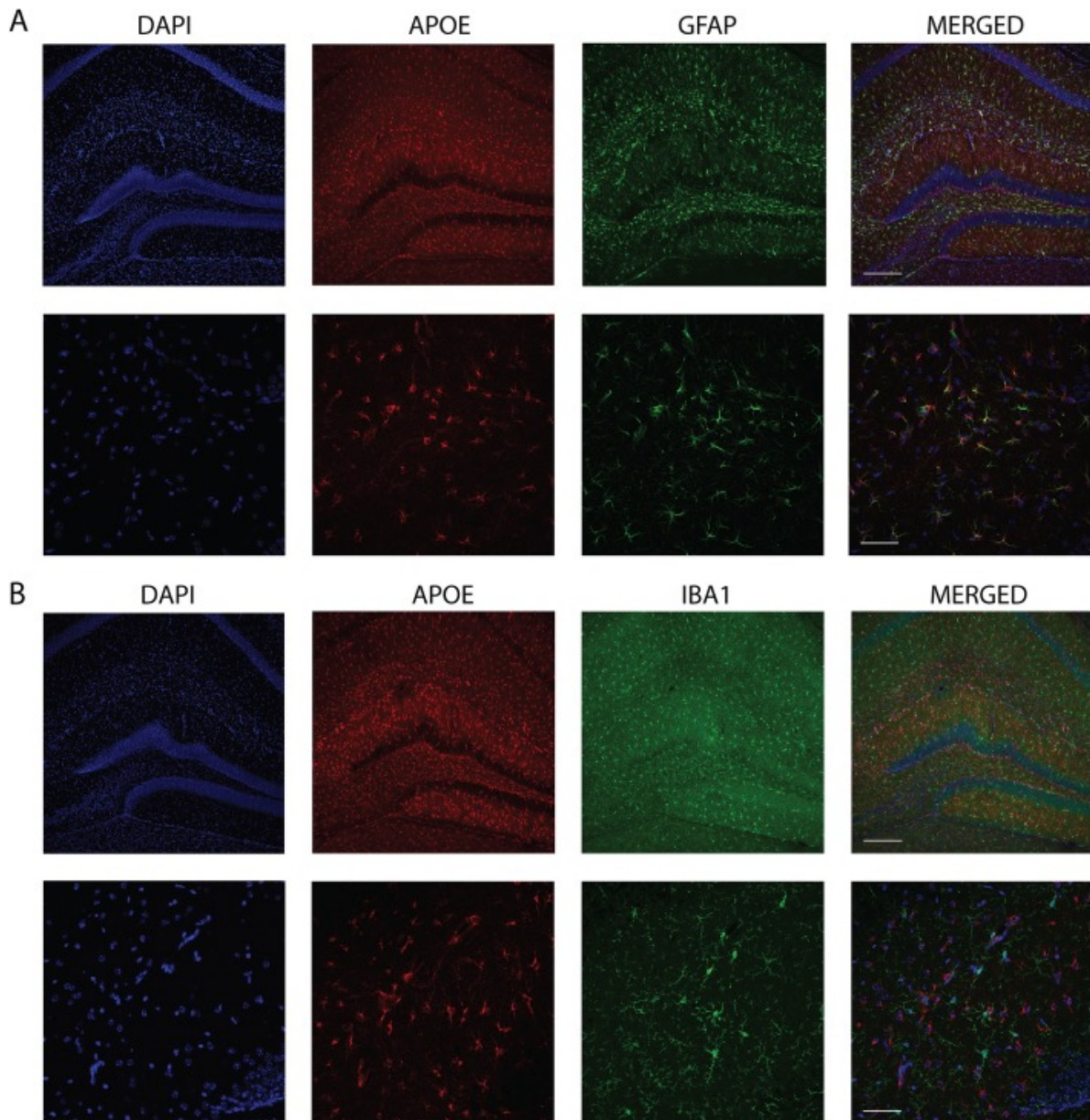
Figure 3.2: Human APOE is expressed in astrocytes in APOE-KI mice.
A) Brain sections from APOE-KI mice were co-stained for nuclei (DAPI), apoE, and GFAP.
Multiple foci of ApoE/GFAP co-localization can be seen at high magnification (bottom panels).
B) Brain sections from APOE-KI mice were co-stained for nuclei (DAPI), apoE, and IBA1. No
overlap of apoE and IBA1 staining was observed. Scale bars = 200 μm (top panels) and 50 μm
(bottom panels). Images are from E4F mice, and are representative of at least 3 random cortical
areas from 3 biological replicates. There were no appreciable qualitative differences between
E2F, E3F, and E4F samples. (Figure from (229))
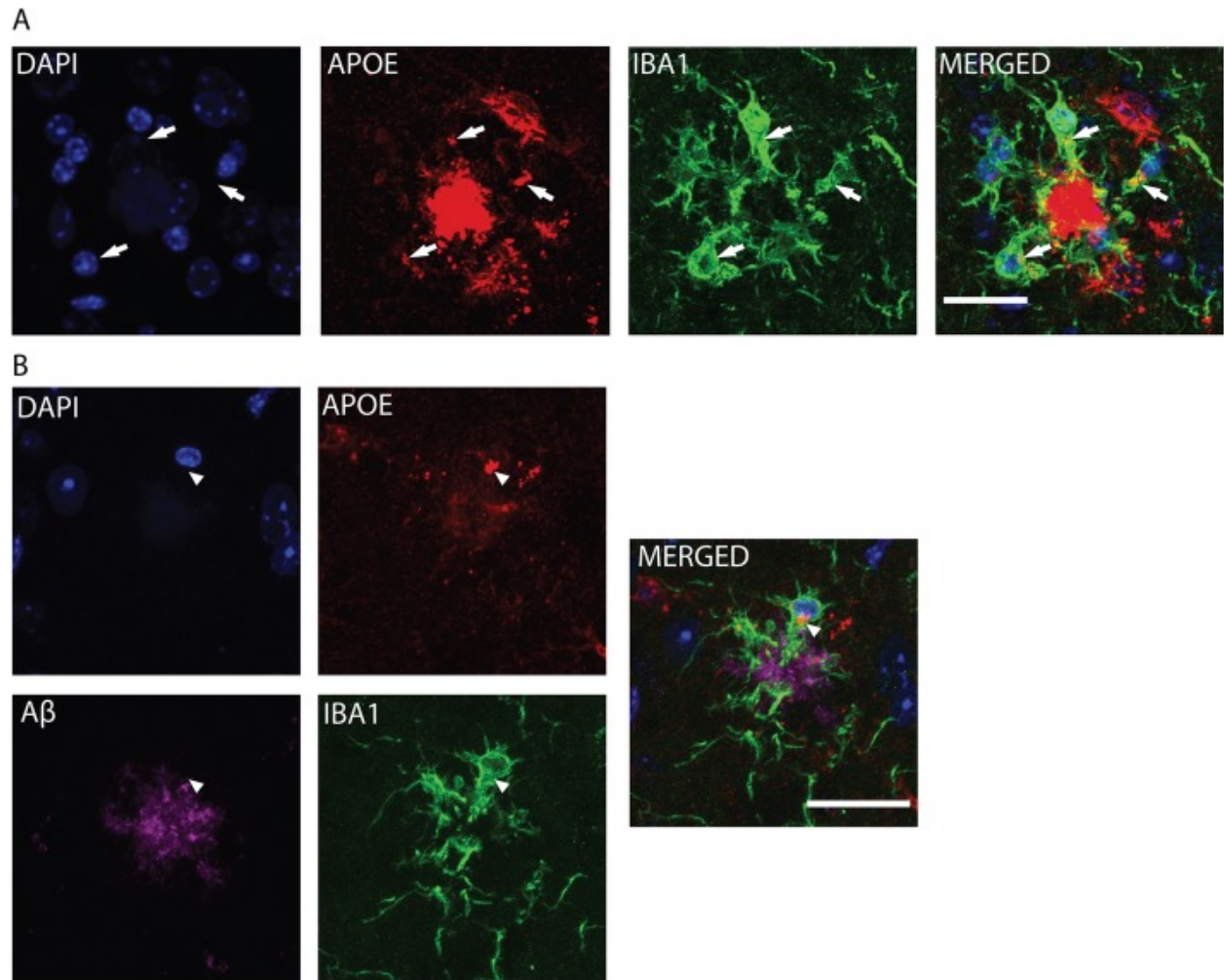
Figure 3.3: Microglial APOE expression in APP/PS1/EKI mice.
A) Brain sections from APPPS1;FE4 mice were co-stained for nuclei (DAPI), apoE, and IBA1.
Multiple foci of apoE/ IBA1 co-localization can be seen (arrows). Scale bar = 20 μm. **B)** Brain
sections from APPPS1;FE4 mice were co-stained with DAPI, apoE, Aβ, and IBA1. ApoE is co-
localized with IBA1 (arrowhead). Scale bar = 25 μm. Images are representative of at least 3
random cortical areas from 3 biological replicates. There were no appreciable qualitative
differences between APPPS1;FE2, APPPS1;FE3, and APPPS1;FE4 samples. (Figure from (229))
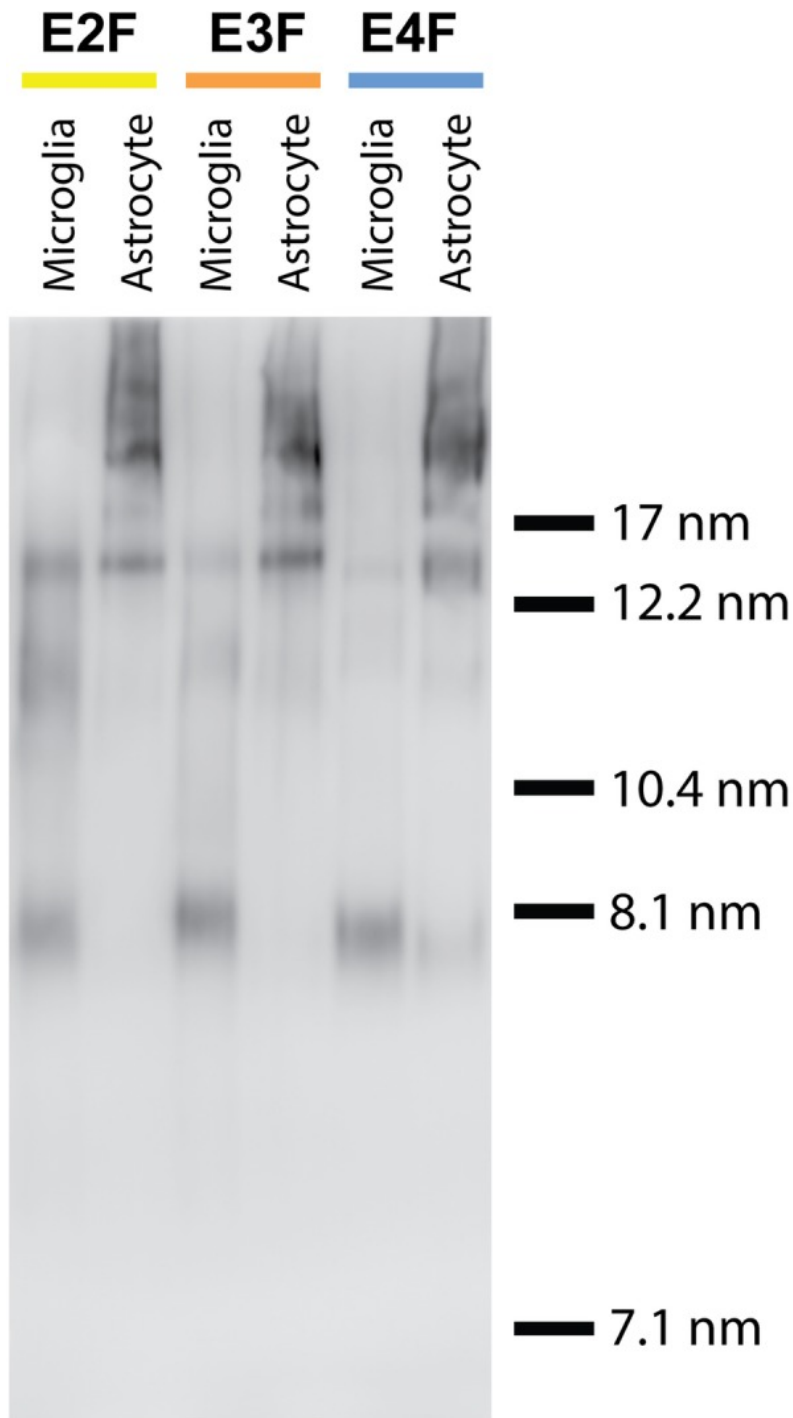
Figure 3.4: Qualitative assessment of microglia and astrocyte-derived apoE particles.
Conditioned media samples from E2F, E3F, and E4F-derived primary cultures enriched for microglia and astrocyte were subjected to non-denaturing 4–20% Tris-glycine gradient gel electrophoresis followed by Western blotting. Approximate hydrated radius of marker proteins, run on the same gel, are shown for comparative purposes. Data shown are representative of 3 independent cultures from different cohorts of mice.
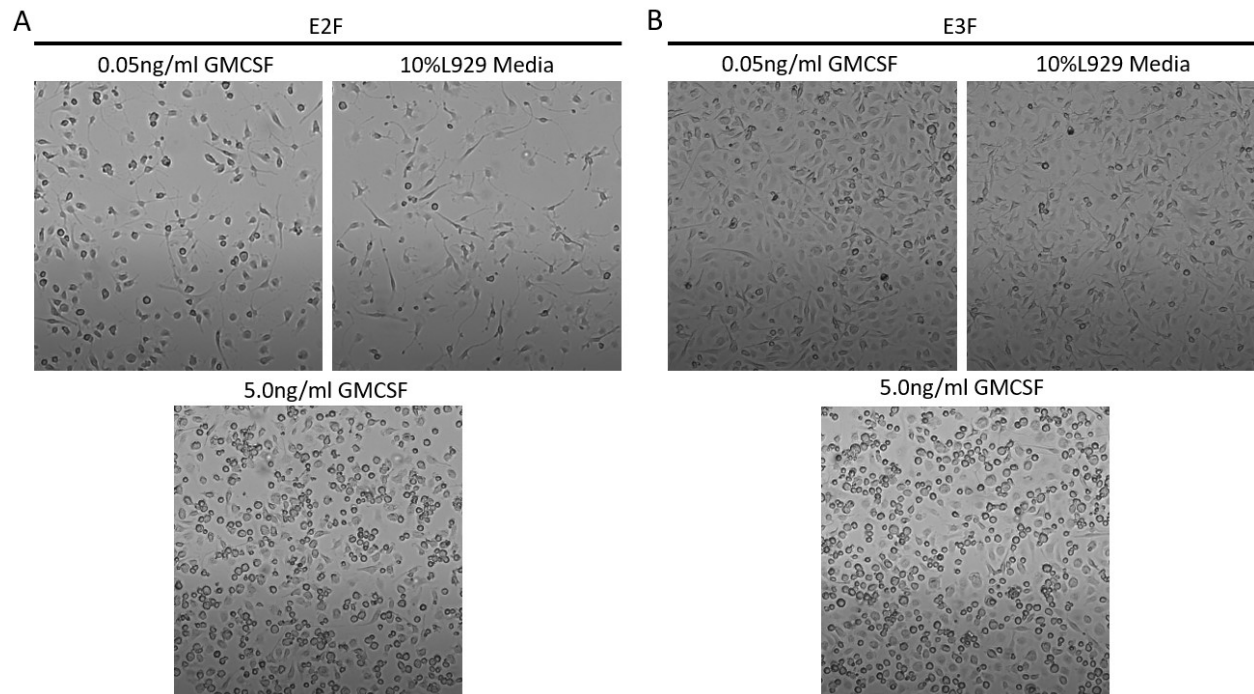
Figure 3.5: Microglial morphology under varying culture conditions.
Images of E2F **(A)** and E3F **(B)** primary microglia cultured in glia media with either 0.05ng/ml GMCSF, 5.0 ng/ml GMCSF, or 10% L929 media. Initial number of cells cultured varied between E2F and E3F.
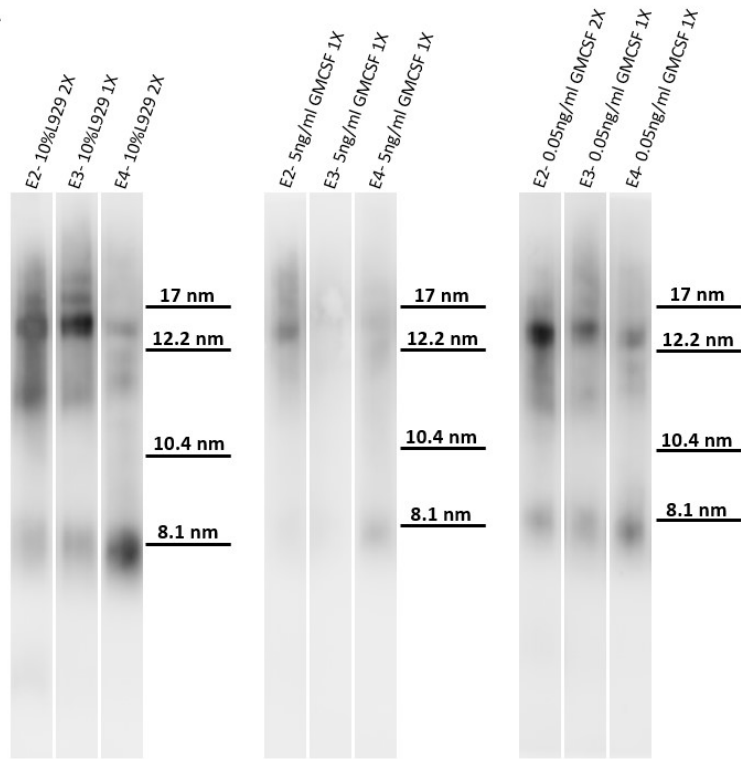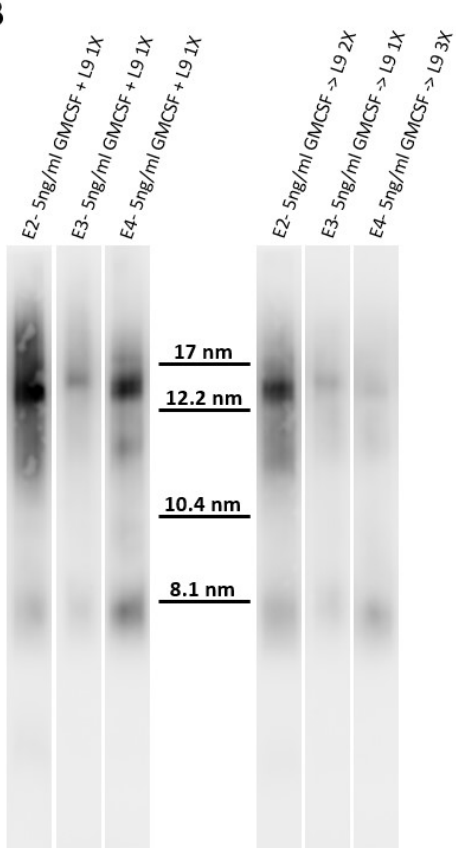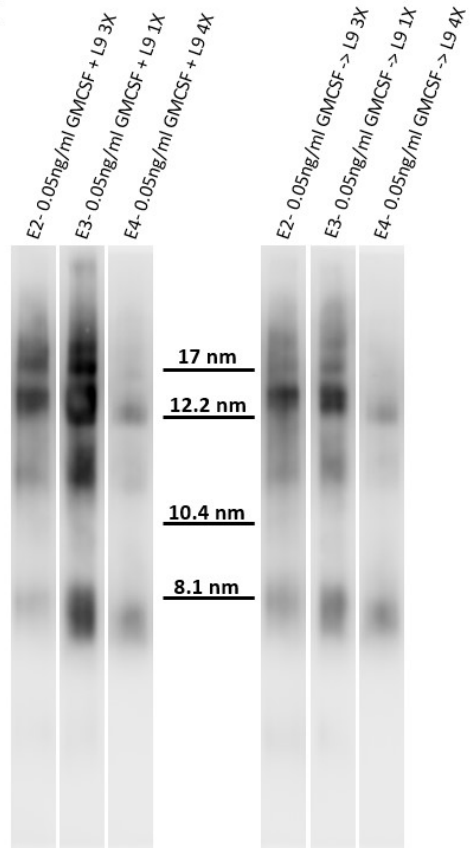
Figure 3.6: Qualitative assessment of microglia-derived apoE particles produced under varying culture conditions.

A) Conditioned media samples from E2F, E3F, and E4F primary microglia cultured in glia media with either 10% L929 media, 5ng/ml GMCSF, or 0.05% GMCSF.

B) Conditioned media samples from E2F, E3F, and E4F primary microglia initially cultured in glia media with 5ng/ml GMCSF and then switched to glia media containing either 5ng/ml GMCSF and 10% L929 media (+L9), or just 10% L929 media (-> L9).

C) Conditioned media samples from E2F, E3F, and E4F primary microglia initially cultured in glia media with 0.05ng/ml GMCSF and then switched to glia media containing either 0.05ng/ml GMCSF and 10% L929 media (+L9), or just 10% L929 media (-> L9).

Samples were loaded with either no dilution (1X), a 2-fold dilution (2X), a 3-fold dilution (3X), or a 4-fold dilution (4X).

Starting Media Condition	APOE Genotype	Final Culture Media Condition	Total Cell Count prior to re-plating	# of cells / well	Final APOE Conc. (ng/ml)	APOE Conc. (ng/ml) per 100K cells
10% L929	APOE2	10% L929	780,000	195000	566.7	290.62
	APOE3	10% L929	1,509,000	252000	387.2	153.64
	APOE4	10% L929	780,000	195000	1049.6	538.26
0.05ng/ml GMCSF	APOE2	0.05ng/ml GMCSF	653,000	218000	444.2	203.76
	APOE3	0.05ng/ml GMCSF	1,283,000	214000	175.4	81.94
	APOE4	0.05ng/ml GMCSF	940,000	188000	403.1	214.41
5ng/ml GMCSF	APOE2	5ng/ml GMCSF	1,981,000	198000	68.8	34.74
	APOE3	5ng/ml GMCSF	4,810,000	200000	16.2	8.09
	APOE4	5ng/ml GMCSF	3,628,000*	186000	111.9	60.16
5ng/ml GMCSF	APOE2	5ng/ml GMCSF + 10% L929	1,981,000	198000	249.3	125.91
	APOE3	5ng/ml GMCSF + 10% L929	4,810,000	200000	111.3	55.66
	APOE4	5ng/ml GMCSF + 10% L929	3,628,000*	186000	736.4	395.91
	APOE2	10% L929	1,981,000	198000	438.0	221.22
	APOE3	10% L929	4,810,000	200000	57.1	28.56
	APOE4	10% L929	3,628,000*	186000	1995.2	1072.69
0.05ng/ml GMCSF	APOE2	0.05ng/ml GMCSF + 10% L929	653,000	218000	872.4	400.18
	APOE3	0.05ng/ml GMCSF + 10% L929	1,283,000	214000	884.4	413.27
	APOE4	0.05ng/ml GMCSF + 10% L929	940,000	188000	2312.1	1229.84
	APOE2	10% L929	653,000	218000	708.7	325.09
	APOE3	10% L929	1,283,000	214000	675.8	315.79
	APOE4	10% L929	940,000	188000	2171.6	1155.11

Table 3.1: APOE levels produced by microglia cultured under varying conditions.
APOE levels were determined using a sandwich ELISA for conditioned media samples from E2F, E3F, and E4F primary microglia cultured in glia media with either 10% L929 media, 5ng/ml GMCSF, or 0.05% GMCSF. A subset of primary microglia were initially cultured in glia media with 5ng/ml GMCSF and then switched to glia media containing either 5ng/ml GMCSF and 10% L929 media (+L9), or just 10% L929 media (-> L9). A subset of primary microglia were initially cultured in glia media with 0.05ng/ml GMCSF and then switched to glia media containing either 0.05ng/ml GMCSF and 10% L929 media (+L9), or just 10% L929 media (-> L9). APOE concentrations were normalized to every 100,000 cells (100K) based upon cell counts that were performed at the time of splitting and re-plating of the microglia. *For E4F 5.0ng/ml GM-CSF the total cell count of 1,305K for the 6cm dish was multiplied by 2.78 to account for the smaller surface area compared to the 10cm dish used for all other conditions.

Chapter 4: Selective reduction of astrocyte apoE3 and apoE4 strongly reduces Aβ accumulation and plaque-related pathology in a mouse model of amyloidosis

This chapter is adapted from a manuscript that has been reviewed. We are in the process of revising it for re-submission:

T.E.M. designed the experiments, performed the research and data analysis, compiled the figures and wrote the manuscript

4.1 Introduction

Alzheimer disease (AD) is the leading cause of dementia, affecting over 6 million Americans and ~50 million people worldwide (7,8). The strongest genetic risk factor for developing late-onset AD is apolipoprotein E (*APOE)* genotype. The influence of *APOE* on AD risk occurs in an isoform-dependent manner (ε2 < ε3 < ε4) (77,78,230,231). One way apoE affects AD risk is through facilitating the formation of amyloid plaques, the earliest detectable pathological hallmark of AD (16,17,232). ApoE is found as a constituent in amyloid plaques, suggesting it can directly facilitate plaque formation, and apoE affects amyloid deposition in an isoform and expression-level dependent manner (138,139,143,146,218,233–235). *APOE4* carriers exhibit more amyloid pathology than non-carriers and mouse models of β-amyloidosis with the human *APOE4* gene knocked in develop more amyloid than those with *APOE3* (142,143,195,236–240). The effect of apoE on Aβ is also dependent on the amount of apoE in the brain. Knockout of *Apoe* strongly reduces amyloid deposition in mouse models of amyloid deposition (138,139,241). Mice that are hemizygous for *APOE* develop less Aβ plaque than mice homozygous for *APOE* (138,143,166,195). Additionally, reduction of apoE levels prior to plaque onset using apoE targeted anti-sense oligonucleotides (ASO's), results in reduced Aβ plaque pathology (171). Conversely, overexpression of ApoE4 during the nascent stages of plaque formation led to an increase in amyloid plaque deposition (172).

Within the brain, *APOE* is predominantly expressed by astrocytes under physiological conditions. However, when damage occurs in the brain, microglia significantly upregulate *APOE* expression (61,62,150). In mouse models of amyloid pathology, plaque-associated microglia exhibit high levels of apoE expression as part of a broader "microglial neurodegenerative

phenotype" (MGnD) or "disease-associated microglia" (DAM) transcriptional profile (61,62,123). Microglial apoE expression may be critical for the microglial responses to injury in the brain since microglial activation is attenuated by germ line *Apoe* KO in mouse models of amyloid or tau pathology (89,241). Previous research from our lab has shown that microglia expressing human *APOE2, APOE3*, or *APOE4* produce apoE-containing lipoprotein particles that are smaller in size than particles produced by astrocytes (229). The difference in apoE particle size in astrocytes and microglia raises the question as to whether or not apoE-containing lipoprotein particles produced by each cell type may have differential effects on the development of Aβ pathology.

Microglia-derived apoE can deposit within amyloid plaques and may contribute to plaque formation and influence morphology (118). Other studies found selective removal of murine apoE from astrocytes in APPPS1ΔE9 mice reduces Aβ plaque burden (242). Conversely, overexpression of *APOE4*, but not *APOE3*, in astrocytes exacerbated Aβ pathology, suggesting that astrocyte-derived human apoE may differentially affect amyloid pathology (172). Whether astrocyte-specific expression of endogenously produced human *APOE* isoforms influences Aβ pathology, glial reactivity to Aβ plaque deposition, or downstream effects of Aβ deposition has not been investigated. To assess how the loss of astrocytic *APOE* impacts Aβ pathology, we used Aldh1l1-Cre/ERT2 BAC transgenic mice, in which the Aldh1l1 promoter drives expression of a tamoxifen-inducible Cre recombinase specifically in astrocytes, crossed with APPPS1-21/APOE3 or APOE4 knock-in mice.

4.2 Methods

Experimental Model and Subject Details. APPPS1-21 mice on a C57BL/6N background (gift from Dr. Mathias Jucker, Department of Cellular Neurology, Hertie Institute for Clinical Brain Research, University of Tübingen, Germany) overexpress human APP bearing both the Swedish mutation and PSEN1 containing an L166P mutation, both driven by the Thy1 promoter (133). ApoE3$^{flox/flox}$ and apoE4$^{flox/flox}$ (FE3 and FE4, respectively), human *APOE* knock-in mice on a C57BL background, were generated by replacing the mouse genomic sequence from the translation initiation codon in exon 2 to the termination codon in exon 4 with its human counterparts flanked by loxP site, driven by the endogenous *APOE* promoter (229). Aldh1l1-Cre/ERT2 mice on a C57BL background were obtained from Jackson Laboratories (Stock No. 031008). To generate APPPS1-21/ apoE3$^{flox/flox}$ or apoE4$^{flox/flox}$ mice (APPPS1;FE3 or APPPS1;FE4, respectively), we crossed APPPS1-21 transgenic mice with FE3 or FE4 for several generations.

To generate Aldh1l1-Cre/ERT2/apoE3$^{flox/flox}$ or apoE4$^{flox/flox}$ mice (AFE3 or AFE4, respectively), we crossed Aldh1l1-Cre/ERT2 mice to FE3 or FE4 for several generations. We then crossed APPPS1;FE3 or APPPS1;FE4 mice to AFE3 or AFE4 mice to produce APPPS1-21/Aldh1l1-Cre/apoE3$^{flox/flox}$ or apoE4$^{flox/flox}$ (APPPS1;AFE3 or APPPS1;AFE4, respectively). Finally, we crossed APPPS1;AFE3 or APPPS1;AFE4 mice to FE3 or FE4 mice to produce experimental mice utilized. All the experimental mice involved in the final analysis were obtained from the same generation. The sex of animals in each specific experiment can be found in the corresponding figure legends. All animal procedures and experiments were performed under guidelines approved by the Institutional Animal Care and Use Committee (IACUC) at

Washington University School of Medicine. All of the phenotyping and data analysis was performed by researchers who were blind to the genotype of the mice.

Tamoxifen administration. Tamoxifen was dissolved in corn oil at a concentration of 20 mg/ml by shaking overnight at 37°C. After preparation, the tamoxifen solution was wrapped by foil, and stored at 4°C for up to a month. Tamoxifen was given at 100 mg tamoxifen/kg body weight and administered via intraperitoneal (IP) injection once every 24 h for 6 consecutive days.

Brain isolation and preparation. Mice were anesthetized with 200 mg/kg pentobarbital and subsequently perfused with cold PBS containing 3 IU/ml heparin. After brain isolation, the left hemisphere was fixed in 4% paraformaldehyde for at least 24 h, and then transferred to 30% sucrose and stored at 4oC until sectioning. The right hemisphere was dissected into various parts (posterior- and anterior-cortex, hippocampus, etc.), all of which were snap-frozen using dry ice and stored at – 80oC until further analysis.

Histology and image acquisition. Hippocampal-containing sections were selected for human apoE (Cell Signaling, 13366, 1:500), GFAP (Abcam, ab53554, 1:500; Millipore, MAB3402B, 1:2000), Iba1 (Abcam, ab5076, 1:500; Wako, 019-19741, 1:5000), Aβ (HJ3.4, in house, mouse monoclonal, 2 μg/ml), Clec7a (InviviGen, mabg-mdect, 1:50), and BACE1 (Abcam, ab108394, 1:100) immunofluorescence staining. Sections were washed in Tris-buffered saline (TBS) buffer for 3 times, 5 min each. After washing, sections were incubated in TBS with 0.25% Triton X-100 (TBSX) for 30 min at room temperature to permeabilize the sections, followed by 1 time TBS washing for 5 min. Then sections were incubated with 2 μM X34 in the X-34 staining buffer (40% ethanol, 60% TBS, 1:500 vol. 10N NaOH) for 20 min. After X-34 staining, sections were washed 3 times for 2 min each in the X-34 washing buffer (40% ethanol and 60% TBS),

followed by 3 times washing in TBS for 5 min each. After washing, sections were blocked by 10% donkey serum in TBSX for 1 h at room temperature to prevent non-specific binding. Then sections were incubated with primary antibodies at 4oC, overnight. After overnight incubation, sections were washed 3 times in TBS for 5 min each. Then sections were incubated with corresponding secondary fluorescence antibodies (Life Technologies) for 2 h at room temperature. After 3 times washing by TBS for 10 min each, sections were mounted to glass slides. Slides were coverslipped by ProLong Glass Antifade Mountant (Invitrogen, P36980) and scanned by Nikon A1Rsi Confocal Microscope, Leica Stellaris 5, or BioTek Cytation5. Representative images in Figure 1E were captured by the BioTek Cytation5 using a 10X objective. Representative images in Figures 2A, 3A, 4B, 5B (top panel), and 6A, were captured by the BioTek Cytation5 using a 4X objective. Representative images in Figure 6C were captured by the BioTek Cytation5 using a 20X objective. Representative images in Figures 1G, 2D, 3F, and 4D were captured by the Leica Stellaris 5 using a 40X objective. Representative images in figure 5B (bottom panel) were captured by the Nikon A1Rsi using a 40X objective.

Image processing and quantification. Acquired images were analyzed by using Image J v1.53c (https://imagej.net/Fiji), Imaris 9 (https://imaris.oxinst.com/), and BioTek Gen5 (https://www.biotek.com/products/software-robotics/) software. ApoE fluorescent staining intensity in Figure 1F was determined using images captured by the BioTek Cytation5. The average pixel intensity for each image was found by setting a minimal threshold to highlight positive staining, running the "Analyze Particle" function to obtain the mean pixel intensity, and then subtracting the average background pixel intensity. The average background pixel intensity was determined by calculating the average pixel intensity of APPPS1EKO images. To determine the percent of hippocampal area or cortical area covered by X-34, HJ3.4, Iba1, GFAP, or BACE1

81

in Figures 2B, 2C, 3B, 3C, 4C, 5C, and 6B, images were analyzed as previously described (216,243). Briefly, Image J software was used to analyze images captured with the BioTek Cytation5. Regions of interest (ROI's) of images were traced, images were thresholded to highlight positive staining, and the "Analyze Particle" function was used to obtain the percent area covered. The average intensity of fibrillar plaques in Figure 2E was also found using ImageJ software to analyze images of X-34 stained sections captured with the BioTek Cytation5 software. The cortex was traced, images were thresholded to highlight positive staining, and the "Analyze Particle" function was used to obtain the average pixel intensity. To determine the percent area of Clec7a staining around X-34 plaques in Figure 4E, ImageJ software was used to analyze images captured with the Leica Stellaris 5 confocal microscope. The images of X-34+ plaques were thresholded to highlight plaques, "Analyze Particles" was run, and the thresholded plaque ROI's were combined and then enlarged by 15µm. The enlarged ROI's were then transferred to the corresponding Clec7a images, images were thresholded, and "Analyze Particles" was run to find the percent area covered. The GFAP volume to X-34 volume in Figure 5D was found using Imaris software to analyze images obtained by the Nikon A1Rsi confocal microscope, as previously described (241). Briefly, Surfaces were created for X-34 and GFAP and the Dilate Xtension was used to dilate the X-34 surfaces by 15 µm. The surface-surface co-localization Xtension was run using the dilated X-34 surfaces and GFAP surfaces and the volume of GFAP within 15 µm of X-34 plaque was determined based on overall X-34 plaque volume. The BACE1 area per X-34 plaque was determined using BioTek Gen5 software to analyze images obtained by the BioTek Cytation5. The Cellular Analysis function was used with the primary mask thresholded and set based on the X-34 staining. The secondary mask was set

82

using a 15 µm expanded distance from the X-34 primary mask, BACE1 staining was thresholded, and the average BACE1 area per X-34 plaque was determined.

Brain tissue sample processing. Mouse posterior cortical tissue samples were sequentially homogenized with cold PBS, and then 5M guanidine buffer in the presence of 1X Complete Protease Inhibitor (Roche, 11697498001) and 1X phosSTOP phosphatase Inhibitor (Roche, 04906845001). First, tissues were weighed, a half spoon of beads (Next Advance, ZrOB05) were added, and samples were homogenized for 45 sec on setting 3, using a bead homogenizer (Next Advance, Bullet Blender Strom 24), in cold PBS buffer at 20 µl buffer/1 mg tissue. Homogenates were centrifuged 30min at 15,000 rpm at 4°C. The supernatant was saved as the PBS soluble fraction. Then the same amount of 5M guanidine buffer was added to the pellet and homogenized on bead homogenizer for 3 min on setting 8, followed by 1h rotation at room temperature. Finally, homogenates were centrifuged for 30 min at 15,000 rpm at 4°C. The supernatant was saved as the 5M guanidine insoluble fraction. All fractions were stored at -80°C until further analyzed.

Sandwich ELISA. The levels of apoE, Aβ40, and Aβ42 in PBS and 5M guanidine fractions were measured by sandwich ELISA and normalized to the tissue weight. The coating antibodies for human apoE, Aβ40, and Aβ42 were HJ15.3 (in house, mouse monoclonal, 5 µg/ml), HJ2 (in house, mouse monoclonal, 20 µg/ml), and HJ7.4 (in house, mouse monoclonal, 10 µg/ml), respectively (229,244). The capture antibodies were HJ15.7-biotinylated (in house, mouse monoclonal, 150 ng/ml) for human apoE and HJ5.1-biotinylated (in house, mouse monoclonal, 90 ng/ml) for both Aβ40 and Aβ42 (229,244).

Fluidigm Biomark HD Real-Time PCR. Female mouse arterial cortex tissues were used for the gene expression analysis. Samples were selected based on the mean values of the X34 plaque load. mRNA was exacted from frozen tissues using RNeasy Micro Kit (Qiagen, 74004) and converted to cDNA using the high-capacity RNA-to-cDNA kit (Applied Biosystems, 4387406), following the manufacturer's instructions. Gene expression was conducted using Fluidigm Biomark HD Real-Time PCR System in collaboration with Genome Technology Access Core at Washington University. Using Taqman primers (Life Technologies). GAPDH mRNA expression level was used as a reference.

 Quantification and Statistical Analysis. All values were reported as mean ± SEM. All statistical analyses were conducted in Prism 8 (GraphPad). Two-way or Three-way ANOVA was used for assessing significance between more than two groups. P values less than 0.05 ($p < 0.05$) were considered significant for all tests. *$p < 0.05$, **$p < 0.01$, ***$p < 0.001$, ****$p < 0.0001$. The significant p values and F values for each experiment can be found in Table 4.1. The value of n per group and what n represents in each specific experiment can be found in the corresponding figure legends and in Table 4.1.

4.3   Results

4.3.1 ApoE levels following tamoxifen administration

In order to assess how the loss of astrocytic apoE impacts Aβ pathology, we used Aldh1l1-Cre/ERT2 BAC transgenic mice to selectively remove *APOE* from astrocytes in a tamoxifen dependent manner. APPPS1;AFE3 and APPPS1;AFE4 mice were created to assess Aβ plaque pathology compared to APPPS1;FE3 and APPPS1;FE4 mice. Once-daily intraperitoneal injections of tamoxifen were administered at 4 weeks of age (2-4 weeks before

the initial formation of Aβ plaques in these mice) for 6 consecutive days (Fig. 1A). A cohort of

APPPS1;AFE3, APPPS1;AFE4, APPPS1;FE3, and APPPS1;FE4 mice were collected at 6 weeks

of age, one week after completing tamoxifen administration, and showed no signs of Aβ

pathology (data not shown). To investigate the efficiency of *APOE* removal from astrocytes after

tamoxifen administration, we first assessed apoE mRNA and protein levels in the brain at 18-

weeks of age (Fig. 1A). ApoE mRNA levels were assessed by qPCR and were significantly

reduced by ~70-90% in both the APPPS1;AFE3 and APPPS1;AFE4 females compared to the

APPPS1;FE3 and APPPS1;FE4 mice (Fig.1B). To assess apoE protein levels, cortex tissue

samples were sequentially extracted in PBS and guanidine buffers to measure soluble and

insoluble apoE, respectively. Soluble apoE levels were also significantly reduced in female

APPPS1;AFE3 and male and female APPPS1;AFE3 and APPPS1;AFE4 mice by ~50-60% with

a trend towards reduction in male APPPS1;AFE3 mice. (Fig.1C). Insoluble apoE levels, which

mostly reflects apoE co-deposition in Aβ plaques (113,245), were also significantly reduced in

male and female APPPS1;AFE3 and APPPS1;AFE4 mice (Fig. 1D).

Next, we assessed the cell-type-specificity of apoE expression after tamoxifen

administration by performing immunofluorescent staining of apoE (Fig. 1D). We observed a

strong overall reduction in the intensity of apoE staining for both the APPPS1;AFE3 and

APPPS1;AFE4 mice as compared to the APPPS1;FE3 and APPPS1;FE4 mice (Fig.1E and F).

Qualitative assessment of the staining for apoE also revealed a strong decrease in the presence of

apoE in GFAP+ astrocytes. In the APPPS1;FE3 and APPPS1;FE4 mice nearly all GFAP[+]

astrocytes were also apoE[+] while the APPPS1;AFE3 and APPPS1;AFE4 mice exhibited only

rare apoE staining in GFAP[+] astrocytes (Fig. 1G). The presence of apoE in Iba1^{+} microglia, did

not appear to be altered as apoE[+] microglia were present in all groups, particularly in the vicinity

of Aβ plaques (Fig. 1G). Therefore, the tamoxifen administration was able to effectively reduce the overall apoE levels and strongly reduce apoE expression in astrocytes, while appearing to not affect microglial apoE expression in the APPPS1;AFE3 and APPPS1;AFE4 mice. Additionally, while the immunostaining showed that overall apoE levels were greatly reduced in the APPPS1;AFE3 and APPPS1;AFE4 mice, there were still intense foci of apoE staining co-localized with the X-34$^+$ amyloid plaques, similar to what was observed in the APPPS1;FE3 and APPPS1;FE4 mice (Fig.1E and 1G).

4.3.2 Aβ plaque accumulation in mice lacking astrocytic *APOE*

The deposition of Aβ into fibrillar amyloid plaques is influenced by the expression level and isoform of apoE. With the targeted removal of astrocytic *APOE* resulting in a significant reduction in overall apoE levels, we investigated what impact this reduction might have on the deposition of Aβ into X34$^+$ fibrillar amyloid plaques (Fig. 2A). In the cortex and hippocampus, there was a large and significant decrease in fibrillar plaque load in APPPS1;AFE3 females and in APPPS1;AFE4 males and females (Fig. 2B and 2C). Overall, the total amyloid burden with the loss of astrocytic apoE was qualitatively similar to that observed in APPPS1;EKO mice (Figure 2B and 2C). An analysis of fibrillar plaque intensity revealed APPPS1;AFE3 and APPPS1;AFE4 mice have a significantly reduced overall intensity compared to the APPPS1;FE3 and APPPS1;FE4 mice (Fig. 2D and 2E) and exhibited a smaller, less dense compact core. However, a qualitative assessment of the APPPS1;EKO mice showed fibrillar plaques form with a core that is even less compact and less intense than the APPPS1;AFE3 and APPPS1;AFE4 mice (Fig. 2D and 2E).

To assess overall Aβ deposition, staining was performed using an anti-Aβ antibody (Fig. 3A. In the cortex, female APPPS1;AFE3 mice showed a trend towards lower Aβ plaque levels compared to female APPPS1;FE3 while both male and female APPPS1;AFE4 had a significant decrease in plaque coverage compared to APPPS1;FE4 (Fig. 3B). In the hippocampus, the APPPS1;AFE3 and APPPS1;AFE4 females had significantly lower Aβ plaque coverage (Fig.3C). Interestingly, a qualitative analysis of the APPPS1;EKO mice revealed a higher Aβ load than the APPPS1;AFE3 and APPPS1;AFE4 mice (Fig. 3B and 3C).

To further analyze the accumulation of Aβ in the brain, the level of insoluble Aβ was assessed in the guanidine soluble (PBS-insoluble) fractions from homogenized cortical tissue samples by ELISA for $A\beta_{40}$ and $A\beta_{42}$ levels. Aβ that is insoluble in PBS and detected in the guanidine fraction serves as a measure of how much Aβ has accumulated in deposits in the brain and constitutes the majority of the Aβ pool once Aβ aggregates. The $A\beta_{40}$ and $A\beta_{42}$ in the PBS soluble fraction showed no difference between each of the groups (data not shown). The $A\beta_{40}$ in the guanidine soluble fraction was significantly decreased in the APPPS1;AFE4 males and both the $A\beta_{40}$ and $A\beta_{42}$ levels were significantly decreased in the APPPS1;AFE3 females and APPPS1;AFE4 females vs. their astrocyte-apoE expressing counterparts (Figs. 3D and 3E). A qualitative assessment of the Aβ staining in the female mice also revealed unique patterns of Aβ deposition in APPPS1;AFE3 and APPPS1;AFE4 mice compared to APPPS1;FE3 and APPPS1;FE4 mice. In the APPPS1;AFE3 and APPPS1;AFE4 mice, the fibrillar Aβ core was smaller with a greater percent of each plaque consisting of non-fibrillar Aβ (Fig. 3F). However, the APPPS1;EKO mice had an even greater and more dispersed accumulation of non-fibrillar Aβ than the APPPS1;AFE3 and APPPS1;AFE4 mice (Fig. 3F). Overall, the biochemical results, combined with the Aβ staining results, show that the loss of astrocytic human apoE leads to a

decrease in overall Aβ pathology compared to mice with no loss of apoE. Additionally, the loss of astrocytic apoE leads to more diffuse, less fibrillar plaques though not as diffuse as is seen with a complete knockout of apoE.

4.3.3 Microglial activation after the loss of astrocytic apoE

The activation state of microglia has been shown to be influenced by apoE isoform and the presence of Aβ plaque pathology in the brain. To better understand how the loss of astrocytic apoE was influencing microglial gene expression, we performed RT-qPCR on cortical tissue samples from female mice. Both APPPS1;FE3 and APPPS1;FE4 mice exhibited an upregulation of DAM-associated transcripts compared to FE3 or FE4 mice, respectively, indicative of a microglial response to amyloid plaques (Fig. 4A). The APPPS1;AFE3 mice showed no significant change in DAM gene expression compared to the APPPS1;FE3 mice. However, the APPPS1;AFE4 mice did show a down-regulation of several DAM genes compared to the APPPS1;FE4 mice, including *Clec7a* (Fig. 4A). To assess if the overall levels of microglia were changed, we stained brain sections for Iba1 (Fig. 4B). Overall, the % area of the cortex covered by Iba1 staining remained unchanged between the APPPS1;AFE3 and APPPS1;FE3 mice and between the APPPS1;AFE4 and APPPS1;FE4 mice (Fig. 4C). Interestingly, immunoreactivity of Clec7a, a marker of DAM microglia, was significantly reduced around fibrillar plaques in the APPPS1;AFE4 and APPPS1;AFE3 mice compared to the APPPS1;FE4 and APPPS1;FE3 mice, respectively (Fig. 4D and 4E), suggesting an impaired microglial response to amyloid pathology in the absence of astrocytic apoE.

4.3.4 Astrocyte activation after the loss of astrocytic apoE

ApoE has been shown to influence certain functions of astrocytes, including responses to pathogenic stimuli (124,246), however it is not fully known if the cell-specific loss of astrocytic apoE alters astrocyte reactivity to Aβ plaques. Therefore, we assessed the expression profile of genes involved with astrocyte reactivity by RT-qPCR. Overall expression of reactive astrocytic genes was increased in APPPS1;FE3 and APPPS1;FE4 mice compared to FE3 and FE4 mice (Fig 5A). H2.T23 and Serpina3n were significantly down-regulated in APPPS1;AFE4 mice compared to APPPS1;FE4 mice (Fig. 5A). Interestingly, GFAP trended downward in the APPPS1;AFE4 mice but not in the APPPS1;AFE3 mice (Fig. 5A). To visualize and further assess astrocyte reactivity, we assessed GFAP levels by immunostaining. Overall GFAP staining was not altered in APPPS1;AFE3 compared to APPPS1;FE3 mice. However, there was a significant reduction in GFAP staining in the cortex of APPPS1;AFE4 mice compared to APPPS1;FE4 mice (Fig. 5B and 5C). The reductions in GFAP gene expression, and in immunostaining, in APPPS1;AFE4 mice could result from either altered astrocyte reactivity to amyloid plaques or from overall reductions in amyloid burden. Therefore, to see if astrocyte reactivity was altered specifically around Aβ plaques, we assessed GFAP staining within 15μm of each plaque (Fig 5B.) No differences were found in the levels of GFAP staining around plaques between the groups (Fig 5D). Since GFAP staining around plaques was unaltered, it suggests the loss of apoE in astrocytes does not alter the ability of astrocytes to respond to Aβ plaques, at least morphologically, but that overall changes to astrocyte reactivity may be driven by the level of total Aβ plaque pathology.

4.3.5 Neuritic dystrophy after the loss of astrocytic apoE

The deposition of Aβ into fibrillar amyloid plaques results in damage to surrounding neuronal processes and leads to the formation of large swollen axons and dendrites around plaques (neuritic dystrophy). These damaged and swollen neurites contain accumulations of various proteins that can act as markers for the dystrophy, including BACE1 (43,247). We used an anti-BACE1 antibody to stain and assess the total amount of dystrophic neurites present in the cortex of mice (Fig. 6A). The BACE1 levels for the APPPS1;AFE3 and APPPS1;AFE4 female mice were significantly decreased compared to the APPPS1;FE3 and APPPS1;FE4 mice, respectively (Fig. 6B). As the BACE-1 positive dystrophic neurites are only present around amyloid plaques, this is consistent with overall reductions in amyloid plaque following removal of astrocyte apoE. When we assessed the area of BACE1 within 15μm of each plaque, we found a significant increase in neuritic dystrophy in the APPPS1;AFE3 males compared to APPPS1;FE3 males, and an increase in both APPPS1;AFE4 males and females compared to APPPS1;FE4 males and females (Fig. 6C and 6D).

4.4 Discussion

The influence of APOE genotype on the development of various neurodegenerative pathologies has been an area of interest for decades. In particular, the strong effect that APOE4 has on an individual's risk for developing Alzheimer disease has been the focus of a tremendous amount of research. Clinical studies have shown that APOE4 carriers develop an earlier onset and faster rate of development of Aβ pathology (15,146). Previous research has revealed several ways apoE may influence the buildup of Aβ and the formation of amyloid plaques (248,249). One way apoE can influence monomeric Aβ levels and its ultimate aggregation is by competing

for clearance via apoE receptors, like the low-density lipoprotein receptor (LDLR) or LDL receptor-related protein 1 (LRP1) (234,243,250). The ability of apoE to inhibit Aβ binding and clearance via LDLR and LRP1 is likely an important factor regulating the levels of Aβ in the brain. In addition, apoE can directly influence Aβ seeding and fibrillogenesis (i.e. the conversion of monomeric Aβ into oligomeric and fibrillar structures) (34,93,101,105,251,252). However, it is not known if astrocytic apoE or microglial apoE may be having different effects on monomeric Aβ clearance and Aβ seeding/fibrillogenesis. While astrocytes are the primary producer of apoE in the CNS, microglia increase their production of apoE during the development of neurodegenerative pathology (61,62). Microglia produce and secrete species of human apoE that have altered glycosylation compared to astrocytes (253). Additionally, the recent finding by our lab that microglia secrete human apoE-containing lipoprotein particles that are smaller and less lipidated than particles produced by astrocytes (229) points to the potential of apoE produced by each cell type having unique effects on the development of Aβ pathology.

For this study, we aimed to answer the question of how apoE3 and apoE4 specifically produced by astrocytes influence the formation of Aβ plaques and the subsequent response of cells to the amyloid pathology. In order to see how astrocytic apoE influences the initial stages of Aβ plaque development, we aimed to remove *APOE* prior to plaque onset. To ensure tamoxifen administration was occurring prior to the formation of Aβ plaque deposition, a cohort of tamoxifen injected mice was collected at 6 weeks of age, and Aβ immunostaining and X-34 staining showed no signs of any Aβ pathology. The 100mg/kg dose of tamoxifen proved to be well tolerated and to efficiently lower *APOE* mRNA transcripts and to specifically lower most detectable protein levels of apoE from astrocytes in the Cre+ mice. However, because insoluble apoE in the guanidine fraction is likely apoE bound to amyloid plaques (113,245), the decrease

in insoluble apoE in the guanidine fraction of the Cre+ mice is likely due to overall Aβ plaque

levels being decreased. While the tamoxifen administration did lower apoE levels overall, there

was some variability seen in the efficiency of the injections. Immunostaining for apoE showed

an overall lowering of apoE and an absence of apoE in the majority of GFAP+ astrocytes;

however, some mice had higher levels of apoE still present and some GFAP+ astrocytes also still

stained positively for apoE. Nevertheless, the tamoxifen injections did prove effective in

removing most astrocytic *APOE*, significantly lowering apoE levels, with a resultant strong

decrease in Aβ pathology.

The reduction in Aβ plaque load observed by selectively decreasing astrocyte apoE3 and

apoE4 levels is similar to the results seen in previous studies that had reduced apoE in a non-cell

specific manner prior to plaque onset (143,171). Additionally, we observed that the complete

loss of apoE in APPPS1;EKO mice results in large deposits of diffuse non-fibrillar Aβ, similar to

what we found previously (241), and that the level of diffuse Aβ deposition in the APPPS1;EKO

compared to the selective removal of astrocyte apoE3 or apoE4 is considerably elevated. The

increased levels of non-fibrillar Aβ deposition in the APPPS1;EKO mice compared to

APPPS1;AFE3 and APPPS1;AFE4 mice suggests that the presence of *APOE* in cells other than

astrocytes may also be influencing overall Aβ deposition to some extent, though the strong

decrease in overall Aβ accumulation resulting from the removal of astrocyte apoE3 and apoE4

suggests astrocytic apoE is a major driver of Aβ accumulation. Furthermore, the shift in fibrillar

plaque formation towards less intense and less compact plaques with the loss of astrocytic *APOE*

indicates astrocytic apoE is influencing the physical structure of the Aβ plaques that form. Since

the structure of Aβ aggregates is likely driven by direct interactions of apoE and Aβ

(34,101,105,251,252), this suggests that a direct interaction between astrocyte apoE and some

92

form of Aβ during the process of seeding or fibrillogenesis is involved in this Aβ structural change. While a complete loss of *APOE* has shown similar effects on fibrillar plaque levels and structure (138,166,237,241), removing only astrocytic *APOE* in the APPPS1;AFE3 and APPPS1;AFE4 mice produced patterns of Aβ deposition distinct from the APPPS1;EKO. Very few β-sheet structured fibrils, as detected by X-34 (170), form in the APPPS1;EKO mice. However, those that do form, have a much more dispersed and mesh-like appearance than the fibrils that form in the APPPS1;AFE3 and APPPS1;AFE4 mice. This suggests the presence or production of *APOE* in other cell types, such as microglia, may also be influencing the structure of Aβ plaque formation to some extent in APPPS1;AFE3 and APPPS1;AFE4 mice. For example, fibrillar amyloid plaques formed in APPPS1;AFE3 and APPPS1;AFE4 mice with strongly reduced astrocytic apoE still contain apoE, which indicates the apoE present in plaques is likely coming from other cellular sources such as microglia.

Another factor that could be impacting the fibrillar plaque structure is the ability of microglia to interact with the plaque surface. Previous studies have shown activated microglia are capable of 'capping' the edge of Aβ plaques to limit the diffusion of Aβ fibrils and aid in the formation of compact plaques (155,159). However, the low levels of Clec7a around plaques in the APPPS1;AFE3 and APPPS1;AFE4 mice suggests microglia are not activated to the same extent as in the APPPS1;FE3 and APPPS1;FE4 mice. The shift in microglia activation to a reactive or DAM/MGnD state has been shown to be apoE dependent (61,62,254–256). Astrocytic apoE lipoprotein particles can influence microglial activation (128,257), and our results support the hypothesis that astrocytic apoE may be involved in signaling pathways between astrocytes and microglia that regulate the apoE-dependent DAM activation state of microglia. The transition to the DAM activation state has been shown to be TREM2-APOE

dependent (61) and apoE is a ligand for TREM2 (175,176,258). Decreasing astrocytic apoE may lower TREM2 activation via decreased apoE binding. Astrocyte-derived apoE may also be involved in microglial activation via another mechanism. Additionally, since activated microglia are a source of plaque-associated apoE (118), decreased microglial activation may result in decreased microglial apoE production and thus a reduction in the amount of microglial apoE binding to Aβ to aid in fibrillar plaque formation and plaque compaction.

The reduction in either astrocytic apoE3 or apoE4 had similar impacts on lowering Aβ plaque levels, as well as on reducing the activation of microglia to Aβ plaques. However, the total DAM gene expression in the cortex did show an isoform-dependent difference. While the decrease in overall DAM gene expression in the APPPS1;AFE4 mice may be driven by the overall Aβ plaque load being lower than the APPPS1;FE4 mice, the APPPS1;AFE3 mice did not show a difference in overall DAM gene expression despite having a similar lowering of overall Aβ plaque load compared to APPPS1;FE3 mice. This difference suggests astrocytic apoE4 may have a differential effect on overall microglial activation compared to astrocytic apoE3, similar to what we have recently reported in a model of tauopathy (259). In fact, some studies have shown that apoE3 can decrease microglial activation while apoE4 increases activation (172,260). In addition to apoE isoform-dependent differences in global microglial activation in the setting of Aβ deposition, we also observed isoform-dependent differences in total astrocyte activation as measured by GFAP staining. Again, while the decrease in overall GFAP levels in the APPPS1;AFE4 mice may be explained by decreased Aβ plaque load, the lack of a difference in overall GFAP levels in APPPS1;AFE3 mice suggests that astrocytic apoE3 may be having a differential effect on reactive astrocytes compared to astrocytic apoE4. Indeed, induced expression of apoE3 by astrocytes has been shown to lower overall GFAP levels (172).

The impact of apoE on microgliosis at sites of Aβ plaque deposition can lead to changes in damage to surrounding cells, including the formation of dystrophic neurites (neuritic dystrophy) (128). Neuritic dystrophy has been shown to be increased around fibrillar plaques with a more dispersed morphology than around dense core plaques with a compact morphology (40,159,241,261,262). The removal of astrocyte apoE strongly reduced the amount of fibrillar plaques and plaque-associated neuritic dystrophy. However, the change in fibrillar plaque formation to a more dispersed and less compact structure observed in the APPPS1;AFE3 and APPPS1;AFE4 mice may be driving the increased neuritic dystrophy around the remaining fibrillar plaques present in these mice (262). Additionally, apoE lipoprotein particles produced by astrocytes have been shown to support neuronal function and recovery following neuronal damage (263–267). The loss of astrocytic apoE could reduce astrocytic support to damaged neuritic processes that develop at sites of Aβ plaques and contribute to the increase in neuritic dystrophy. Further studies are needed to better understand how the loss of astrocytic apoE is impacting overall neuronal function.

4.4.1 Final Conclusions:

We demonstrate that reducing astrocytic apoE3 and apoE4 results in a strong decrease in both fibrillar amyloid plaques and overall Aβ plaque deposition in APPPS1;AFE3 and APPPS1;AFE4 mice. We also found that the loss of astrocytic apoE results in the structure and pattern of Aβ deposition being altered in a unique manner compared to the complete loss of apoE in APPPS1;EKO mice. Furthermore, the decrease in microglial activation surrounding fibrillar plaques following removal of astrocyte apoE demonstrates astrocytic apoE may be playing a critical role in regulating microglial responses to Aβ pathology. Isoform-dependent effects on glial activation were also seen and suggest astrocytic apoE3 may act to reduce overall glial

activation. Finally, while the more dispersed fibrillar plaque structures seen in the APPPS1;AFE3 and APPPS1;AFE4 mice were shown to induce an increase in neuritic dystrophy at the site of Aβ plaque deposition, the ability of reducing astrocytic apoE to lower Aβ plaque levels led to an overall decrease in levels of neuritic dystrophy. These results demonstrate the therapeutic potential of using targeted cell-specific reduction of astrocytic apoE to ameliorate Aβ pathology that is found in Alzheimer disease.

4.5 Figures and Table
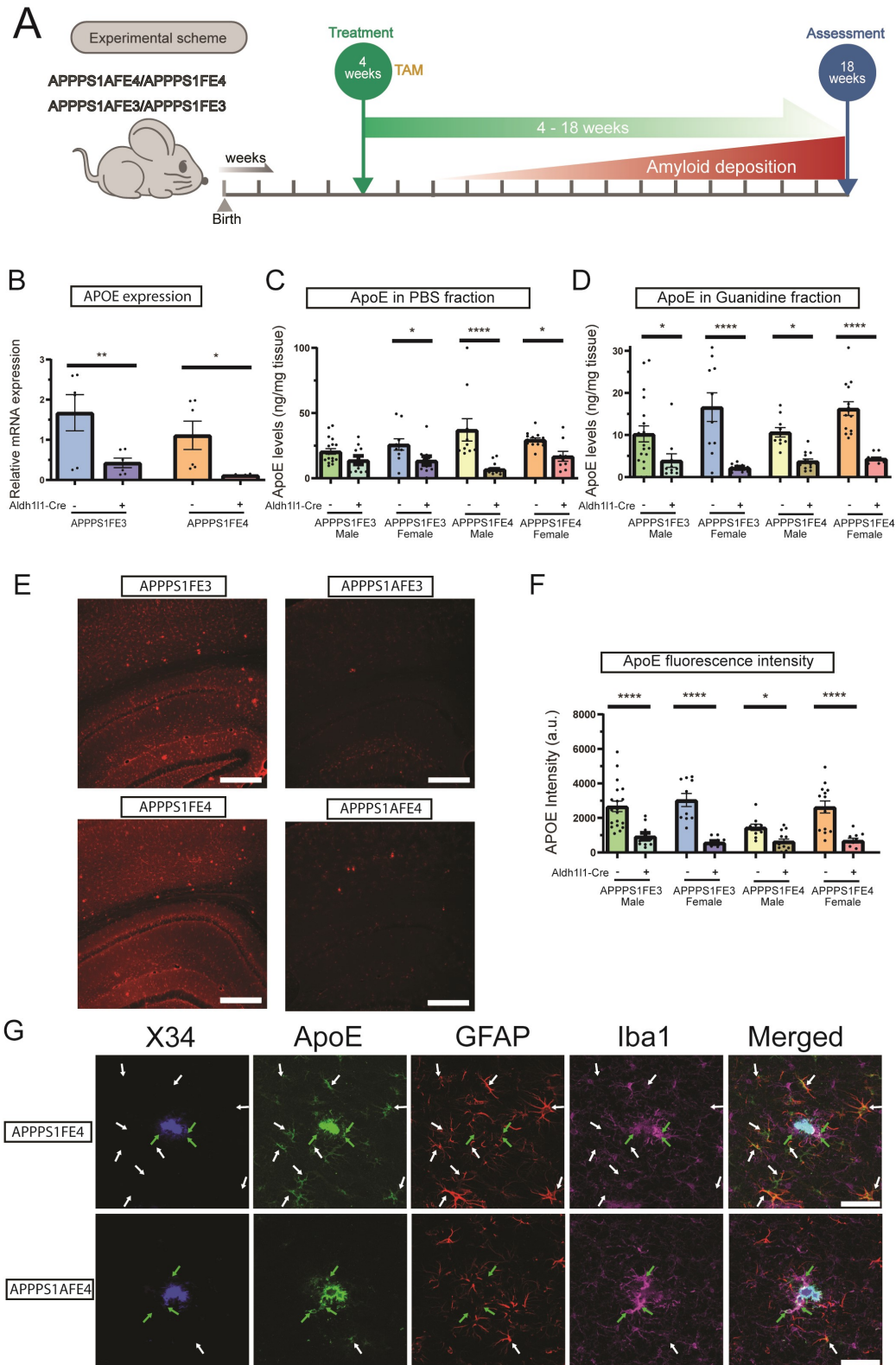
Figure 4.1: Tamoxifen administration reduces ApoE levels in Aldh1l1-Cre+ APPPS1;FE3 and APPPS1;FE4 mice

(**A**) Timeline of the experimental scheme. Mice were given once-daily IP injections of tamoxifen (TAM) (100mg TAM/kg body weight) at 4 weeks of age for 6 consecutive days. Sample collection and analysis occurred at 18 weeks of age. (**B**) *APOE* mRNA expression levels in female Cre- or Cre+ APPPS1;FE3 and Cre- or Cre+ APPPS1;FE4 mice. Cortical tissue samples were analyzed by qPCR (n = 6). (**C**) Soluble apoE levels in the cortex of Cre- or Cre+ APPPS1;FE3 and Cre- or Cre+ APPPS1;FE4 mice. Cortical tissue samples were homogenized in PBS and PBS-soluble apoE protein levels were analyzed by ELISA (n = 9-19). (**D**) Insoluble apoE levels in the cortex of Cre- or Cre+ APPPS1;FE3 and Cre- or Cre+ APPPS1;FE4 mice. PBS-insoluble cortex tissue samples from (C) were further homogenized in 5M guanidine HCl to determine the amount of PBS-insoluble apoE that was guanidine-soluble. Protein levels were analyzed by ELISA (n = 9-19). (**E**) ApoE immunostaining in the cortex and hippocampus of APPPS1;FE3, APPPS1;AFE3, APPPS1;FE4, and APPPS1;AFE4 mice. Representative images are of brain sections stained with an anti-apoE antibody. Scale bars = 300µm. (**F**) Intensity of fluorescent apoE staining in Cre- or Cre+ APPPS1;FE3 and Cre- or Cre+ APPPS1;FE4 mice. The average pixel intensity was analyzed from images of apoE immunostained brain sections (n=10-19). (**G**) Brain sections from APPPS1;FE4 and APPPS1;AFE4 mice co-stained for X-34 (blue), apoE (green), GFAP (red), and Iba1 (magenta). White arrows indicate co-localization of apoE with GFAP and green arrows indicate co-localization of apoE with Iba1. Scale bars = 50µm. (**A-G**) * $p \leq 0.05$, ** $p \leq 0.01$, and **** $p \leq 0.0001$; two-way ANOVA and Sidak's post hoc test in (B), three-way ANOVA and Sidak's post hoc test in (D); three-way ANOVA and uncorrected Fisher's LSD test in (C) and (F). Data are expressed as mean ± SEM. See Table 4.1 for detailed statistics.

A

APPPS1FE3   APPPS1AFE3   APPPS1FE4   APPPS1AFE4   APPPS1EKO

X-34

B Fibrillar plaque load in Cortex

C Fibrillar plaque load in Hippocampus

D

APPPS1FE3   APPPS1AFE3   APPPS1FE4   APPPS1AFE4   APPPS1EKO

Intensity

Heatmap

E Fibrillar plaque intensity
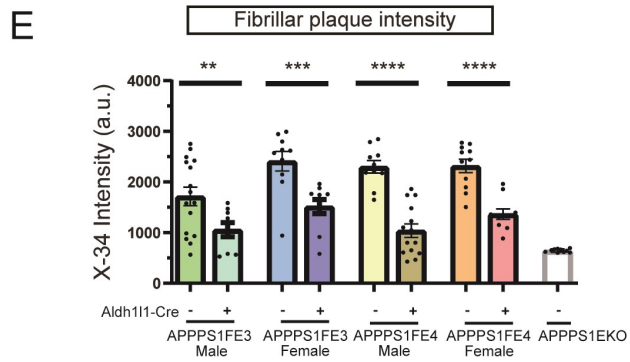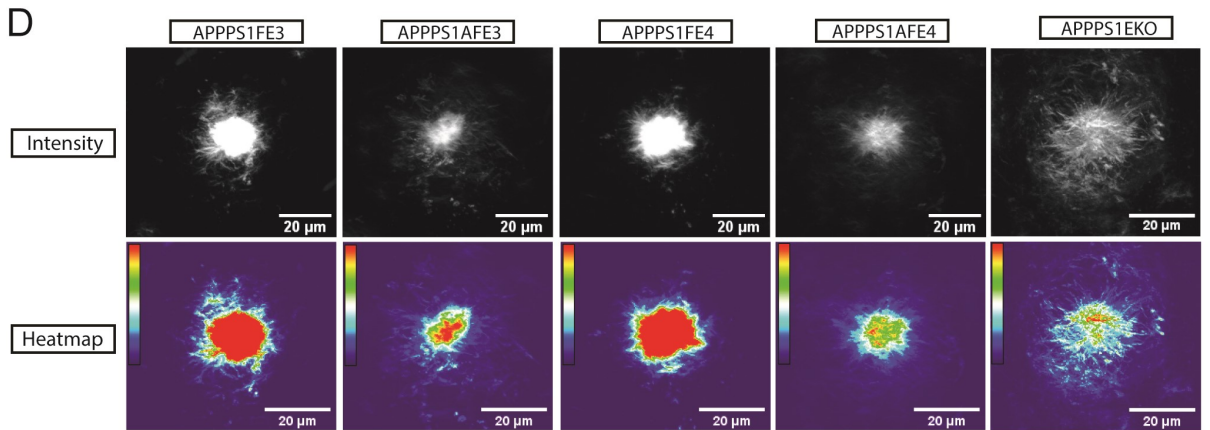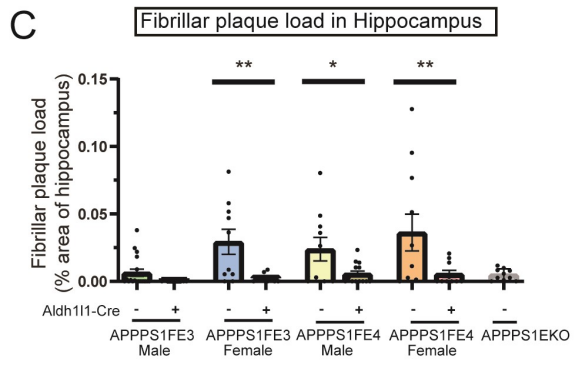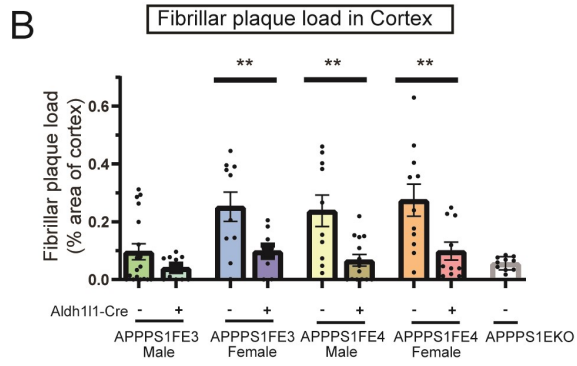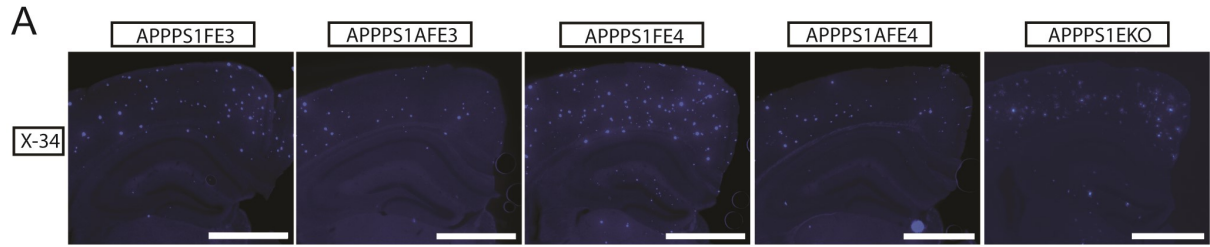
Figure 4.2: Reducing astrocytic apoE decreases fibrillar plaque levels and plaque intensity
(**A**) Fibrillar amyloid plaque staining in the cortex and hippocampus of APPPS1;FE3, APPPS1;AFE3, APPPS1;FE4, APPPS1;AFE4, and APPPS1EKO mice. Representative images are of X-34 (blue) stained brain sections. Scale bars = 1000μm (**B**) Fibrillar plaque load in the cortex of Cre- or Cre+ APPPS1;FE3, Cre- or Cre+ APPPS1;FE4, and APPPS1EKO mice. Percent of cortex area covered by fibrillar plaque was determined by analyzing X-34 stained brain sections (n = 10-18). (**C**) Fibrillar plaque load in hippocampus of Cre- or Cre+ APPPS1;FE3, Cre- or Cre+ APPPS1;FE4, and APPPS1EKO mice. Percent of hippocampus area covered by fibrillar plaque was determined by analyzing X-34 stained brain sections (n = 10-18). (**D**) Intensity of fibrillar amyloid plaques in APPPS1;FE3, APPPS1;AFE3, APPPS1;FE4, APPPS1;AFE4, and APPPS1EKO mice. Representative images are of X-34 stained amyloid plaques. Scale bars = 20μm. (**E**) Measure of average pixel intensity of X-34 stained fibrillar plaques in the cortex of Cre- or Cre+ APPPS1;FE3, Cre- or Cre+ APPPS1;FE4, and APPPS1EKO mice (n = 9-16). (**A-E**) * $p \leq 0.05$, ** $p \leq 0.01$, *** $p \leq 0.001$, and **** $p \leq 0.0001$; three-way ANOVA and uncorrected Fisher's LSD test in (B), (C), and (E). Data are expressed as mean ± SEM. See Table 4.1 for detailed statistics.

A APPPS1FE3 | APPPS1AFE3 | APPPS1FE4 | APPPS1AFE4 | APPPS1EKO

Aβ

B Aβ plaque load in Cortex

C Aβ plaque load in Hippocampus

D Aβ$_{40}$ in Guanidine fraction

E Aβ$_{42}$ in Guanidine fraction

F X-34 | Aβ | Merged

APPPS1FE4

APPPS1AFE4
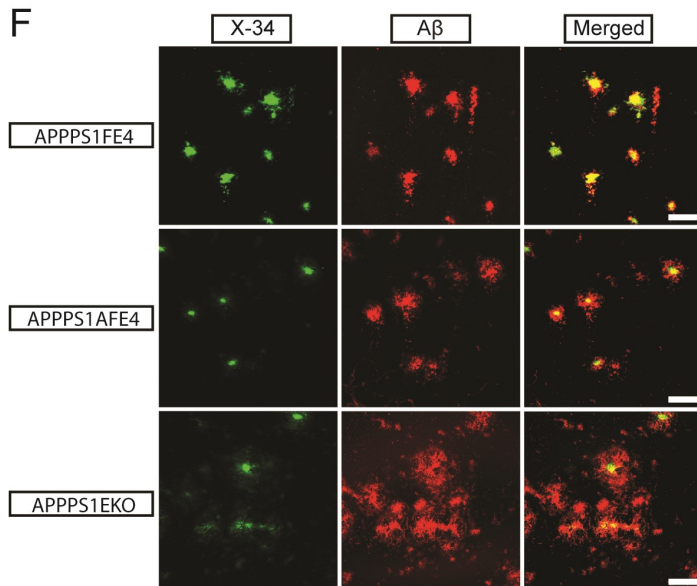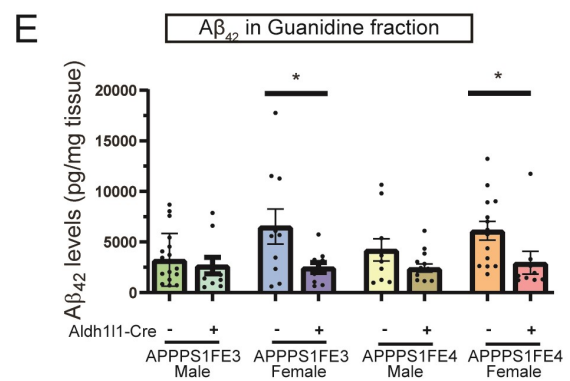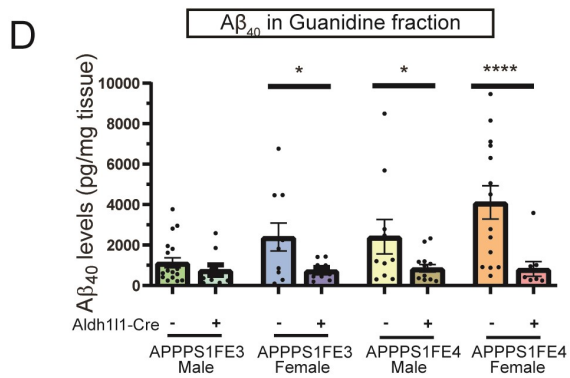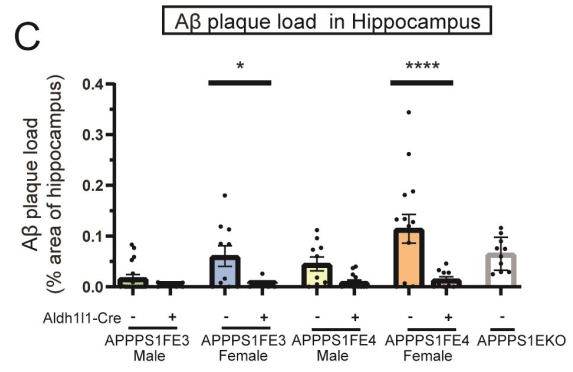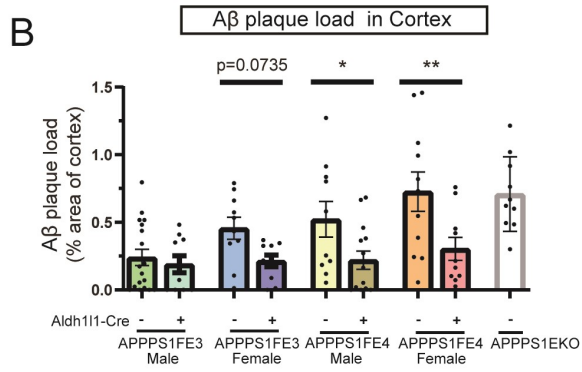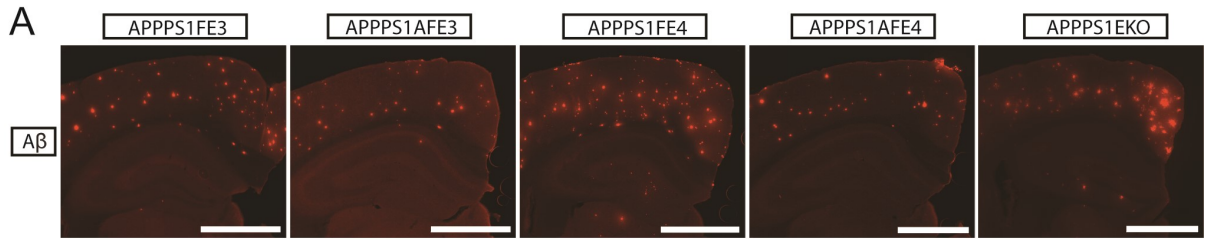
APPPS1EKO

Figure 4.3: Reducing astrocytic apoE decreases Aβ plaque levels and alters Aβ deposition
(**A**) Aβ plaque staining in the cortex and hippocampus of APPPS1;FE3, APPPS1;AFE3, APPPS1;FE4, APPPS1;AFE4, and APPPS1EKO mice. Representative images are of Aβ immunostained brain sections using the HJ3.4 anti-Aβ antibody (orange). Scale bars = 1000μm. (**B**) Aβ plaque load in cortex of Cre- or Cre+ APPPS1;FE3, Cre- or Cre+ APPPS1;FE4, and APPPS1EKO mice. Percent of cortex area covered by Aβ plaque was determined by analyzing HJ3.4 stained brain sections (n = 10-18). (**C**) Aβ plaque load in the hippocampus of Cre- or Cre+ APPPS1;FE3, Cre- or Cre+ APPPS1;FE4, and APPPS1EKO mice. Percent of hippocampus area covered by Aβ plaque was determined by analyzing HJ3.4 stained brain sections (n = 10-18). (**D**) Insoluble $A\beta_{40}$ levels in the cortex of Cre- or Cre+ APPPS1;FE3 and Cre- or Cre+ APPPS1;FE4 mice. PBS-insoluble cortical tissue samples that were further homogenized in 5M guanidine HCl were analyzed by ELISA to determine the guanidine-soluble $A\beta_{40}$ levels (n = 9-19). (**E**) Insoluble $A\beta_{42}$ levels in the cortex of Cre- or Cre+ APPPS1;FE3 and Cre- or Cre+ APPPS1;FE4 mice. PBS-insoluble cortex tissue samples that were further homogenized in 5M guanidine HCl were analyzed by ELISA to determine the guanidine-soluble $A\beta_{42}$ levels (n = 9-19). (**F**) Deposition pattern of Aβ plaque and fibrillar amyloid plaque staining in APPPS1;FE4, APPPS1;AFE4, and APPPS1EKO mice. Representative images are of X-34 (green) and HJ3.4 (red) co-stained brain sections. Scale bars = 50μm. (**A-F**) * $p \leq 0.05$, ** $p \leq 0.01$, and **** $p \leq 0.0001$; three-way ANOVA and Sidak's post hoc test in (B) and (C); three-way ANOVA and uncorrected Fisher's LSD test in (D) and (E). Data are expressed as mean ± SEM. See Table 4.1 for detailed statistics.
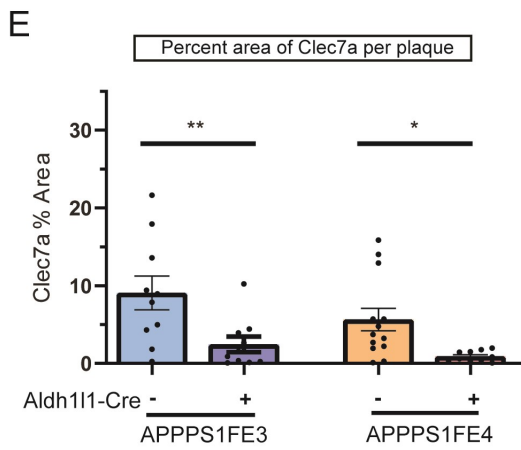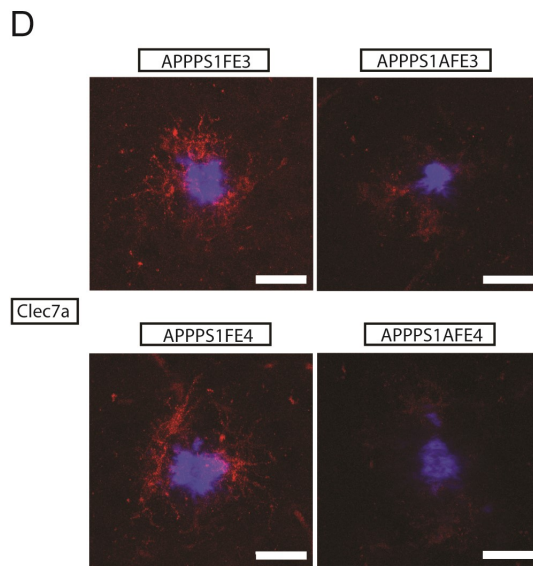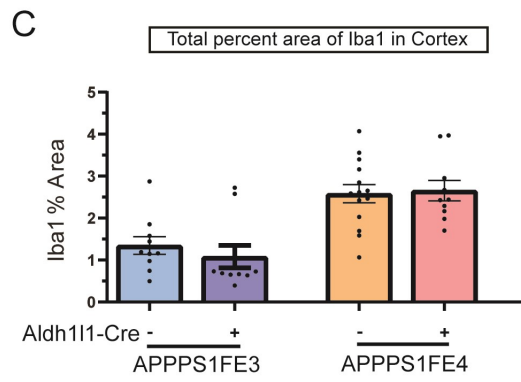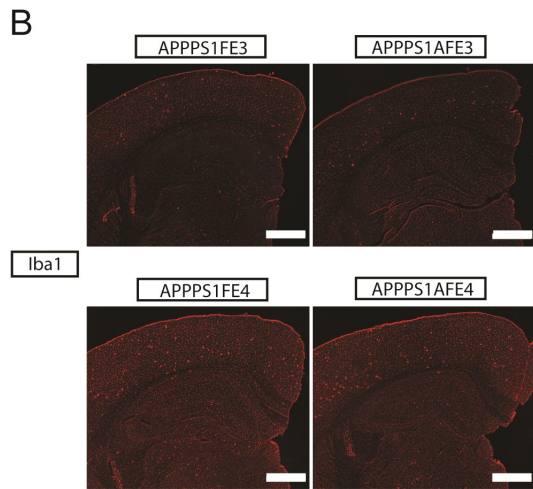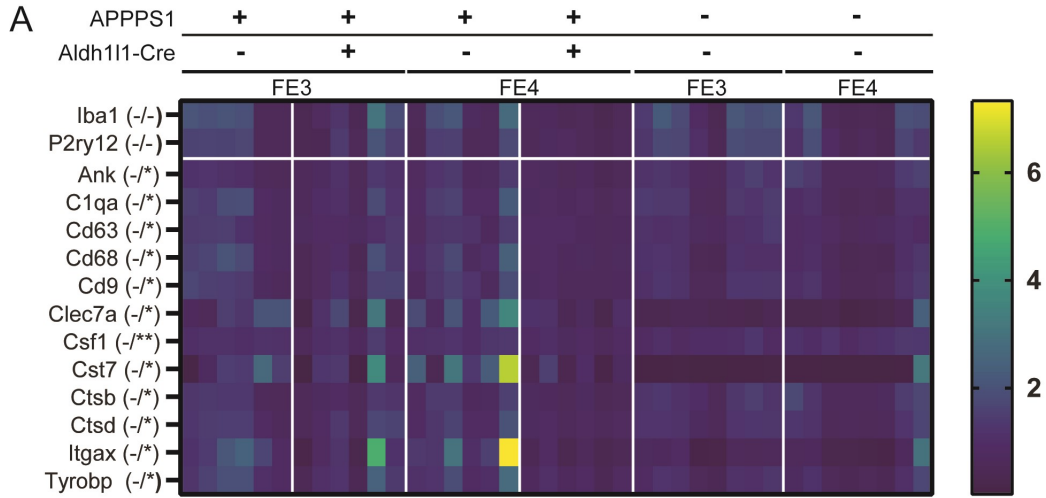
Figure 4.4: Microglial activation is reduced in mice with a decrease in astrocytic apoE
(**A**) Microglial gene expression analysis in female Cre- or Cre+ APPPS1;FE3, Cre- or Cre+ APPPS1;FE4, FE3, and FE4 mice. Heatmap is of microglial genes assessed by qPCR from cortical tissue samples (n = 6-8). In the parentheses, the first symbol before the slash indicates significance between the Cre- and Cre+ APPPS1;FE3 groups and the second symbol after the slash indicates significance between the Cre- and Cre+ APPPS1;FE4 groups. - $p > 0.05$, * $p \leq 0.05$, ** $p \leq 0.01$. (**B**) Microglia staining in the cortex and hippocampus of female APPPS1;FE3, APPPS1;AFE3, APPPS1;FE4, and APPPS1;AFE4 mice. Representative images are of brain sections immunostained using an anti-Iba1 antibody (red). Scale bars = 200μm. (**C**) Microglial coverage in the cortex of female Cre- or Cre+ APPPS1;FE3 and Cre- or Cre+ APPPS1;FE4 mice. Percent of cortex area covered by microglia was determined by analyzing Iba1 stained brain sections (n = 10-14). (**D**) Activated microglia around fibrillar amyloid plaques in female APPPS1;FE3, APPPS1;AFE3, APPPS1;FE4, and APPPS1;AFE4 mice. Representative images are of Clec7a immunostaining (red), using an anti-Clec7a antibody, around X-34 stained (blue) amyloid plaques. Scale bars = 20μm. (**E**) Coverage of activated microglia around fibrillar amyloid plaques in female Cre- or Cre+ APPPS1;FE3 and Cre- or Cre+ APPPS1;FE4 mice. Percent of area covered by activated microglia around fibrillar amyloid plaques was determined by analyzing the level of cleca7a staining within 15μm of X-34 stained plaques (n = 10-14). (**A-E**) * $p \leq 0.05$, ** $p \leq 0.01$; three-way ANOVA and uncorrected Fisher's LSD test in (A); two-way ANOVA and Sidak's post hoc test in (C) and (E). Data are expressed as mean ± SEM. See Table 4.1 for detailed statistics.

A

		FE3		FE4		FE3	FE4
APPPS1	+	+	+	+	-	-
Aldh1l1-Cre	-	+	-	+	-	-

S100B (-/-)

GFAP (-/0.092)

H2.T23 (-/*)

Ptgs2 (*/-)

S1pr3 (-/0.058)

Serpina3n (-/0.011)

B

APPPS1FE3 APPPS1AFE3 APPPS1FE4 APPPS1AFE4

GFAP

GFAP

C Total percent area of GFAP in Cortex

GFAP % Area

Aldh1l1-Cre   -   +   -   +

APPPS1FE3   APPPS1FE4

D Volume of GFAP per plaque

GFAP Vol./ X-34 Vol.

Aldh1l1-Cre   -   +   -   +   -   +   -   +

APPPS1FE3 Male APPPS1FE3 Female APPPS1FE4 Male APPPS1FE4 Female
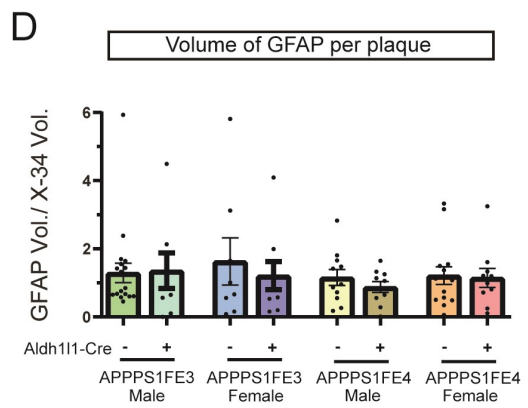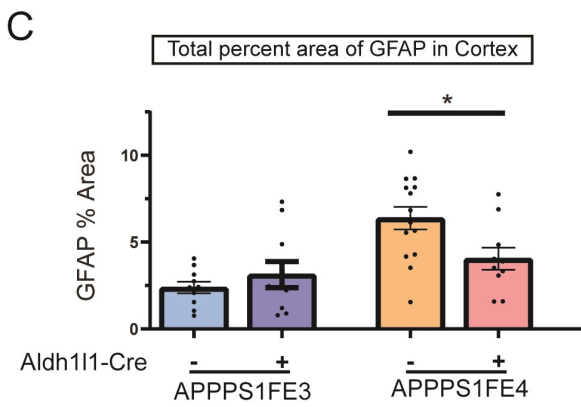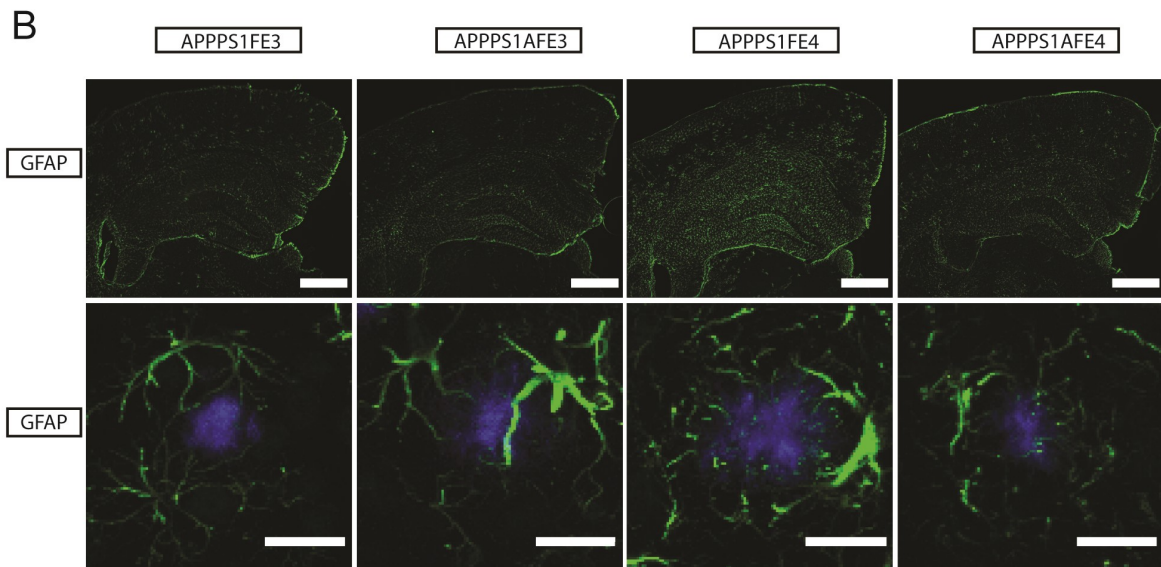
Figure 4.5: Astrocyte activation is reduced in APPPS1;AFE4 mice

(**A**) Astrocyte gene expression analysis in female Cre- or Cre + APPPS1;FE3, Cre- or Cre+ APPPS1;FE4, FE3, and FE4 mice. Heatmap is of astrocyte genes assessed by qPCR from cortical tissue samples (n = 6-8). In the parentheses, the first symbol before the slash indicates significance between the Cre- and Cre+ APPPS1;FE3 groups and the second symbol after the slash indicates significance between the Cre- and Cre+ APPPS1;FE4 groups. - $p > 0.05$, * $p \leq 0.05$. (**B**) Activated astrocyte staining in female APPPS1;FE3, APPPS1;AFE3, APPPS1;FE4, and APPPS1;AFE4 mice. Representative images in the top panel are of the cortex and hippocampus from brain sections immunostained using an anti-GFAP antibody (green). Images in the bottom panels are of GFAP immunostaining (green), using an anti-GFAP antibody, around X-34 stained amyloid plaques (blue). Scale bars = 200µm (top panels), 20um (bottom panels). (**C**) Astrocyte activation in the cortex of female Cre- or Cre+ APPPS1;FE3 and Cre- or Cre+ APPPS1;FE4 mice. Percent of cortical area covered by activated astrocytes was determined by analyzing GFAP stained brain sections (n = 10-14). (**D**) Astrocyte activation around fibrillar amyloid plaques in female Cre- or Cre+ APPPS1;FE3 and Cre- or Cre+ APPPS1;FE4 mice. The volume of activated astrocyte processes around fibrillar amyloid plaques was determined by analyzing the amount of GFAP staining within 15µm of X-34 stained plaques. GFAP volume was divided by the X-34 volume to normalize to the amount of plaque and account for differences in plaque size (n = 8-19). (**A-D**) * $p \leq 0.05$; three way ANOVA and uncorrected Fisher's LSD test in (A), and (D); two-way ANOVA and Sidak's post hoc test in (C). Data are expressed as mean ± SEM. See Table 4.1 for detailed statistics.
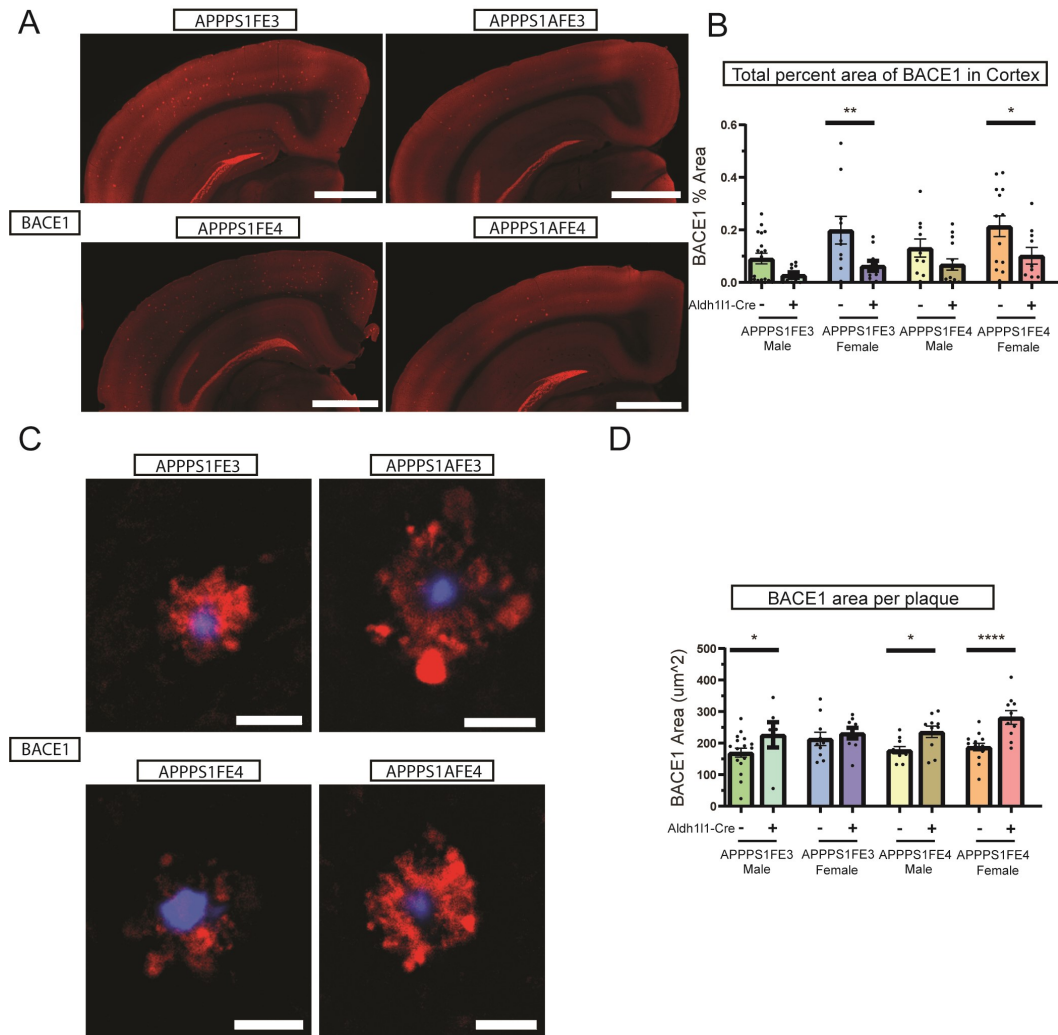
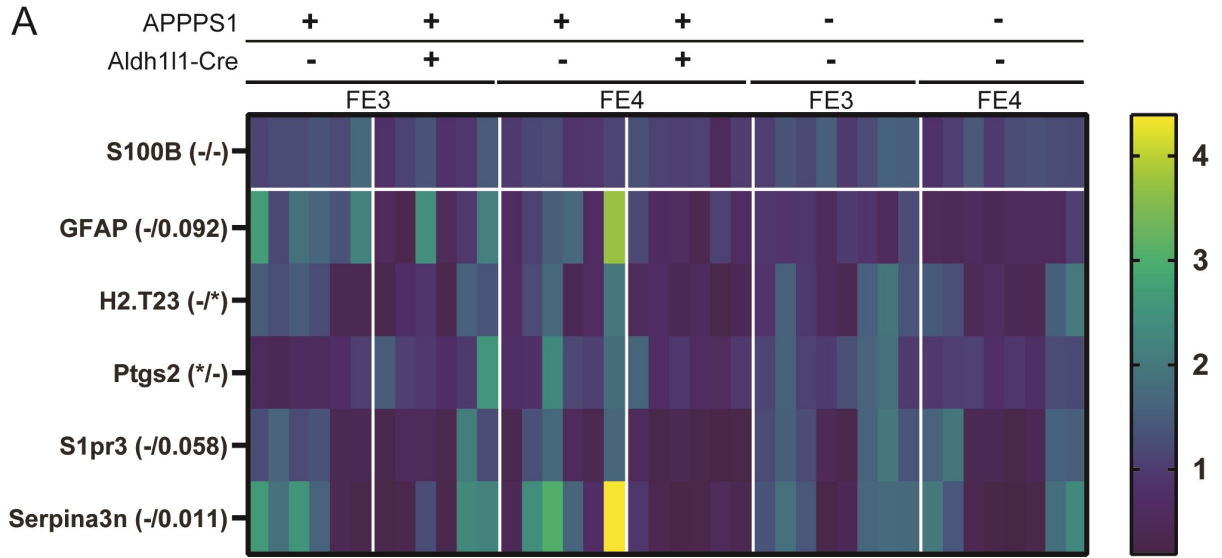**Figure 4.6: Neuritic dystrophy is increased around plaques, but decreased overall, with a reduction in astrocytic apoE**

(**A**) Dystrophic neurite staining in the cortex and hippocampus of APPPS1;FE3, APPPS1;AFE3, APPPS1;FE4 and APPPS1;AFE4 mice. Representative images are of brain sections immunostained using an anti-BACE1 antibody (red). Scale bars = 1000μm. (**B**) Level of neuritic dystrophy in the cortex of Cre- or Cre+ APPPS1;FE3 and Cre- or Cre+ APPPS1;FE4 mice. Percent of cortical area covered by dystrophic neurites was determined by analyzing BACE1 stained brain sections (n = 10-19). (**C**) Dystrophic neurites around fibrillar amyloid plaques in APPPS1;FE3, APPPS1;AFE3, APPPS1;FE4, and APPPS1;AFE4 mice. Representative images are of BACE1 immunostaining (red), using an anti-BACE1 antibody, around X-34 stained (blue) amyloid plaques. Scale bars = 20μm. (**D**) Level of neuritic dystrophy around fibrillar amyloid plaques in Cre- or Cre+ APPPS1;FE3 and Cre- or Cre+ APPPS1;FE4 mice. Percent of area covered by dystrophic neurites around fibrillar amyloid plaques was determined by analyzing the level of BACE1 staining within 15μm of X-34 stained plaques (n = 6-18). (**A-D**) * $p \leq 0.05$, ** $p \leq 0.01$, and **** $p \leq 0.0001$; three-way ANOVA and Sidak's post hoc test in (B); three-way ANOVA and uncorrected Fisher's LSD test in (D). Data are expressed as mean ± SEM. See Table 4.1 for detailed statistics.

**Table 4.1: Detailed statistical information.**

Figure	Sample size	Statistic information table
Figure 1B	N=6 per group	Cre F (1,20) = 14.74, p=0.0010; p=0.0068 in APPPS1AFE3 vs. APPPS1FE3; p=0.0258 in APPPS1AFE4 vs. APPPS1FE4
Figure 1C	APPPS1FE4-male: n=10; APPPS1AFE4-male: n=14; APPPS1FE4-female: n=14; APPPS1AFE4-female: n=9;	Cre F (1,88) = 35.09, p<0.0001; Cre and APOE interaction F(1,88) = 5.160, p=0.0256; Cre, APOE, and Sex interaction F(1,88) = 4.932, p=0.0289; p=0.0285 in APPPS1AFE3-female vs. APPPS1FE3-female; p<0.0001 in APPPS1AFE4-male vs. APPPS1FE4-male; p=0.0194 in APPPS1AFE4-female vs. APPPS1FE4-female
Figure 1E	APPPS1FE3-male: n=19; APPPS1AFE3-male: n=10; APPPS1FE3-female: n=10; APPPS1AFE3-female: n=10	Cre F (1,88) = 13.31, p=0.0004; Sex F(1,88) = 4.439, p=0.0380; p=0.0048 in APPPS1AFE3-female vs. APPPS1FE3-female; p=0.0197 in APPPS1AFE4-female vs. APPPS1FE4-female
Figure 1F	APPPS1FE4-male: n=10; APPPS1AFE4-male: n=14; APPPS1FE4-female: n=14; APPPS1AFE4-female: n=10; APPPS1FE3-male: n=19; APPPS1AFE3-male: n=10; APPPS1FE3-female: n=10; APPPS1AFE3-female: n=10	Cre F (1,89) = 77.81, p<0.0001; APOE F(1,89) = 5.272, p=0.0240; Cre and Sex interaction F(1,89) = 4.439, p=0.0380; p<0.0001 in APPPS1AFE3-male vs. APPPS1FE3-male; p<0.0001 in APPPS1AFE3-female vs. APPPS1FE3-female; p<0.0001 in APPPS1AFE4-female vs. APPPS1FE4-female
Figure 2B	APPPS1FE4-male: n=10; APPPS1AFE4-male: n=14; APPPS1FE4-female: n=11;	Cre F (1,85) = 28.61, p<0.0001; Sex F(1,89) = 7.305, p=0.0083; p=0.0063 in APPPS1AFE3-female vs. APPPS1FE3-female; p=0.0012 in APPPS1AFE4-male vs. APPPS1FE4-male; p=0.0015 in APPPS1AFE4-female vs. APPPS1FE4-female
Figure 2C	APPPS1AFE4-female: n=10; APPPS1FE3-male: n=18; APPPS1AFE3-male: n=10; APPPS1FE3-female: n=10; APPPS1AFE3-female: n=10; APPPS1EKO: n=10	Cre F (1,85) = 20.80, p<0.0001; Sex F(1,89) = 4.152, p=0.0447; p=0.0051 in APPPS1AFE3-female vs. APPPS1FE3-female; p=0.0419 in APPPS1AFE4-male vs. APPPS1FE4-male; p=0.0014 in APPPS1AFE4-female vs. APPPS1FE4-female
Figure 2E	APPPS1FE4-male: n=10; APPPS1AFE4-male: n=14; APPPS1FE4-female: n=11; APPPS1AFE4-female: n=10; APPPS1FE3-male: n=16; APPPS1AFE3-male: n=9; APPPS1FE3-female: n=10; APPPS1AFE3-female: n=10; APPPS1EKO: n=10	Cre F (1,82) = 71.6, p<0.0001; Sex F(1,82) = 11.31, p=0.0012; p=0.0032 in APPPS1AFE3-male vs. APPPS1FE3-male; p=0.0002 in APPPS1AFE3-female vs. APPPS1FE3-female; p<0.0001 in APPPS1AFE4-male vs. APPPS1FE4-male; p<0.0001 in APPPS1AFE4-female vs. APPPS1FE4-female
Figure 3B	APPPS1FE4-male: n=10; APPPS1AFE4-male: n=14; APPPS1FE4-female: n=11; APPPS1AFE4-female: n=10; APPPS1FE3-male: n=18; APPPS1AFE3-male: n=10; APPPS1FE3-female: n=10; APPPS1AFE3-female: n=10; APPPS1EKO: n=10	Cre F (1,85) = 16.23, p=0.0001; APOE F (1,85) = 7.091, p=0.0093; Sex F(1,85) = 4.396, p=0.0396; p=0.0735 in APPPS1AFE3-female vs. APPPS1FE3-female; p=0.0163 in APPPS1AFE4-male vs. APPPS1FE4-male; p=0.0017 in APPPS1AFE4-female vs. APPPS1FE4-female
Figure 3C	APPPS1FE4-male: n=10; APPPS1AFE4-male: n=14; APPPS1FE4-female: n=14; APPPS1AFE4-female: n=10; APPPS1FE3-male: n=18; APPPS1AFE3-male: n=10; APPPS1FE3-female: n=10; APPPS1AFE3-female: n=10; APPPS1EKO: n=10	Cre F (1,88) = 23.96, p<0.0001; APOE F (1,88) = 5.427, p=0.0221; Sex F(1,88) = 8.147, p=0.0; Cre and Sex interaction F(1,88) = 6.426, p=0.0130; p=0.0151 in APPPS1AFE3-female vs. APPPS1FE3-female; p=0.0904 in APPPS1AFE4-male vs. APPPS1FE4-male; p<0.0001 in APPPS1AFE4-female vs. APPPS1FE4-female
Figure 3D	APPPS1FE4-male: n=10; APPPS1AFE4-male: n=14; APPPS1FE4-female: n=14; APPPS1AFE4-female: n=9;	Cre F (1,88) = 21.33, p<0.0001; APOE F (1,88) = 4.503, p=0.0366; Cre and Sex interaction F(1,88) = 4.098, p=0.0460; p=0.0403 in APPPS1AFE3-female vs. APPPS1FE3-female; p=0.0353 in APPPS1AFE4-male vs. APPPS1FE4-male; p<0.0001 in APPPS1AFE4-female vs. APPPS1FE4-female
Figure 3E	APPPS1FE3-male: n=19; APPPS1AFE3-male: n=10; APPPS1FE3-female: n=10; APPPS1AFE3-female: n=10	Cre F (1,88) = 13.31, p=0.0004; Sex F (1,88) = 4.439, p=0.0380; p=0.0048 in APPPS1AFE3-female vs. APPPS1FE3-female; p=0.0197 in APPPS1AFE4-female vs. APPPS1FE4-female
Figure 4A	N=6 in APPPS1 positive groups; n=8 in APPPS1 negative groups	Ank: p=0.0276 in APPPS1AFE4 vs. APPPS1FE4; C1qa: Cre F(1,20) = 6.206, p=0.0216; p=0.0408 in APPPS1AFE4 vs. APPPS1FE4; CD63: Cre F(1,20) = 6.937, p=0.0159; p=0.0328 in APPPS1AFE4 vs. APPPS1FE4; CD68: Cre F(1,20) = 7.081, p=0.0150; p=0.0383 in APPPS1AFE4 vs. APPPS1FE4;

		CD9: Cre F(1,20) = 5.233, p=0.0332; p=0.0397 in APPPS1AFE4 vs. APPPS1FE4; Clec7a: p=0.0311 in APPPS1AFE4 vs. APPPS1FE4; Csf1: Cre F(1,20) = 8.878, p=0.0074; p=0.0063 in APPPS1AFE4 vs. APPPS1FE4; Cst7: p=0.0212 in APPPS1AFE4 vs. APPPS1FE4; Ctsb: Cre F(1,20) = 6.683, p=0.0177; p=0.0209 in APPPS1AFE4 vs. APPPS1FE4; Ctsd: p=0.0294 in APPPS1AFE4 vs. APPPS1FE4; Itgax: p=0.0290 in APPPS1AFE4 vs. APPPS1FE4; Tyrobp: p=0.0448 in APPPS1AFE4 vs. APPPS1FE4
Figure 4C	APPPS1FE4-female: n=14;	APOE F(1,40) = 34.91, p<0.0001
Figure 4E	APPPS1AFE4-female: n=10; APPPS1FE3-female: n=10; APPPS1AFE3-female: n=10	Cre F (1,39) = 15.59, p=0.0003; p=0.0060 in APPPS1AFE3-female vs. APPPS1FE3-female; p=0.0422 in APPPS1AFE4-female vs. APPPS1FE4-female
Figure 5A	N=6 in APPPS1 positive groups; n=8 in APPPS1 negative groups	GFAP: Cre F(1,20) = 5.243, p=0.0330; p=0.0920 in APPPS1AFE4 vs. APPPS1FE4; H2.T23: p=0.0395 in APPPS1AFE4 vs. APPPS1FE4; Ptgs2: Cre and APOE interaction F(1,20) = 6.316, p=0.0206; p=0.0408 in APPPS1AFE3 vs. APPPS1FE3; S1pr3: p=0.0583 in APPPS1AFE4 vs. APPPS1FE4; Serpina3n: Cre F(1,20) = 6.503, p=0.0191; p=0.0108 in APPPS1AFE4 vs. APPPS1FE4
Figure 5C	APPPS1FE4-female: n=14; APPPS1AFE4-female: n=10; APPPS1FE3-female: n=10; APPPS1AFE3-female: n=10	APOE F (1,40) = 14.98, p=0.0004; APOE and Cre interaction F(1,40) = 5.863, p=0.0201; p=0.0201 in APPPS1AFE4-female vs. APPPS1FE4-female
Figure 5D	APPPS1FE4-male: n=11; APPPS1AFE4-male: n=10; APPPS1FE4-female: n=14; APPPS1AFE4-female: n=10; APPPS1FE3-male: n=19; APPPS1AFE3-male: n=8; APPPS1FE3-female: n=8; APPPS1AFE3-female: n=9	N/A
Figure 6B	APPPS1FE4-male: n=10; APPPS1AFE4-male: n=14; APPPS1FE4-female: n=14; APPPS1AFE4-female: n=10; APPPS1FE3-male: n=19; APPPS1AFE3-male: n=10; APPPS1FE3-female: n=10; APPPS1AFE3-female: n=10	Cre F (1,89) = 17.93, p<0.0001; Sex F (1,89) = 8.648, p=0.0042; p=0.0051 in APPPS1AFE3-female vs. APPPS1FE3-female; p=0.0121 in APPPS1AFE4-female vs. APPPS1FE4-female
Figure 6D	APPPS1FE4-male: n=10; APPPS1AFE4-male: n=10; APPPS1FE4-female: n=14; APPPS1AFE4-female: n=10; APPPS1FE3-male: n=18; APPPS1AFE3-male: n=6; APPPS1FE3-female: n=10; APPPS1AFE3-female: n=9	Cre F (1,79) = 18.20, p<0.0001; p=0.0461 in APPPS1AFE3-male vs. APPPS1FE3-male; p=0.0316 in APPPS1AFE4-male vs. APPPS1FE4-male; p=0.0003 in APPPS1AFE4-female vs. APPPS1FE4-female

Chapter 5: Conclusions and future directions

Ever since Dr. Alois Alzheimer first characterized senile dementia in Auguste Deter over one hundred years ago, researchers have continued to not only ask why AD develops, but also how can it be stopped. As mankind continues to live longer with advances in medicine and technology, the incidence of diseases of aging, like AD, will only continue to increase. AD not only impacts those afflicted with the disease, it also takes a tremendous toll on their loved ones and caregivers as well. In addition, the cost of care is poised to increase at an unsustainable rate if effective treatments are not developed in the very near future. While advancements in therapeutic treatments targeting Aβ have provided hope that the pathobiology of AD can be kept at bay by removing Aβ early in the course of the disease, the failure of many of these drugs in initial clinical trials has led many to question and wonder if other therapeutic targets might provide improvements in clinical outcomes.

Despite the many setbacks from clinical trials targeting Aβ, a tremendous amount of knowledge has been gained about the time course and the pathobiology of the disease. One of the most important lessons came from understanding that when trying to modulate Aβ levels to improve disease outcomes, timing is everything. In particular, many have realized that participants who have clinical symptoms of AD already have high loads of Aβ that have caused additional downstream pathologies to develop, like tau pathology. With this in mind, more recent trials have focused on providing these treatments earlier in the time course of the disease. However, to date only one monoclonal antibody treatment targeting Aβ, aducanumab, has received approval through the FDA's accelerated approval program. While the approach of trying to prevent the development of AD early in the disease course by targeting Aβ holds promise, continued research into ways to target and alter the course of AD are needed. Given that apoE is the strongest genetic risk factor for LOAD, and LOAD accounts for the greatest number

of AD cases, identifying ways that apoE can be targeted and manipulated to improve AD pathology remains a promising approach.

5.1 Apolipoprotein E, Alzheimer disease, and β-amyloidogenesis

A tremendous amount of research has been performed to elucidate the role apoE plays in the development of AD pathology, but several questions still remain as to precisely how apoE contributes to the various aspects of the disease. Researchers have known for decades that apoE has a dramatic effect on the accumulation of Aβ in the brain and in the ability of Aβ to form highly-ordered fibrillar amyloid plaques. Post-mortem samples of human AD brain tissue samples have shown that Aβ can form a variety of plaque types in the brain and that apoE can deposit in these plaques. Characterization of these plaques has revealed that compact dense core plaques tend to be more likely to contain apoE and recent findings have even described a coarse-grained plaque that is associated with homozygous *APOE4* carriers (268). We found that either a complete loss of Aβ or just the loss of astrocytic apoE has a tremendous impact on not only the level of fibrillar Aβ plaques that deposit, but also on the way that the fibrils form. Indeed, the morphology of the fibrillar plaques was altered in a way that made the plaques more dispersed and wispy-like in appearance with the global apoE KO resulting in little to no plaques having a compact dense core. While previous studies using apoE KO mice had shown similar changes in the level of Aβ plaques (139,166), little work had been done to see how the loss of apoE impacted cellular responses to the plaques.

The impact of a complete loss of apoE on microgliosis that we show here is quite striking. The reduction in the ability of microglia to become activated and cluster around the

fibrillar Aβ plaques has provided some of the initial evidence that apoE is playing a critical role in the activation of microglia in the setting of AD. Interestingly, in a collaboration with Dr. Marco Collona, we have also shown a similar effect on microgliosis with the loss of the microglia receptor TREM2 (269). These findings led to a better understanding that TREM2 and apoE are linked and necessary for microglial activation under disease conditions (61,123). Additionally, recent findings that apoE is a ligand for TREM2 (175,176,258,270) raise the possibility that the TREM2-APOE dependent microglial activation could stem from a requirement of plaque-bound apoE to bind TREM2. Recent development of our labs anti-apoE antibody, HAE-4, which binds to de-lipidated forms of apoE, has shown that Aβ plaques contain de-lipidated apoE (116,117). Since plaques that form in apoE KO mice lack any apoE, the impaired microgliosis that we observed could be the result of the loss of this de-lipidated apoE ligand. Another alternative explanation could be that the impaired microgliosis we observed is the result of the loss of endogenous microglial apoE. At the time of the finding that microgliosis around Aβ plaques was apoE dependent, apoE was primarily thought of as being an astrocytic protein and subsequent research showing that microglial apoE is upregulated in DAM/MGnD microglia (61,62) had yet to be described. Additional studies have since shown that microglial apoE is necessary for microglial responses to damaged neurons (61) and that a reduced activation of microglia, and subsequent prevention of an increase in microglial apoE, causes a significant decrease in plaque-associated apoE (118).

5.2 Microglial Apolipoprotein E and its potential roles in Alzheimer disease

The increased recognition that microglial apoE is playing an important role in the development of Aβ pathology, and may have a potential role in developing tau pathology (89,271), provides ample reason for further investigations into whether there are characteristics of microglial apoE and microglial produced apoE-containing lipoprotein particles that are unique and thus may have distinct roles and impacts in AD. Our results clearly show that microglia produce a greater amount of smaller apoE particles compared to astrocytes and that there is likely an isoform-dependent difference in apoE particles produced by microglia. The smaller 8nm sized apoE particles, which appeared to be most prevalent in the APOE4 expressing microglia, are likely to be less lipidated and thus could be more prone to shedding what lipids are present in the particle to become fully de-lipidated. This may lead microglial apoE, in particular APOE4 produced by microglia, to be more susceptible to becoming de-lipidated and then subsequently incorporated into fibrillar Aβ plaques. It is therefore critical for future work to look more in depth at apoE itself to see whether apoE produced by microglia may be post-translationally modified in a unique manner compared to astrocytic apoE and to see if any modifications are unique to certain apoE isoforms. In fact, recent work has shown that astrocytic apoE is glycosylated in a different manner than microglial apoE (253). Furthermore, lipidomic analysis of the lipids and cholesterols found in lipoprotein particles containing each isoform of apoE that are produced from microglia is warranted. These types of investigations could provide additional insight in to whether specific lipid or cholesterol species are contained in these particles and if they may be influencing certain cellular functions or signaling pathways. In

particular, the possibility exists that apoE particles could be playing a role in signaling between different cell types, like from astrocytes to microglia, as Aβ pathology develops.

Furthermore, the ability of two key factors involved in macrophage activation and polarization, M-CSF and GM-CSF, to have drastically different effects on microglial apoE secretion, and for these effects to show differences based on apoE isoform, warrants further exploration. The high concentration of 5.0ng/ml GM-CSF is above the typical range seen in plasma, which is 20-100pg/ml (272–274). However, in certain circumstances, including with inflammatory stimuli, GM-CSF levels have been shown to reach upwards of 8.0ng/ml (275). The question still remains as to whether microglia encounter GM-CSF in the ng/ml range in the brain, and whether or not Aβ pathology could induce inflammation capable of increasing GM-CSF production locally that could be in the ng/ml range. Nevertheless, the ability of GM-CSF to significantly lower microglial apoE production compared to M-CSF provides evidence that the activation state of microglia plays a key role in regulating microglial apoE. In addition, the development of AD pathology goes through many different stages and the state of microglial is likely to shift as the disease progresses. The changes in microglial activation during different stages of AD might also mean that the level of production of apoE may vary in these different stages and the type and size of apoE particles produced may also vary.

5.3   The impact of Apolipoprotein E on Alzheimer disease neuropathology and potential therapeutic interventions

One of the pathologies that is seen in the early stages of AD as Aβ plaques are accumulating is neuritic dystrophy (276,277). Here we have reported that reducing astrocytic apoE levels leads to an overall decrease in neuritic dystrophy, which likely can be attributed to

the overall reduction in Aβ plaque load. However, the increase in damage to neuronal processes locally around plaques does present a potential issue, especially when it comes to thinking about possible apoE-targeted therapies. There are a few potential explanations that could underlie why the damage to neurons is increased with the loss of apoE either globally or from astrocytes. One reason could be simply that the loss of apoE causes unique apoE-deficient fibrillar structures to form that are more dispersed, and thus more capable of interacting with and causing damage to neurites. Another explanation could be the lack of microglial activation. If astrocytic apoE provides a signal that aids in the activation of microglia, the loss of astrocytic apoE could be inhibiting this activation. With microglia not being activated at the plaque site, they may not be providing adequate phagocytosis and uptake of Aβ and may be deficient in 'capping' the edge of the plaque. This may explain the change in plaque structure to a more dispersed and widespread morphology that is capable of inducing a greater amount of damage to neuronal processes.

The ability to reduce Aβ plaque levels by specifically reducing astrocytic apoE does provide promise for the development of cell-specific targeted therapies. While we clearly showed a significant effect on reducing Aβ pathology by reducing astrocytic apoE, one caveat to our results was the variability in the amount of apoE reduction in astrocytes. The tamoxifen injections were not always consistent and, while astrocytic apoE was significantly reduced, some astrocytic apoE still remained and made it hard to tell whether the remaining astrocytic apoE influenced any of the results we were seeing. Another issue with a potential treatment targeting astrocytic apoE is the dystrophic neurites accruing to a greater extent around plaques when apoE has been reduced. One way to address such an issue could come from the use of a combination therapy. If neuritic dystrophy is developing because of the lack of microglial activation with the loss of astrocytic apoE, other targeted therapies might be able to activate and boost microglial

116

function in a more beneficial manner and could thus be used in conjunction with the apoE-targeted therapies.

The complexity of AD and the issues that have arisen from the failed clinical trials targeting Aβ have led many researchers to believe that no one therapeutic treatment will be capable of addressing all instances of AD pathology that develop. In addition, while one therapy might work for one individual at an early stage of the disease, the same therapy may not work for someone else who is at a later stage. It is also important to remember that there are various underlying factors that cause AD to develop in different populations. While *APOE4* is the strongest genetic risk factor for LOAD, it does not have as much of an impact on the risk of those with ADAD or for individuals with Down syndrome, who have very unique drivers of the disease. Additionally, as mentioned earlier, *APOE4* status has different influences based on sex and ethnic background that need to be considered. It stands to reason that an APOE4-targeted therapy may be more effective for some, like those with LOAD, but that other therapies, or a combination of therapies, may be needed for those with ADAD, Down syndrome, or other unique types of AD.

References

1. Yang HD, Kim DH, Lee SB, Young LD. History of Alzheimer's Disease. Dement Neurocognitive Disord. 2016;15(4):115.

2. Hippius H, Neundörfer G. The discovery of Alzheimer's disease. Dialogues Clin Neurosci. 2003;5(1):101.

3. Alzheimer A. Über einen eigenartigen schweren Erkrankungsprozeß der Hirnrinde. Neurol Cent. 1906;23:1129–1136.

4. MB G, S K, E G-F, HJ M, P M. Histopathology and APOE genotype of the first Alzheimer disease patient, Auguste D. Neurogenetics. 1998;1(3):223–8.

5. Ramirez-Bermudez J. Alzheimer's Disease: Critical Notes on the History of a Medical Concept. Arch Med Res. 2012 Nov 1;43(8):595–9.

6. Kraepelin E. Psychiatrie: Ein Lehrbuch für Studierende und Ärzte. In 1910. p. 593–632.

7. 2021 Alzheimer's disease facts and figures. Alzheimer's Dement. 2021 Mar 1;17(3):327–406.

8. International AD, Guerchet M, Prince M. Numbers of people with dementia around the world. 2020 Nov.

9. Alzheimer's Facts and Figures Report | Alzheimer's Association [Internet]. [cited 2021 May 10]. Available from: https://www.alz.org/alzheimers-dementia/facts-figures

10. 2020 Alzheimer's disease facts and figures. Alzheimer's Dement. 2020 Mar 1;16(3):391–460.

11. GM M, DS K, H C, BT H, CR J, CH K, et al. The diagnosis of dementia due to Alzheimer's disease: recommendations from the National Institute on Aging-Alzheimer's Association workgroups on diagnostic guidelines for Alzheimer's disease. Alzheimers Dement. 2011;7(3):263–9.

12. Musiek ES, Holtzman DM. Three dimensions of the amyloid hypothesis: time, space and "wingmen." Nat Neurosci. 2015;

13. O'Brien RJ, Wong PC. Amyloid Precursor Protein Processing and Alzheimer's Disease. Annu Rev Neurosci. 2011 Jul 21;34:185.

14. C H, C K, G T, S S. Trafficking and proteolytic processing of APP. Cold Spring Harb Perspect Med. 2012;2(5).

15. Long JM, Holtzman DM. Alzheimer Disease: An Update on Pathobiology and Treatment

Strategies. Vol. 179, Cell. Cell Press; 2019. p. 312–39.

16.   Jack CR, Holtzman DM. Biomarker modeling of alzheimer's disease. Vol. 80, Neuron. Cell Press; 2013. p. 1347–58.

17.   Bateman RJ, Xiong C, Benzinger TLS, Fagan AM, Goate A, Fox NC, et al. Clinical and Biomarker Changes in Dominantly Inherited Alzheimer's Disease. N Engl J Med. 2012 Aug 30;367(9):795–804.

18.   Dorszewska J, Prendecki M, Oczkowska A, Dezor M, Kozubski W. Molecular Basis of Familial and Sporadic Alzheimer's Disease. Curr Alzheimer Res. 2016 Jul 27;13(9):952–63.

19.   Bekris LM, Yu C-E, Bird TD, Tsuang DW. Genetics of Alzheimer Disease. J Geriatr Psychiatry Neurol. 2010 Dec;23(4):213.

20.   Bateman RJ, Aisen PS, De Strooper B, Fox NC, Lemere CA, Ringman JM, et al. Autosomal-dominant Alzheimer's disease: a review and proposal for the prevention of Alzheimer's disease. Alzheimer's Res Ther 2011 31. 2011 Jan 6;3(1):1–13.

21.   Hartley D, Blumenthal T, Carrillo M, DiPaolo G, Esralew L, Gardiner K, et al. Down syndrome and Alzheimer's disease: Common pathways, common goals. Alzheimer's Dement. 2015 Jun 1;11(6):700–9.

22.   Head E, Powell D, Gold BT, Schmitt FA. Alzheimer's Disease in Down Syndrome. Eur J Neurodegener Dis. 2012;1(3):353.

23.   M M, P M, E R, P D, R C, N M. A prospective 20-year longitudinal follow-up of dementia in persons with Down syndrome. J Intellect Disabil Res. 2017 Sep 1;61(9):843–52.

24.   JA H, DC A, A B, AD B, GT C, R C, et al. Cross-Sectional Exploration of Plasma Biomarkers of Alzheimer's Disease in Down Syndrome: Early Data from the Longitudinal Investigation for Enhancing Down Syndrome Research (LIFE-DSR) Study. J Clin Med. 2021 Apr 28;10(9):1907.

25.   B R, R R, C H, G S, G M, R M, et al. Amyloid A4 protein and its precursor in Down's syndrome and Alzheimer's disease. N Engl J Med. 1989 Jun;320(22):1446–52.

26.   Perl DP. Neuropathology of Alzheimer's Disease. Mt Sinai J Med. 2010 Jan;77(1):32.

27.   Price JL, Ko AI, Wade MJ, Tsou SK, McKeel DW, Morris JC. Neuron Number in the Entorhinal Cortex and CA1 in Preclinical Alzheimer Disease. Arch Neurol. 2001 Sep 1;58(9):1395–402.

28.   Hardy JA, Higgins GA. Alzheimer's disease: the amyloid cascade hypothesis. Science. 1992 Apr 10;256(5054):184–5.

29.   Hu X, Crick SL, Bu G, Frieden C, Pappu R V., Lee JM. Amyloid seeds formed by cellular uptake, concentration, and aggregation of the amyloid-beta peptide. Proc Natl Acad Sci U

S A. 2009 Dec 1;106(48):20324–9.

30. Dickson T., Vickers J. The morphological phenotype of β-amyloid plaques and associated neuritic changes in Alzheimer's disease. Neuroscience. 2001 Jul;105(1):99–107.

31. Golabek AA, Soto C, Vogel T, Wisniewski T. The interaction between apolipoprotein E and Alzheimer's amyloid beta-peptide is dependent on beta-peptide conformation. J Biol Chem. 1996 May 3;271(18):10602–6.

32. Golabek A, Marques MA, Lalowski M, Wisniewski T. Amyloid β binding proteins in vitro and in normal human cerebrospinal fluid. Neurosci Lett. 1995 May 19;191(1–2):79–82.

33. Venegas C, Kumar S, Franklin BS, Dierkes T, Brinkschulte R, Tejera D, et al. Microglia-derived ASC specks cross-seed amyloid-β in Alzheimer's disease. Nat 2017 5527685. 2017 Dec 21;552(7685):355–61.

34. Wisniewski T, Castaño EM, Golabek A, Vogel T, Frangione B. Acceleration of Alzheimer's fibril formation by apolipoprotein E in vitro. Am J Pathol. 1994 Nov;145(5):1030–5.

35. LN N, KR B, G D, MN G, D M, SM P, et al. Alpha-1-antichymotrypsin promotes beta-sheet amyloid plaque deposition in a transgenic mouse model of Alzheimer's disease. J Neurosci. 2001 Mar 1;21(5):1444–51.

36. Shirahama T, Skinner M, Westermark P, Rubinow A, Cohen AS, Brun A, et al. Senile cerebral amyloid. Prealbumin as a common constituent in the neuritic plaque, in the neurofibrillary tangle, and in the microangiopathic lesion. Am J Pathol. 1982;107(1):41.

37. Gião T, Saavedra J, Cotrina E, Quintana J, Llop J, Arsequell G, et al. Undiscovered Roles for Transthyretin: From a Transporter Protein to a New Therapeutic Target for Alzheimer's Disease. Int J Mol Sci. 2020 Mar 2;21(6).

38. Bussière T, Bard F, Barbour R, Grajeda H, Guido T, Khan K, et al. Morphological characterization of Thioflavin-S-positive amyloid plaques in transgenic Alzheimer mice and effect of passive Abeta immunotherapy on their clearance. Am J Pathol. 2004 Sep;165(3):987–95.

39. DM W, MN G, D M. Quantification of cerebral amyloid angiopathy and parenchymal amyloid plaques with Congo red histochemical stain. Nat Protoc. 2006 Aug;1(3):1591–5.

40. Yuan P, Condello C, Keene CD, Wang Y, Bird TD, Paul SM, et al. TREM2 Haplodeficiency in Mice and Humans Impairs the Microglia Barrier Function Leading to Decreased Amyloid Compaction and Severe Axonal Dystrophy. Neuron. 2016 May 18;90(4):724–39.

41. Urbanc B, Cruz L, Le R, Sanders J, Ashe KH, Duff K, et al. Neurotoxic effects of thioflavin S-positive amyloid deposits in transgenic mice and Alzheimer's disease. Proc Natl Acad Sci. 2002 Oct 29;99(22):13990–5.

42. Heath JE, Siedlak SL, Zhu X, Lee H-G, Thakur A, Yan R, et al. Widespread distribution of reticulon-3 in various neurodegenerative diseases. Neuropathology. 2010 Dec;30(6):574–9.

43. Sadleir KR, Kandalepas PC, Buggia-Prévot V, Nicholson DA, Thinakaran G, Vassar R. Presynaptic dystrophic neurites surrounding amyloid plaques are sites of microtubule disruption, BACE1 elevation, and increased Aβ generation in Alzheimer's disease. Acta Neuropathol. 2016 Aug 18;132(2):235–56.

44. Gowrishankar S, Yuan P, Wu Y, Schrag M, Paradise S, Grutzendler J, et al. Massive accumulation of luminal protease-deficient axonal lysosomes at Alzheimer's disease amyloid plaques. Proc Natl Acad Sci. 2015 Jul 14;112(28):E3699–708.

45. Dickson TC, King CE, McCormack GH, Vickers JC. Neurochemical diversity of dystrophic neurites in the early and late stages of Alzheimer's disease. Exp Neurol. 1999;156(1):100–10.

46. Zhang X, Li Y, Xu H, Zhang Y. The γ-secretase complex: from structure to function. Front Cell Neurosci. 2014 Dec 11;8(DEC).

47. Xu X. γ-Secretase Catalyzes Sequential Cleavages of the AβPP Transmembrane Domain. J Alzheimers Dis. 2009;16(2):211.

48. MA F, JA K, T F, MS W. Alzheimer presenilin-1 mutations dramatically reduce trimming of long amyloid β-peptides (Aβ) by γ-secretase to increase 42-to-40-residue Aβ. J Biol Chem. 2014 Nov 7;289(45):31043–52.

49. McNaughton D, Knight W, Guerreiro R, Ryan N, Lowe J, Poulter M, et al. Duplication of amyloid precursor protein (APP), but not prion protein (PRNP) gene is a significant cause of early onset dementia in a large UK series. Neurobiol Aging. 2012;33(2):426.e13.

50. Panza F, Lozupone M, Logroscino G, Imbimbo BP. A critical appraisal of amyloid-β-targeting therapies for Alzheimer disease. Nat Rev Neurol 2018 152. 2019 Jan 4;15(2):73–88.

51. Mintun MA, Lo AC, Evans CD, Wessels AM, Ardayfio PA, Andersen SW, et al. Donanemab in Early Alzheimer's Disease. https://doi.org/101056/NEJMoa2100708. 2021 Mar 13;384(18):1691–704.

52. Swanson CJ, Zhang Y, Dhadda S, Wang J, Kaplow J, Lai RYK, et al. A randomized, double-blind, phase 2b proof-of-concept clinical trial in early Alzheimer's disease with lecanemab, an anti-Aβ protofibril antibody. Alzheimer's Res Ther 2021 131. 2021 Apr 17;13(1):1–14.

53. Cummings J, Aisen P, Lemere C, Atri A, Sabbagh M, Salloway S. Aducanumab produced a clinically meaningful benefit in association with amyloid lowering. Alzheimer's Res Ther 2021 131. 2021 May 10;13(1):1–3.

54. Yiannopoulou KG, Anastasiou AI, Zachariou V, Pelidou S-H. Reasons for Failed Trials of

Disease-Modifying Treatments for Alzheimer Disease and Their Contribution in Recent Research. Biomedicines. 2019 Dec 1;7(4).

55.   Aisen PS, Cummings J, Doody R, Kramer L, Salloway S, Selkoe DJ, et al. The Future of Anti-Amyloid Trials. J Prev Alzheimer's Dis. 2020 Mar 1;7(3):146–51.

56.   Bateman RJ, Benzinger TL, Berry S, Clifford DB, Duggan C, Fagan AM, et al. The DIAN-TU Next Generation Alzheimer's prevention trial: adaptive design and disease progression model. Alzheimers Dement. 2017 Jan 1;13(1):8.

57.   Bennett DA, Schneider JA, Arvanitakis Z, Wilson RS. OVERVIEW AND FINDINGS FROM THE RELIGIOUS ORDERS STUDY. Curr Alzheimer Res. 2012 Jul 25;9(6):628.

58.   CM R, C X, JP M, JC M. Education and Alzheimer disease without dementia: support for the cognitive reserve hypothesis. Neurology. 2007 Jan;68(3):223–8.

59.   Getz GS, Reardon CA. Apoprotein E as a lipid transport and signaling protein in the blood, liver, and artery wall. J Lipid Res. 2009 Apr;50(Suppl):S156.

60.   Fagan AM, Holtzman DM, Munson G, Mathur T, Schneider D, Chang LK, et al. Unique lipoproteins secreted by primary astrocytes from wild type, apoE (-/-), and human apoE transgenic mice. J Biol Chem. 1999 Oct 15;274(42):30001–7.

61.   Krasemann S, Madore C, Cialic R, Baufeld C, Calcagno N, El Fatimy R, et al. The TREM2-APOE Pathway Drives the Transcriptional Phenotype of Dysfunctional Microglia in Neurodegenerative Diseases. Immunity. 2017 Sep 19;47(3):566-581.e9.

62.   Keren-Shaul H, Spinrad A, Weiner A, Matcovitch-Natan O, Dvir-Szternfeld R, Ulland TK, et al. A Unique Microglia Type Associated with Restricting Development of Alzheimer's Disease. Cell. 2017 Jun;169(7):1276-1290.e17.

63.   Mauch DH, Nägler K, Schumacher S, Göritz C, Müller E-C, Otto A, et al. CNS Synaptogenesis Promoted by Glia-Derived Cholesterol. Science (80-). 2001 Nov 9;294(5545):1354–7.

64.   MJ I, EM S, RE P, RW M. Lipoprotein uptake by neuronal growth cones in vitro. Science. 1987;236(4804):959–62.

65.   Frieden C, Garai K. Structural differences between apoE3 and apoE4 may be useful in developing therapeutic agents for Alzheimer's disease. Proc Natl Acad Sci U S A. 2012 Jun 5;109(23):8913.

66.   Mahley RW, Weisgraber KH, Huang Y. Apolipoprotein E: structure determines function, from atherosclerosis to Alzheimer's disease to AIDS. J Lipid Res. 2009 Apr 1;50(SUPPL.):S183–8.

67.   J D, RE G, CF S. Apolipoprotein E polymorphism and atherosclerosis. Arteriosclerosis. 1988;8(1):1–21.

68.   Steinmetz A, Jakobs C, Motzny S, Kaffarnik H. Differential distribution of apolipoprotein

E isoforms in human plasma lipoproteins. Arterioscler An Off J Am Hear Assoc Inc. 1989;9(3):405–11.

69.   Gregg RE, Zech LA, Schaefer EJ, Stark D, Wilson D, Brewer HB. Abnormal in vivo metabolism of apolipoprotein E4 in humans. J Clin Invest. 1986 Sep 1;78(3):815–21.

70.   Peng D, Song C, Reardon CA, Liao S, Getz GS. Lipoproteins produced by ApoE-/- astrocytes infected with adenovirus expressing human ApoE. J Neurochem. 2003 Sep;86(6):1391–402.

71.   DeMattos RB, Brendza RP, Heuser JE, Kierson M, Cirrito JR, Fryer J, et al. Purification and characterization of astrocyte-secreted apolipoprotein E and J-containing lipoproteins from wild-type and human apoE transgenic mice. Neurochem Int. 2001 Nov 1;39(5–6):415–25.

72.   Peng D, Song C, Reardon CA, Liao S, Getz GS. Lipoproteins produced by ApoE–/– astrocytes infected with adenovirus expressing human ApoE. J Neurochem. 2003;

73.   Lanfranco MF, Ng CA, Rebeck GW. ApoE Lipidation as a Therapeutic Target in Alzheimer's Disease. Int J Mol Sci. 2020 Sep 1;21(17):1–19.

74.   Y F, J Z, Y A, HM N, CC L, H Z, et al. Apolipoprotein E lipoprotein particles inhibit amyloid-β uptake through cell surface heparan sulphate proteoglycan. Mol Neurodegener. 2016 May 5;11(1).

75.   Namba Y, Tomonaga M, Kawasaki H, Otomo E, Ikeda K. Apolipoprotein E immunoreactivity in cerebral amyloid deposits and neurofibrillary tangles in Alzheimer's disease and kuru plaque amyloid in Creutzfeldt-Jakob disease. Vol. 541, Brain Research. 1991.

76.   T W, B F. Apolipoprotein E: a pathological chaperone protein in patients with cerebral and systemic amyloid. Neurosci Lett. 1992 Feb 3;135(2):235–8.

77.   Corder EH, Saunders AM, Strittmatter WJ, Schmechel DE, Gaskell PC, Small GW, et al. Gene dose of apolipoprotein E type 4 allele and the risk of Alzheimer's disease in late onset families. Science. 1993 Aug 13;261(5123):921–3.

78.   Strittmatter WJ, Saunders AM, Schmechel D, Pericak-Vance M, Enghild J, Salvesen GS, et al. Apolipoprotein E: high-avidity binding to beta-amyloid and increased frequency of type 4 allele in late-onset familial Alzheimer disease. Proc Natl Acad Sci U S A. 1993 Mar 1;90(5):1977–81.

79.   AD R. Apolipoprotein E alleles as risk factors in Alzheimer's disease. Annu Rev Med. 1996;47:387–400.

80.   Gomez-Isla T, West HL, Rebeck GW, Harr SD, Growdon JH, Locascio JJ, et al. Clinical and pathological correlates of apolipoprotein E ε4 in Alzheimer's disease. Ann Neurol. 1996 Jan 1;39(1):62–70.

81.   Hsu M, Dedhia M, Crusio WE, Delprato A. Sex differences in gene expression patterns

associated with theAPOE4 allele. F1000Research. 2019;8.

82. Neu SC, Pa J, Kukull W, Beekly D, Kuzma A, Gangadharan P, et al. Apolipoprotein E genotype and sex risk factors for Alzheimer disease: A meta-analysis. JAMA Neurol. 2017 Oct 1;74(10):1178–89.

83. A A, L T, VW H, MD G. Sex modifies the APOE-related risk of developing Alzheimer disease. Ann Neurol. 2014;75(4):563–73.

84. F S, E V, MJ de L, D A, J P, V M, et al. APOE-by-sex interactions on brain structure and metabolism in healthy elderly controls. Oncotarget. 2015;6(29):26663–74.

85. Turney IC, Chesebro AG, Rentería MA, Lao PJ, Beato JM, Schupf N, et al. APOE ε4 and resting-state functional connectivity in racially/ethnically diverse older adults. Alzheimer's Dement Diagnosis, Assess Dis Monit. 2020 Jan 1;12(1):e12094.

86. Wilkins CH, Grant EA, Schmitt SE, McKeel DW, Morris JC. The Neuropathology of Alzheimer Disease in African American and White Individuals. Arch Neurol. 2006 Jan 1;63(1):87–90.

87. Beydoun MA, Weiss J, Beydoun HA, Hossain S, Maldonado AI, Shen B, et al. Race, APOE genotypes, and cognitive decline among middle-aged urban adults. Alzheimer's Res Ther 2021 131. 2021 Jun 30;13(1):1–16.

88. Morris JC, Schindler SE, McCue LM, Moulder KL, Benzinger TLS, Cruchaga C, et al. Assessment of Racial Disparities in Biomarkers for Alzheimer Disease. JAMA Neurol. 2019 Mar 1;76(3):264–73.

89. Shi Y, Yamada K, Liddelow SA, Smith ST, Zhao L, Luo W, et al. ApoE4 markedly exacerbates tau-mediated neurodegeneration in a mouse model of tauopathy. Nature. 2017 Sep 20;549(7673):523–7.

90. DS Y, JD S, Z Z, SE G, RN M. Characterization of the binding of amyloid-beta peptide to cell culture-derived native apolipoprotein E2, E3, and E4 isoforms and to isoforms from human plasma. J Neurochem. 1997;68(2):721–5.

91. S A, CR A, VI Z. Interaction of nascent ApoE2, ApoE3, and ApoE4 isoforms expressed in mammalian cells with amyloid peptide beta (1-40). Relevance to Alzheimer's disease. Biochemistry. 1997 Aug 26;36(34):10571–80.

92. Ladutl MJ, Faldutonll MT, Manellill AM, Reardons CA, Getz8 GS, Frail7 DE. Isoform-specific binding of apolipoprotein E to beta-amyloid. J Biol Chem. 1994;269(38):23403–6.

93. Islam T, Gharibyan AL, Golchin SA, Pettersson N, Brännström K, Hedberg I, et al. Apolipoprotein E impairs amyloid-β fibril elongation and maturation. FEBS J. 2020 Mar 1;287(6):1208–19.

94. Verghese PB, Castellano JM, Garai K, Wang Y, Jiang H, Shah A, et al. ApoE influences amyloid-β (Aβ) clearance despite minimal apoE/Aβ association in physiological

conditions. Proc Natl Acad Sci U S A. 2013 May 7;110(19):E1807-16.

95. Sanan DA, Weisgraber KH, Russell SJ, Mahley RW, Huang D, Saunders A, et al. Apolipoprotein E associates with beta amyloid peptide of Alzheimer's disease to form novel monofibrils. Isoform apoE4 associates more efficiently than apoE3. J Clin Invest. 1994 Aug 1;94(2):860–9.

96. Strittmatter WJ, Weisgraber KH, Huang DY, Dong LM, Salvesen GS, Pericak-Vance M, et al. Binding of human apolipoprotein E to synthetic amyloid beta peptide: isoform-specific effects and implications for late-onset Alzheimer disease. Proc Natl Acad Sci. 1993 Sep 1;90(17):8098–102.

97. Carter DB. The interaction of amyloid-beta with ApoE. Vol. 38, Sub-cellular biochemistry. Springer, Boston, MA   ; 2005. p. 255–72.

98. Basak JM, Verghese PB, Yoon H, Kim J, Holtzman DM. Low-density lipoprotein receptor represents an apolipoprotein E-independent pathway of Aβ uptake and degradation by astrocytes. J Biol Chem. 2012 Apr 20;287(17):13959–71.

99. Kanekiyo T, Xu H, Bu G. ApoE and Aβ in Alzheimer's disease: accidental encounters or partners? Neuron. 2014 Feb 19;81(4):740–54.

100. Zhao N, Liu C-C, Qiao W, Bu G. Apolipoprotein E, Receptors, and Modulation of Alzheimer's Disease. Biol Psychiatry. 2018 Feb 15;83(4):347–57.

101. Ma J, Yee A, Brewer HB, Das S, Potter H. Amyloid-associated proteins α1-antichymotrypsin and apolipoprotein E promote assembly of Alzheimer β-protein into filaments. Nature. 1994 Nov 3;372(6501):92–4.

102. Evans KC, Berger EP, Cho CG, Weisgraber KH, Lansbury PT. Apolipoprotein E is a kinetic but not a thermodynamic inhibitor of amyloid formation: implications for the pathogenesis and treatment of Alzheimer disease. Proc Natl Acad Sci. 1995 Jan 31;92(3):763–7.

103. Stephen J. Wood, Winnie Chan and, Wetzel* R. Seeding of Aβ Fibril Formation Is Inhibited by All Three Isotypes of Apolipoprotein E. Biochemistry. 1996;35(38):12623–8.

104. U B, J P. ApoE associated with lipid has a reduced capacity to inhibit beta-amyloid fibril formation. Neuroreport. 1998 Oct 5;9(14):3321–3.

105. Garai K, Verghese PB, Baban B, Holtzman DM, Frieden C. The Binding of Apolipoprotein E to Oligomers and Fibrils of Amyloid-β Alters the Kinetics of Amyloid Aggregation. Biochemistry. 2014 Oct 14;53(40):6323–31.

106. Huynh T-P V., Davis AA, Ulrich JD, Holtzman DM. Apolipoprotein E and Alzheimer's disease: the influence of apolipoprotein E on amyloid-β and other amyloidogenic proteins: Thematic Review Series: ApoE and Lipid Homeostasis in Alzheimer's Disease. J Lipid Res. 2017 May 1;58(5):824–36.

107. Tokuda T, Calero M, Matsubara E, Vidal R, Kumar A, Permanne B, et al. Lipidation of

apolipoprotein E influences its isoform-specific interaction with Alzheimer's amyloid beta peptides. Biochem J. 2000 Jun 1;348 Pt 2(2):359–65.

108. Suidan GL, Ramaswamy G. Targeting Apolipoprotein E for Alzheimer's Disease: An Industry Perspective. Int J Mol Sci. 2019 May 1;20(9).

109. Williams T, Borchelt DR, Chakrabarty P. Therapeutic approaches targeting Apolipoprotein E function in Alzheimer's disease. Mol Neurodegen 2020 151. 2020 Jan 31;15(1):1–19.

110. Wahrle SE, Jiang H, Parsadanian M, Legleiter J, Han X, Fryer JD, et al. ABCA1 is required for normal central nervous system ApoE levels and for lipidation of astrocyte-secreted apoE. J Biol Chem. 2004 Sep 24;279(39):40987–93.

111. Koldamova R, Staufenbiel M, Lefterov I. Lack of ABCA1 considerably decreases brain ApoE level and increases amyloid deposition in APP23 mice. J Biol Chem. 2005 Dec 30;280(52):43224–35.

112. Hirsch-Reinshagen V, Zhou S, Burgess BL, Bernier L, McIsaac SA, Chan JY, et al. Deficiency of ABCA1 impairs apolipoprotein E metabolism in brain. J Biol Chem. 2004 Sep 24;279(39):41197–207.

113. Hirsch-Reinshagen V, Maia LF, Burgess BL, Blain J-F, Naus KE, McIsaac SA, et al. The absence of ABCA1 decreases soluble ApoE levels but does not diminish amyloid deposition in two murine models of Alzheimer disease. J Biol Chem. 2005 Dec 30;280(52):43243–56.

114. Fitz NF, Cronican AA, Saleem M, Fauq AH, Chapman R, Lefterov I, et al. Abca1 deficiency affects Alzheimer's disease-like phenotype in human ApoE4 but not in ApoE3-targeted replacement mice. J Neurosci. 2012 Sep 19;32(38):13125–36.

115. Wahrle SE, Jiang H, Parsadanian M, Kim J, Li A, Knoten A, et al. Overexpression of ABCA1 reduces amyloid deposition in the PDAPP mouse model of Alzheimer disease. J Clin Invest. 2008 Feb;118(2):671–82.

116. Liao F, Li A, Xiong M, Bien-Ly N, Jiang H, Zhang Y, et al. Targeting of nonlipidated, aggregated apoE with antibodies inhibits amyloid accumulation. J Clin Invest. 2018 May 1;128(5):2144–55.

117. Xiong M, Jiang H, Serrano JR, Gonzales ER, Wang C, Gratuze M, et al. APOE immunotherapy reduces cerebral amyloid angiopathy and amyloid plaques while improving cerebrovascular function. Sci Transl Med. 2021 Feb 17;13(581):7522.

118. Parhizkar S, Arzberger T, Brendel M, Kleinberger G, Deussing M, Focke C, et al. Loss of TREM2 function increases amyloid seeding but reduces plaque-associated ApoE. Nat Neurosci. 2019 Feb 1;22(2):191–204.

119. Mills CD, Kincaid K, Alt JM, Heilman MJ, Hill AM. M-1/M-2 Macrophages and the Th1/Th2 Paradigm. J Immunol. 2000 Jun 15;164(12):6166–73.

120. Lacey DC, Achuthan A, Fleetwood AJ, Dinh H, Roiniotis J, Scholz GM, et al. Defining GM-CSF– and Macrophage-CSF–Dependent Macrophage Responses by In Vitro Models. J Immunol. 2012;188(11).

121. Hamilton TA, Zhao C, Pavicic PGJ, Datta S. Myeloid Colony-Stimulating Factors as Regulators of Macrophage Polarization. Front Immunol. 2014;0(NOV):554.

122. Ransohoff RM. A polarizing question: do M1 and M2 microglia exist? Nat Neurosci 2016 198. 2016 Aug 1;19(8):987–91.

123. Pimenova AA, Marcora E, Goate AM. A Tale of Two Genes: Microglial Apoe and Trem2. Vol. 47, Immunity. 2017. p. 398–400.

124. Perez-Nievas BG, Serrano-Pozo A. Deciphering the astrocyte reaction in Alzheimer's disease. Vol. 10, Frontiers in Aging Neuroscience. Frontiers Media S.A.; 2018. p. 114.

125. Liddelow SA, Guttenplan KA, Clarke LE, Bennett FC, Bohlen CJ, Schirmer L, et al. Neurotoxic reactive astrocytes are induced by activated microglia. Nature. 2017 Jan 26;541(7638):481.

126. J H, MJ L, LJ VE. Apolipoprotein E attenuates beta-amyloid-induced astrocyte activation. J Neurochem. 1998;71(4):1626–34.

127. Maezawa I, Maeda N, Montine TJ, Montine KS. Apolipoprotein E-specific innate immune response in astrocytes from targeted replacement mice. J Neuroinflammation 2006 31. 2006 Apr 7;3(1):1–6.

128. Fernandez CG, Hamby ME, McReynolds ML, Ray WJ. The role of apoE4 in disrupting the homeostatic functions of astrocytes and microglia in aging and Alzheimer's disease. Front Aging Neurosci. 2019 Feb 11;10(FEB):14.

129. Sullivan PM, Mezdour H, Aratani Y, Knouff C, Najib J, Reddick RL, et al. Targeted Replacement of the Mouse Apolipoprotein E Gene with the Common Human APOE3 Allele Enhances Diet-induced Hypercholesterolemia and Atherosclerosis *. J Biol Chem. 1997 Jul 18;272(29):17972–80.

130. Götz J, Bodea L-G, Goedert M. Rodent models for Alzheimer disease. Nat Rev Neurosci 2018 1910. 2018 Sep 7;19(10):583–98.

131. AM S, L S, P S-C, M C-T, L E, R L de M, et al. Overexpression of wild-type human APP in mice causes cognitive deficits and pathological features unrelated to Abeta levels. Neurobiol Dis. 2009 Mar;33(3):369–78.

132. Sasaguri H, Nilsson P, Hashimoto S, Nagata K, Saito T, Strooper B De, et al. APP mouse models for Alzheimer's disease preclinical studies. EMBO J. 2017 Sep 1;36(17):2473–87.

133. Radde R, Bolmont T, Kaeser SA, Coomaraswamy J, Lindau D, Stoltze L, et al. Abeta42-driven cerebral amyloidosis in transgenic mice reveals early and robust pathology. EMBO Rep. 2006 Sep 1;7(9):940–6.

134. Jankowsky JL, Fadale DJ, Anderson J, Xu GM, Gonzales V, Jenkins NA, et al. Mutant presenilins specifically elevate the levels of the 42 residue -amyloid peptide in vivo: evidence for augmentation of a 42-specific secretase. Hum Mol Genet. 2003 Nov 25;13(2):159–70.

135. Webster SJ, Bachstetter AD, Nelson PT, Schmitt FA, Eldik LJ Van. Using mice to model Alzheimer's dementia: an overview of the clinical disease and the preclinical behavioral changes in 10 mouse models. Front Genet. 2014;5(APR).

136. Jankowsky JL, Zheng H. Practical considerations for choosing a mouse model of Alzheimer's disease. Mol Neurodegener. 2017 Dec 22;12(1).

137. Saito T, Matsuba Y, Mihira N, Takano J, Nilsson P, Itohara S, et al. Single App knock-in mouse models of Alzheimer's disease. Nat Neurosci. 2014 May;17(5):661–3.

138. Bales KR, Verina T, Cummins DJ, Du Y, Dodel RC, Saura J, et al. Apolipoprotein E is essential for amyloid deposition in the APP(V717F) transgenic mouse model of Alzheimer's disease. Proc Natl Acad Sci U S A. 1999 Dec 21;96(26):15233–8.

139. Holtzman DM, Fagan AM, Mackey B, Tenkova T, Sartorius L, Paul SM, et al. Apolipoprotein E facilitates neuritic and cerebrovascular plaque formation in an Alzheimer's disease model. Ann Neurol. 2000;47(6):739–47.

140. TB R, JS K, KL R, AJ L. Evolution of apolipoprotein E: mouse sequence and evidence for an 11-nucleotide ancestral unit. Proc Natl Acad Sci U S A. 1985;82(23):8085–9.

141. Liao F, Zhang TJ, Jiang H, Lefton KB, Robinson GO, Vassar R, et al. Murine versus human apolipoprotein E4: differential facilitation of and co-localization in cerebral amyloid angiopathy and amyloid plaques in APP transgenic mouse models. Acta Neuropathol Commun. 2015 Nov 10;3(1):70.

142. Castellano JM, Kim J, Stewart FR, Jiang H, DeMattos RB, Patterson BW, et al. Human apoE Isoforms Differentially Regulate Brain Amyloid-β Peptide Clearance. Sci Transl Med. 2011;3(89).

143. Kim J, Jiang H, Park S, Eltorai AEM, Stewart FR, Yoon H, et al. Haploinsufficiency of human APOE reduces amyloid deposition in a mouse model of amyloid-β amyloidosis. J Neurosci. 2011 Dec 7;31(49):18007–12.

144. TV H, F L, CM F, GO R, JR S, H J, et al. Age-Dependent Effects of apoE Reduction Using Antisense Oligonucleotides in a Model of β-amyloidosis. Neuron. 2017 Dec 6;96(5):1013-1023.e4.

145. Aguzzi A, Barres BA, Bennett ML. Microglia: scapegoat, saboteur, or something else? Science. 2013 Jan 11;339(6116):156–61.

146. Musiek ES, Holtzman DM. Three dimensions of the amyloid hypothesis: time, space and "wingmen." Nat Neurosci. 2015 May 26;18(6):800–6.

147. Bell RD, Sagare AP, Friedman AE, Bedi GS, Holtzman DM, Deane R, et al. Transport

Pathways for Clearance of Human Alzheimer's Amyloid β-Peptide and Apolipoproteins E and J in the Mouse Central Nervous System: http://dx.doi.org/101038/sj.jcbfm9600419. 2006 Nov 1;27(5):909–18.

148.   Deane R, Sagare A, Hamm K, Parisi M, Lane S, Finn MB, et al. apoE isoform–specific disruption of amyloid β peptide clearance from mouse brain. J Clin Invest. 2008 Dec 1;118(12):4002–13.

149.   Uchihara T, Duyckaerts C, He Y, Kobayashi K, Seilhean D, Amouyel P, et al. ApoE immunoreactivity and microglial cells in Alzheimer's disease brain. Neurosci Lett. 1995;195(1):5–8.

150.   Butovsky O, Jedrychowski MP, Cialic R, Krasemann S, Murugaiyan G, Fanek Z, et al. Targeting miR-155 restores abnormal microglia and attenuates disease in SOD1 mice. Ann Neurol. 2015 Jan;77(1):75–99.

151.   Naj AC, Jun G, Beecham GW, Wang L-S, Vardarajan BN, Buros J, et al. Common variants at MS4A4/MS4A6E, CD2AP, CD33 and EPHA1 are associated with late-onset Alzheimer's disease. Nat Genet 2011 435. 2011 Apr 3;43(5):436–41.

152.   Griciuc A, Serrano-Pozo A, Parrado AR, Lesinski AN, Asselin CN, Mullin K, et al. Alzheimer's Disease Risk Gene CD33 Inhibits Microglial Uptake of Amyloid Beta. Neuron. 2013 May 22;78(4):631–43.

153.   Guerreiro R, Wojtas A, Bras J, Carrasquillo M, Rogaeva E, Majounie E, et al. *TREM2* Variants in Alzheimer's Disease. N Engl J Med. 2013 Jan 10;368(2):117–27.

154.   Jonsson T, Stefansson H, Steinberg S, Jonsdottir I, Jonsson P V., Snaedal J, et al. Variant of *TREM2* Associated with the Risk of Alzheimer's Disease. N Engl J Med. 2013 Jan 10;368(2):107–16.

155.   Condello C, Yuan P, Schain A, Grutzendler J. Microglia constitute a barrier that prevents neurotoxic protofibrillar Aβ42 hotspots around plaques. Nat Commun. 2015 Jan 29;6:6176.

156.   Heneka MT, Golenbock DT, Latz E. Innate immunity in Alzheimer's disease. Nat Immunol 2015 163. 2015 Feb 17;16(3):229–36.

157.   Ulrich JD, Finn MB, Wang Y, Shen A, Mahan TE, Jiang H, et al. Altered microglial response to Abeta plaques in APPPS1-21 mice heterozygous for TREM2. Mol Neurodegener. 2014;9(1):20.

158.   Wang Y, Cella M, Mallinson K, Ulrich JD, Young KL, Robinette ML, et al. TREM2 Lipid Sensing Sustains the Microglial Response in an Alzheimer's Disease Model. Cell. 2015;160(6):1061–71.

159.   Wang Y, Ulland TK, Ulrich JD, Song W, Tzaferis JA, Hole JT, et al. TREM2-mediated early microglial response limits diffusion and toxicity of amyloid plaques. J Exp Med. 2016;213(5).

160. Jay TR, Hirsch AM, Broihier ML, Miller CM, Neilson LE, Ransohoff RM, et al. Disease Progression-Dependent Effects of TREM2 Deficiency in a Mouse Model of Alzheimer's Disease. J Neurosci. 2017 Jan 18;37(3):637–47.

161. Song W, Hooli B, Mullin K, Jin SC, Cella M, Ulland TK, et al. Alzheimer's disease-associated TREM2 variants exhibit either decreased or increased ligand-dependent activation. Alzheimer's Dement. 2017 Apr 1;13(4):381–7.

162. Ulland TK, Song WM, Ching S, Huang -Cheng, Artyomov MN, Holtzman DM, et al. TREM2 Maintains Microglial Metabolic Fitness in Alzheimer's Disease In Brief The Alzheimer's disease risk factor TREM2 regulates microglial function through modulation of cellular biosynthetic metabolism. TREM2 Maintains Microglial Metabolic Fitness in Alzheimer's Disease. Cell. 2017;170:649-656.e13.

163. Bales KR, Verina T, Dodel RC, Du Y, Altstiel L, Bender M, et al. Lack of apolipoprotein E dramatically reduces amyloid beta-peptide deposition. Nat Genet. 1997 Nov;17(3):263–4.

164. Holtzman DM, Bales KR, Wu S, Bhat P, Parsadanian M, Fagan a M, et al. Expression of human apolipoprotein E reduces amyloid-beta deposition in a mouse model of Alzheimer's disease. J Clin Invest. 1999;103(6):R15–21.

165. Katsouri L, Georgopoulos S. Lack of ldl receptor enhances amyloid deposition and decreases glial response in an alzheimer's disease mouse model. Block ML, editor. PLoS One. 2011 Jul 6;6(7):e21880.

166. Irizarry MC, Cheung BS, Rebeck GW, Paul SM, Bales KR, Hyman BT. Apolipoprotein E affects the amount, form, and anatomical distribution of amyloid β-peptide deposition in homozygous APP V717F transgenic mice. Acta Neuropathol. 2000 Nov 28;100(5):451–8.

167. Fagan AM, Watson M, Parsadanian M, Bales KR, Paul SM, Holtzman DM. Human and murine apoE markedly alters Aβ metabolism before and after plaque formation in a mouse model of Alzheimer's Disease. Neurobiol Dis. 2002;9(3):305–18.

168. Klingstedt T, Åslund A, Simon RA, Johansson LBG, Mason JJ, Nyström S, et al. Synthesis of a library of oligothiophenes and their utilization as fluorescent ligands for spectral assignment of protein aggregates. Org Biomol Chem. 2011;9(24):8356.

169. Nyström S, Psonka-Antonczyk KM, Ellingsen PG, Johansson LBG, Reitan N, Handrick S, et al. Evidence for Age-Dependent *in Vivo* Conformational Rearrangement within Aβ Amyloid Deposits. ACS Chem Biol. 2013 Jun 21;8(6):1128–33.

170. Styren, SD, Hamilton RL, Styren GC, Klunk WE. X-34, A Fluorescent Derivative of Congo Red: A Novel Histochemical Stain for Alzheimer's Disease Pathology. J Histochem Cytochem. 2000 Sep;48(9):1223–32.

171. Huynh T-PV, Liao F, Francis CM, Robinson GO, Serrano JR, Jiang H, et al. Age-Dependent Effects of apoE Reduction Using Antisense Oligonucleotides in a Model of β-amyloidosis. Neuron. 2017;96(5).

172. Liu CC, Zhao N, Fu Y, Wang N, Linares C, Tsai CW, et al. ApoE4 Accelerates Early Seeding of Amyloid Pathology. Neuron. 2017 Dec 6;96(5):1024-1032.e3.

173. Klingstedt T, Blechschmidt C, Nogalska A, Prokop S, Häggqvist B, Danielsson O, et al. Luminescent Conjugated Oligothiophenes for Sensitive Fluorescent Assignment of Protein Inclusion Bodies. ChemBioChem. 2013 Mar 18;14(5):607–16.

174. Magnusson K, Simon R, Sjölander D, Sigurdson CJ, Hammarström P, Nilsson KPR. Multimodal fluorescence microscopy of prion strain specific PrP deposits stained by thiophene-based amyloid ligands. Prion. 2014;8(4):319–29.

175. Atagi Y, Liu C-C, Painter MM, Chen X-F, Verbeeck C, Zheng H, et al. Apolipoprotein E Is a Ligand for Triggering Receptor Expressed on Myeloid Cells 2 (TREM2). J Biol Chem. 2015 Oct 23;290(43):26043–50.

176. Yeh FL, Wang Y, Tom I, Gonzalez LC, Sheng M. TREM2 Binds to Apolipoproteins, Including APOE and CLU/APOJ, and Thereby Facilitates Uptake of Amyloid-Beta by Microglia. Neuron. 2016 Jul 20;91(2):328–40.

177. Srinivasan K, Friedman BA, Larson JL, Lauffer BE, Goldstein LD, Appling LL, et al. Untangling the brain's neuroinflammatory and neurodegenerative transcriptional responses. Nat Commun 2016 71. 2016 Apr 21;7(1):1–16.

178. Gutierrez EG, Banks WA, Kastin AJ. Murine tumor necrosis factor alpha is transported from blood to brain in the mouse. J Neuroimmunol. 1993 Sep 1;47(2):169–76.

179. Grainger DJ, Reckless J, McKilligin E. Apolipoprotein E Modulates Clearance of Apoptotic Bodies In Vitro and In Vivo, Resulting in a Systemic Proinflammatory State in Apolipoprotein E-Deficient Mice. J Immunol. 2004 Nov 15;173(10):6366–75.

180. Bell RD, Winkler EA, Singh I, Sagare AP, Deane R, Wu Z, et al. Apolipoprotein E controls cerebrovascular integrity via cyclophilin A. Nat 2012 4857399. 2012 May 16;485(7399):512–6.

181. Chung W-S, Verghese PB, Chakraborty C, Joung J, Hyman BT, Ulrich JD, et al. Novel allele-dependent role for APOE in controlling the rate of synapse pruning by astrocytes. Proc Natl Acad Sci. 2016 Sep 6;113(36):10186–91.

182. Hafezi-Moghadam A, Thomas KL, Wagner DD. ApoE deficiency leads to a progressive age-dependent blood-brain barrier leakage. https://doi.org/101152/ajpcell005632005. 2007 Apr;292(4):1256–62.

183. Zenaro E, Pietronigro E, Bianca V Della, Piacentino G, Marongiu L, Budui S, et al. Neutrophils promote Alzheimer's disease–like pathology and cognitive decline via LFA-1 integrin. Nat Med 2015 218. 2015 Jul 27;21(8):880–6.

184. Zhou X, Stemme S, Hansson GK. Evidence for a local immune response in atherosclerosis. CD4+ T cells infiltrate lesions of apolipoprotein-E-deficient mice. Am J Pathol. 1996 Aug;149(2):359.

185. Su Z, Li Y, James JC, McDuffie M, Matsumoto AH, Helm GA, et al. Quantitative Trait Locus Analysis of Atherosclerosis in an Intercross Between C57BL/6 and C3H Mice Carrying the Mutant Apolipoprotein E Gene. Genetics. 2006 Mar 1;172(3):1799–807.

186. Rodriguez GA, Tai LM, LaDu MJ, Rebeck GW. Human APOE4 increases microglia reactivity at Aβ plaques in a mouse model of Aβ deposition. J Neuroinflammation. 2014 Jun 19;11:111.

187. Serrano-Pozo A, Muzikansky A, Gómez-Isla T, Growdon JH, Betensky RA, Frosch MP, et al. Differential relationships of reactive astrocytes and microglia to fibrillar amyloid deposits in Alzheimer disease. J Neuropathol Exp Neurol. 2013 Jun;72(6):462–71.

188. Butovsky O, Jedrychowski MP, Moore CS, Cialic R, Lanser AJ, Gabriely G, et al. Identification of a unique TGF-β-dependent molecular and functional signature in microglia. Nat Neurosci. 2014 Jan;17(1):131–43.

189. Shin S, Walz KA, Archambault AS, Sim J, Bollman BP, Koenigsknecht-Talboo J, et al. Apolipoprotein E mediation of neuro-inflammation in a murine model of multiple sclerosis. J Neuroimmunol. 2014 Jun 15;271(1–2):8–17.

190. H H, Y K-F, K S, M K, R S, Y M, et al. Altered cholesterol metabolism in human apolipoprotein E4 knock-in mice. Hum Mol Genet. 2000 Feb 12;9(3):353–61.

191. H H, U I, H H, M K, SC F, WG W, et al. Cholesterol is increased in the exofacial leaflet of synaptic plasma membranes of human apolipoprotein E4 knock-in mice. Neuroreport. 2002 Mar 25;13(4):383–6.

192. WJ J, R O, DL K, BM T, P S, FR V, et al. Prevalence of cerebral amyloid pathology in persons without dementia: a meta-analysis. JAMA. 2015 May 19;313(19):1924–38.

193. Bales KR, Liu F, Wu S, Lin S, Koger D, DeLong C, et al. Human APOE Isoform-Dependent Effects on Brain β-Amyloid Levels in PDAPP Transgenic Mice. J Neurosci. 2009;29(21).

194. JC M, CM R, C X, AM F, AM G, DM H, et al. APOE predicts amyloid-beta but not tau Alzheimer pathology in cognitively normal aging. Ann Neurol. 2010;67(1):122–31.

195. Bien-Ly N, Gillespie AK, Walker D, Yoon SY, Huang Y. Reducing human Apolipoprotein E levels attenuates age-dependent Aβ accumulation in mutant human amyloid precursor protein transgenic mice. J Neurosci. 2012 Apr 4;32(14):4803–11.

196. D T, JB L, OL L, RL H, DA B, JA S, et al. APOE ε4 increases risk for dementia in pure synucleinopathies. JAMA Neurol. 2013;70(2):223–8.

197. Koriath C, Lashley T, Taylor W, Druyeh R, Dimitriadis A, Denning N, et al. ApoE4 lowers age at onset in patients with frontotemporal dementia and tauopathy independent of amyloid-β copathology. Alzheimer's Dement Diagnosis, Assess Dis Monit. 2019 Dec 1;11(1):277–80.

198. DW D, MG H, ME M, AI S, RL W, NN D, et al. APOE ε4 is associated with severity of

Lewy body pathology independent of Alzheimer pathology. Neurology. 2018 Sep 18;91(12):E1182–95.

199. Pitas RE, Boyles JK, Lee SH, Foss D, Mahley RW. Astrocytes synthesize apolipoprotein E and metabolize apolipoprotein E-containing lipoproteins. Biochim Biophys Acta - Lipids Lipid Metab. 1987 Jan 13;917(1):148–61.

200. Stone DJ, Rozovsky I, Morgan TE, Anderson CP, Hajian H, Finch CE. Astrocytes and Microglia Respond to Estrogen with Increased apoE mRNAin Vivoandin Vitro. Vol. 143, Experimental Neurology. 1997.

201. K F, K N, UV M, C S, A F. Production of macrophage colony-stimulating factor by astrocytes and brain macrophages. J Neuroimmunol. 1992;40(2–3):189–95.

202. Malipiero U V, Frei K, Fontana A. Production of hemopoietic colony-stimulating factors by astrocytes. J Immunol. 1990;144(10).

203. Sawada M, Suzumura A, Yamamoto H, Marunouchi T. Activation and proliferation of the isolated microglia by colony stimulating factor-1 and possible involvement of protein kinase C. Vol. 509, Brain Research. 1990.

204. AT B, CL O, D G, JA B. Differentiation of human monocytes in vitro with granulocyte-macrophage colony-stimulating factor and macrophage colony-stimulating factor produces distinct changes in cGMP phosphodiesterase expression. Cell Signal. 2004;16(3):365–74.

205. Heap RE, Marín-Rubio JL, Peltier J, Heunis T, Dannoura A, Moore A, et al. Proteomics characterisation of the L929 cell supernatant and its role in BMDM differentiation. bioRxiv. 2020 Nov 14;2020.08.20.259515.

206. Draijer C, Penke LRK, Peters-Golden M. Distinctive Effects of GM-CSF and M-CSF on Proliferation and Polarization of Two Major Pulmonary Macrophage Populations. J Immunol. 2019 May 1;202(9):2700–9.

207. SH Z, GF E, L O. Cytokine regulation of macrophage apo E secretion: opposing effects of GM-CSF and TGF-beta. Atherosclerosis. 1992;96(2–3):203–14.

208. Braesch-Andersen S, Paulie S, Smedman C, Mia S, Kumagai-Braesch M. ApoE Production in Human Monocytes and Its Regulation by Inflammatory Cytokines. PLoS One. 2013 Nov 14;8(11):79908.

209. Masliah E, Mallory M, Ge N, Alford M, Veinbergs I, Roses AD. Neurodegeneration in the Central Nervous System of apoE-Deficient Mice. Exp Neurol. 1995;136(2):107–22.

210. I V, M M, M M, E M. Neurotrophic effects of Cerebrolysin in animal models of excitotoxicity. J Neural Transm Suppl. 2000;59(59):273–80.

211. TB S, E R, D A, D O, MS S. Apolipoprotein E deficiency promotes increased oxidative stress and compensatory increases in antioxidants in brain tissue. Free Radic Biol Med. 2002 Oct 15;33(8):1115–20.

212. SM F, GA S, WJ S, WD M. Impairment of the blood-nerve and blood-brain barriers in apolipoprotein e knockout mice. Exp Neurol. 2001;169(1):13–22.

213. DH M, K N, S S, C G, EC M, A O, et al. CNS synaptogenesis promoted by glia-derived cholesterol. Science. 2001 Nov 9;294(5545):1354–7.

214. J P, A B, D D, S G. Cholesterol synthesis and lipoprotein reuptake during synaptic remodelling in hippocampus in adult rats. Neuroscience. 1993;55(1):81–90.

215. Bero AW, Bauer AQ, Stewart FR, White BR, Cirrito JR, Raichle ME, et al. Bidirectional Relationship between Functional Connectivity and Amyloid-β Deposition in Mouse Brain. J Neurosci. 2012 Mar 28;32(13):4334–40.

216. Bero AW, Yan P, Roh JH, Cirrito JR, Stewart FR, Raichle ME, et al. Neuronal activity regulates the regional vulnerability to amyloid-β deposition. Nat Neurosci. 2011 Jun;14(6):750–6.

217. DeMattos RB, Bales KR, Cummins DJ, Dodart JC, Paul SM, Holtzman DM. Peripheral anti-A beta antibody alters CNS and plasma A beta clearance and decreases brain A beta burden in a mouse model of Alzheimer's disease. Proc Natl Acad Sci U S A. 2001 Jul 17;98(15):8850–5.

218. Wisniewski T, Frangione B. Apolipoprotein E: A pathological chaperone protein in patients with cerebral and systemic amyloid. Neurosci Lett. 1992;135(2):235–8.

219. Wahrle SE, Jiang H, Parsadanian M, Hartman RE, Bales KR, Paul SM, et al. Deletion of Abca1 increases Abeta deposition in the PDAPP transgenic mouse model of Alzheimer disease. J Biol Chem. 2005 Dec 30;280(52):43236–42.

220. Xu Q, Li Y, Cyras C, Sanan DA, Cordell B. Isolation and Characterization of Apolipoproteins from Murine Microglia: IDENTIFICATION OF A LOW DENSITY LIPOPROTEIN-LIKE APOLIPOPROTEIN J-RICH BUT E-POOR SPHERICAL PARTICLE. J Biol Chem. 2000 Oct 13;275(41):31770–7.

221. Guzman-Martinez L, Maccioni RB, Andrade V, Navarrete LP, Pastor MG, Ramos-Escobar N. Neuroinflammation as a Common Feature of Neurodegenerative Disorders. Front Pharmacol. 2019;0(SEP):1008.

222. Bachiller S, Jiménez-Ferrer I, Paulus A, Yang Y, Swanberg M, Deierborg T, et al. Microglia in Neurological Diseases: A Road Map to Brain-Disease Dependent-Inflammatory Response. Front Cell Neurosci. 2018 Dec 18;0:488.

223. Leng F, Edison P. Neuroinflammation and microglial activation in Alzheimer disease: where do we go from here? Nat Rev Neurol 2020 173. 2020 Dec 14;17(3):157–72.

224. Cherry JD, Olschowka JA, O'Banion MK. Neuroinflammation and M2 microglia: the good, the bad, and the inflamed. J Neuroinflammation 2014 111. 2014 Jun 3;11(1):1–15.

225. Pons V, Rivest S. New Therapeutic Avenues of mCSF for Brain Diseases and Injuries. Front Cell Neurosci. 2018 Dec 20;12.

226. Aram J, Francis A, Tanasescu R, Constantinescu CS. Granulocyte-Macrophage Colony-Stimulating Factor as a Therapeutic Target in Multiple Sclerosis. Neurol Ther. 2019 Jun 1;8(1):45.

227. Lotfi N, Thome R, Rezaei N, Zhang G-X, Rezaei A, Rostami A, et al. Roles of GM-CSF in the Pathogenesis of Autoimmune Diseases: An Update. Front Immunol. 2019;0(JUN):1265.

228. ED P, LP S, K M, J P-V, D V, BN D. GM-CSF production by autoreactive T cells is required for the activation of microglial cells and the onset of experimental autoimmune encephalomyelitis. J Immunol. 2007 Jan 1;178(1):39–48.

229. Huynh TP V., Wang C, Tran AC, Tabor GT, Mahan TE, Francis CM, et al. Lack of hepatic apoE does not influence early Aβ deposition: Observations from a new APOE knock-in model. Mol Neurodegener. 2019;14(1).

230. Holtzman DM, Herz J, Bu G. Apolipoprotein E and apolipoprotein E receptors: Normal biology and roles in Alzheimer disease. Cold Spring Harb Perspect Med. 2012 Mar 1;2(3):a006312.

231. Jansen WJ, Ossenkoppele R, Knol DL, Tijms BM, Scheltens P, Verhey FRJ, et al. Prevalence of cerebral amyloid pathology in persons without dementia: A meta-analysis. JAMA - J Am Med Assoc. 2015 May 19;313(19):1924–38.

232. Tosun D, Veitch D, Aisen P, Jack CR, Jagust WJ, Petersen RC, et al. Detection of β-amyloid positivity in Alzheimer's Disease Neuroimaging Initiative participants with demographics, cognition, MRI and plasma biomarkers. Brain Commun. 2021 Apr 5;3(2).

233. Namba Y, Tomonaga M, Kawasaki H, Otomo E, Ikeda K. Apolipoprotein E immunoreactivity in cerebral amyloid deposits and neurofibrillary tangles in Alzheimer's disease and kuru plaque amyloid in Creutzfeldt-Jakob disease. Brain Res. 1991 Feb 8;541(1):163–6.

234. Castellano JM, Kim J, Stewart FR, Jiang H, DeMattos RB, Patterson BW, et al. Human apoE isoforms differentially regulate brain amyloid-β peptide clearance. Sci Transl Med. 2011 Jun 29;3(89):89ra57.

235. William Rebeck G, Reiter JS, Strickland DK, Hyman BT. Apolipoprotein E in sporadic Alzheimer's disease: Allelic variation and receptor interactions. Neuron. 1993 Oct 1;11(4):575–80.

236. Kim J, Basak JM, Holtzman DM. The role of apolipoprotein E in Alzheimer's disease. Neuron. 2009 Aug 13;63(3):287–303.

237. Holtzman DM, Bales KR, Tenkova T, Fagan AM, Parsadanian M, Sartorius LJ, et al. Apolipoprotein E isoform-dependent amyloid deposition and neuritic degeneration in a mouse model of Alzheimer's disease. Proc Natl Acad Sci U S A. 2000 Mar 14;97(6):2892–7.

238. Fagan AM, Watson M, Parsadanian M, Bales KR, Paul SM, Holtzman DM. Human and Murine ApoE Markedly Alters Aβ Metabolism before and after Plaque Formation in a Mouse Model of Alzheimer's Disease. Neurobiol Dis. 2002;9(3):305–18.

239. Yamazaki Y, Zhao N, Caulfield TR, Liu C-C, Bu G. Apolipoprotein E and Alzheimer disease: pathobiology and targeting strategies. Nat Rev Neurol 2019 159. 2019 Jul 31;15(9):501–18.

240. Youmans KL, Tai LM, Nwabuisi-Heath E, Jungbauer L, Kanekiyo T, Gan M, et al. APOE4-specific Changes in Aβ Accumulation in a New Transgenic Mouse Model of Alzheimer Disease. J Biol Chem. 2012 Dec 7;287(50):41774–86.

241. Ulrich JD, Ulland TK, Mahan TE, Nyström S, Nilsson KP, Song WM, et al. ApoE facilitates the microglial response to amyloid plaque pathology. J Exp Med. 2018 Apr 2;215(4):1047 LP – 1058.

242. Zheng J yu, Sun J, Ji C mei, Shen L, Chen Z jun, Xie P, et al. Selective deletion of apolipoprotein E in astrocytes ameliorates the spatial learning and memory deficits in Alzheimer's disease (APP/PS1) mice by inhibiting TGF-β/Smad2/STAT3 signaling. Neurobiol Aging. 2017 Jun 1;54:112–32.

243. Kim J, Castellano JM, Jiang H, Basak JM, Parsadanian M, Pham V, et al. Overexpression of low-density lipoprotein receptor in the brain markedly inhibits amyloid deposition and increases extracellular A beta clearance. Neuron. 2009 Dec 10;64(5):632–44.

244. Liao F, Zhang TJ, Jiang H, Lefton KB, Robinson GO, Vassar R, et al. Murine versus human apolipoprotein E4: differential facilitation of and co-localization in cerebral amyloid angiopathy and amyloid plaques in APP transgenic mouse models. Acta Neuropathol Commun. 2015 Dec 10;3(1):70.

245. Youmans KL, Leung S, Zhang J, Maus E, Baysac K, Bu G, et al. Amyloid-β42 Alters Apolipoprotein E Solubility in Brains of Mice with Five Familial AD Mutations. J Neurosci Methods. 2011 Mar 15;196(1):51.

246. Lin YT, Seo J, Gao F, Feldman HM, Wen HL, Penney J, et al. APOE4 Causes Widespread Molecular and Cellular Alterations Associated with Alzheimer's Disease Phenotypes in Human iPSC-Derived Brain Cell Types. Neuron. 2018 Jun 27;98(6):1141-1154.e7.

247. Leyns CEG, Gratuze M, Narasimhan S, Jain N, Koscal LJ, Jiang H, et al. TREM2 function impedes tau seeding in neuritic plaques. Nat Neurosci. 2019 Aug 1;22(8):1217–22.

248. Mulder SD, Nielsen HM, Blankenstein MA, Eikelenboom P, Veerhuis R. Apolipoproteins E and J interfere with amyloid-beta uptake by primary human astrocytes and microglia *in vitro*. Glia. 2014 Apr;62(4):493–503.

249. Nielsen HM, Mulder SD, Beliën JAM, Musters RJP, Eikelenboom P, Veerhuis R. Astrocytic Aβ1-42 uptake is determined by Aβ-aggregation state and the presence of

amyloid-associated proteins. Glia. 2010 Aug 1;58(10):1235–46.

250. Martiskainen H, Haapasalo A, Kurkinen KM, Pihlajamäki J, Soininen H, Hiltunen M. Targeting ApoE4/ApoE receptor LRP1 in Alzheimer's disease. Vol. 17, Expert Opinion on Therapeutic Targets. Taylor & Francis; 2013. p. 781–94.

251. Golabek AA, Soto C, Vogel T, Wisniewski T. The Interaction between apolipoprotein E and Alzheimer's amyloid β-peptide is dependent on β-peptide conformation. J Biol Chem. 1996 May 3;271(18):10602–6.

252. Castano EM, Prelli F, Wisniewski T, Golabek A, Kumar RA, Soto C, et al. Fibrillogenesis in Alzheimer's disease of amyloid beta peptides and apolipoprotein E. Biochem J. 1995 Mar 1;306 (Pt 2)(Pt 2):599–604.

253. Lanfranco MF, Sepulveda J, Kopetsky G, Rebeck GW. Expression and secretion of apoE isoforms in astrocytes and microglia during inflammation. Glia. 2021 Jun 1;69(6):1478–93.

254. Yin Z, Raj D, Saiepour N, Van Dam D, Brouwer N, Holtman IR, et al. Immune hyperreactivity of Aβ plaque-associated microglia in Alzheimer's disease. Neurobiol Aging. 2017 Jul 1;55:115–22.

255. von Bernhardi R, Eugenín-von Bernhardi L, Eugenín J. Microglial cell dysregulation in brain aging and neurodegeneration. Front Aging Neurosci. 2015;7:124.

256. Villegas-Llerena C, Phillips A, Garcia-Reitboeck P, Hardy J, Pocock JM. Microglial genes regulating neuroinflammation in the progression of Alzheimer's disease. Curr Opin Neurobiol. 2016 Feb;36:74–81.

257. Fitz NF, Nam KN, Wolfe CM, Letronne F, Playso BE, Iordanova BE, et al. Phospholipids of APOE lipoproteins activate microglia in an isoform-specific manner in preclinical models of Alzheimer's disease. Nat Commun. 2021 Dec 7;12(1):3416.

258. Bailey CC, DeVaux LB, Farzan M. The Triggering Receptor Expressed on Myeloid Cells 2 Binds Apolipoprotein E. J Biol Chem. 2015 Oct 23;290(43):26033–42.

259. Wang C, Xiong M, Gratuze M, Bao X, Shi Y, Andhey PS, et al. Selective removal of astrocytic APOE4 strongly protects against tau-mediated neurodegeneration and decreases synaptic phagocytosis by microglia. Neuron. 2021;109(10):1657-1674.e7.

260. Iannucci J, Sen A, Grammas P. Isoform-Specific Effects of Apolipoprotein E on Markers of Inflammation and Toxicity in Brain Glia and Neuronal Cells In Vitro. Curr Issues Mol Biol. 2021 May 27;43(1):215–25.

261. Dickson T., Vickers J. The morphological phenotype of β-amyloid plaques and associated neuritic changes in Alzheimer's disease. Neuroscience. 2001;105(1):99–107.

262. Huang Y, Happonen KE, Burrola PG, O'Connor C, Hah N, Huang L, et al. Microglia use TAM receptors to detect and engulf amyloid β plaques. Nat Immunol. 2021 May 1;22(5):586–94.

263. Li X, Zhang J, Li D, He C, He K, Xue T, et al. Astrocytic ApoE reprograms neuronal cholesterol metabolism and histone-acetylation-mediated memory. Neuron. 2021 Mar 17;109(6):957-970.e8.

264. Zhang J, Liu Q. Cholesterol metabolism and homeostasis in the brain. Protein Cell. 2015 Apr 1;6(4):254–64.

265. Yu T-S, Tensaouti Y, Stephanz EP, Rafikian EE, Yang M, Kernie SG. Astrocyte-derived ApoE is Required for the Maturation of Injury-induced Hippocampal Neurons and Regulates Cognitive Recovery After Traumatic Brain Injury Abbreviated Title: ApoE is required for Injury-induced Neurogenesis. bioRxiv. 2021 Jan 14;2021.01.13.425890.

266. Laskowitz DT, Horsburgh K, Roses AD. Apolipoprotein E and the CNS response to injury. Vol. 18, Journal of Cerebral Blood Flow and Metabolism. Nature Publishing Group; 1998. p. 465–71.

267. Zhao J, Davis MD, Martens YA, Shinohara M, Graff-Radford NR, Younkin SG, et al. APOE ϵ4/ϵ4 diminishes neurotrophic function of human iPSC-derived astrocytes. Hum Mol Genet. 2017 Jul 15;26(14):2690–700.

268. Boon BDC, Bulk M, Jonker AJ, Morrema THJ, van den Berg E, Popovic M, et al. The coarse-grained plaque: a divergent Aβ plaque-type in early-onset Alzheimer's disease. Acta Neuropathol. 2020 Sep 14;1:3.

269. Y W, TK U, JD U, W S, JA T, JT H, et al. TREM2-mediated early microglial response limits diffusion and toxicity of amyloid plaques. J Exp Med. 2016 May 2;213(5):667–75.

270. Kober DL, Stuchell-Brereton MD, Kluender CE, Dean HB, Strickland MR, Steinberg DF, et al. Functional insights from biophysical study of TREM2 interactions with ApoE and Aβ1-42. bioRxiv. 2020 Feb 25;2020.02.24.963264.

271. Y S, M M, J L, K W, PM S, J RS, et al. Microglia drive APOE-dependent neurodegeneration in a tauopathy mouse model. J Exp Med. 2019 Nov 1;216(11):2546–61.

272. Lee J, Kim Y, Lim J, Kim M, Han K. G-CSF and GM-CSF Concentrations and Receptor Expression in Peripheral Blood Leukemic Cells from Patients with Chronic Myelogenous Leukemia. 2008;

273. Conti L, Gessani S. GM-CSF in the generation of dendritic cells from human blood monocyte precursors: Recent advances. Immunobiology. 2008 Nov 6;213(9–10):859–70.

274. Bhattacharya P, Thiruppathi M, Elshabrawy HA, Alharshawi K, Kumar P, Prabhakar BS. GM-CSF: An Immune Modulatory Cytokine that can Suppress Autoimmunity. Cytokine. 2015 Oct 1;75(2):261.

275. Cebon J, Layton JE, Maher D, Morstyn G. Endogenous haemopoietic growth factors in neutropenia and infection. Br J Haematol. 1994;86(2):265–74.

276. Braak H, Alafuzoff I, Arzberger T, Kretzschmar H, Del Tredici K. Staging of Alzheimer

disease-associated neurofibrillary pathology using paraffin sections and immunocytochemistry. Acta Neuropathol 2006 1124. 2006 Aug 12;112(4):389–404.

277. Knowles JK, Rajadas J, Nguyen T-V V., Yang T, LeMieux MC, Griend L Vander, et al. The p75 Neurotrophin Receptor Promotes Amyloid-β(1-42)-Induced Neuritic Dystrophy In Vitro and In Vivo. J Neurosci. 2009 Aug 26;29(34):10627–37.

Curriculum Vitae

Thomas Edward Mahan

EDUCATION

Doctor of Philosophy in Neuroscience Washington University in St. Louis School of Medicine, St. Louis, MO
August 2014 – December 2021

Master of Science in Biochemistry/Biotechnology University of Missouri – St. Louis, St. Louis, MO
GPA of 3.70/4.0 May 2011

Bachelor of Science in Biology McKendree University, Lebanon, IL
Minor in Biochemistry December 2007
GPA of 3.51/4.0

RELEVANT COURSEWORK

Ph.D Coursework:
Fundamentals of Molecular Cell Biology, Cellular Neurobiology, Neural Systems, Statistics for Medical Researchers, Pathobiology of Human Disease States

M.S. Coursework:
Advanced Molecular Biology, Advanced Plant Biology and Biotechnology, Advanced Virology, Advanced Biochemistry, Advanced Molecular Cell Biology, Bioinformatics, Biotechnology Lab, Advanced Nucleic Acid Structure and Function, Graduate Seminar: RNA Functions, and Special Topics in Biochemistry - Proteins as Polymers.

B.S. Coursework:
Physics I and II and Labs, Statistics, Microbiology and Labs, Organic and Inorganic Chemistry and Labs, Genetics and Labs, Cell Biology and Labs, Analytical Chemistry and Labs, Biochemistry I and II, Human Anatomy and Physiology and Labs, Plant Physiology. Senior Research: RNA Isolation Techniques of the Marine Chlorophyte *Tetraselmis suecica*.

WORK EXPERIENCE

Washington University in St. Louis School of Medicine
Research Assistant – Department of Neurology October 2011-August 2014

- Perform perfusions of mice, including perfusion with paraformaldehyde and gluteraldehyde for EM imaging.
- Collect serum and plasma samples from mice.
- Extract and dissect the brains of mice into regions of interest for biochemical analysis.
- Section half and whole brains of mice and human brain sections using microtome.
- Perform and optimize bright field and fluorescent immunohistochemistry staining on sections of mouse and human brain.
- Mount tissue on microscope slides; obtain images by using nanozoomer and digital imaging microscope.
- Perform volumetric analysis on regions of interest for mouse brain sections.
- Quantification of staining levels of amyloid beta plaques and tau pathology using ImageJ software.

Sigma-Aldrich
Chemist 1 and 2 January 2008-October 2011

- Perform biochemical processing for protein and enzyme purifications from various mammalian, plant, and yeast sources.
- Trained on multiple operating procedures, and quality documentation.
- Performed protein analysis using HPLC chromatography, UV/Vis spectrophotometry, SDS Page and Agarose gel electrophoresis, Karl-Fischer, and Biuret, Bradford, and Lowry Protein Reagents.
- Utilized various resin chromatography techniques (affinity, size exclusion, dye, and ion-exchange), various filtration techniques, diafiltration, dialysis, heat steps, and protein salt precipitations, for protein purifications.
- Promoted to a Chemist 2 based on continually meeting and exceeding company goals for cost savings, on-time delivery of products, zero-blown batches, and quality documentation.
- Member of Safety Committee 2009-2010: Performed safety inspections and audit reviews to ensure proper safety requirements were being implemented within the Dekalb facility.

PUBLICATIONS

- Lall D, Lorenzini I, Mota TA, Bell S, Mahan TE, Ulrich JD, Davtyan H, Rexach JE, Muhammad AKMG, Shelest O, Landeros J, Vazquez M, Kim J, Ghaffari L, O'Rourke JG, Geschwind DH, Blurton-Jones M, Holtzman DM, Sattler R, Baloh RH. (2021) C9orf72 deficiency promotes microglial-mediated synaptic loss in aging and amyloid accumulation. *Neuron*. S0896-6273(21)00373-1.

- Huynh TV, Wang C, Tran AC, Tabor GT, Mahan TE, Francis CM, Finn MB, Spellman R, Manis M, Tanzi RE, Ulrich JD, Holtzman DM. (2019) Lack of hepatic apoE does not influence early Aβ deposition: observations from a new APOE knock-in model. *Mol Neurodegener*. 14(1):37.

- Holth JK, Fritschi SK, Wang C, Pedersen NP, Cirrito JR, Mahan TE, Finn MB, Manis M, Geerling JC, Fuller PM, Lucey BP, Holtzman DM. (2019) The sleep-wake cycle regulates brain interstitial fluid tau in mice and CSF tau in humans. *Science*. 363(6429):880-884.

- Lessard CB, Malnik SL, Zhou Y, Ladd TB, Cruz PE, Ran Y, Mahan TE, Chakrabaty P, Holtzman DM, Ulrich JD, Colonna M, Golde TE. (2018) High-affinity interactions and signal transduction between Aβ oligomers and TREM2. *EMBO Mol Med*. 10(11) pii: e9027.

- Ulrich JD, Ulland TK, Mahan TE, Nyström S, Nilsson KP, Song WM, Zhou Y, Reinartz M, Choi S, Jiang H, Stewart FR, Anderson E, Wang Y, Colonna M, Holtzman DM. (2018) ApoE facilitates the microglial response to amyloid plaque pathology. *J Exp Med*. 215(4):1047-1058.

- Huynh TPV, Liao F, Robinson GO, Serrano J, Jiang H, Roh J, Finn MB, Sullivan P, Mahan TE, Ulrich JD, Francis C, Cole T, and Holtzman DM. (2017) Age-dependent effects of apoE reduction using antisense oligonucleotides in a model of β-amyloidosis, *Neuron*. 96(5):1013-1023.

- Holth JK, Mahan TE, Robinson GO, Rocha A, Holtzman DM. (2017) Altered sleep and EEG power in the P301S Tau transgenic mouse model, *Ann Clin Transl Neurol*. 4(3):180-190.

- Wang Y, Ulland TK, Ulrich JD, Song W, Tzaferis JA, Hole JT, Yuan P, Mahan TE, Shi Y, Gilfillan S, Cella M, Grutzendler J, DeMattos RB, Cirrito JR, Holtzman DM, Colonna M. (2016) TREM2-mediated early microglial response limits diffusion and toxicity of amyloid plaques, *J Exp Med*. 213(5):667-75

- Yamada K, Patel TK, Hochgräfe K, Mahan TE, Jiang H, Stewart FR, Mandelkow EM, Holtzman DM. (2015) Analysis of in vivo turnover of tau in a mouse model of tauopathy. *Mol Neurodegener,* 10, 55.

- Macauley SL, Stanley M, Caesar EE, Yamada SA, Raichle ME, Perez R, Mahan TE, Sutphen CL, Holtzman DM. (2015) Hyperglycemia modulates extracellular amyloid-β concentrations and neuronal activity in vivo. *J Clin Invest,* 125(6):2463-7.

- Liao F, Jiang H, Srivatsan S, Xiao Q, Lefton KB, Yamada K, Mahan TE, Lee JM, Shaw AS, Holtzman DM. (2015) Effects of CD2-associated protein deficiency on amyloid-β in neuroblastoma cells and in an APP transgenic mouse model. *Mol Neurodegener,* 10, 12.

- Yanamandra K, Jiang H, Mahan TE, Maloney SE, Wozniak DF, Diamond MI, Holtzman DM. (2015) Anti-tau antibody reduces insoluble tau and decreases brain atrophy. *Ann Clin Transl Neurol,* 2(3), 278-88.

- Roh JH, Jiang H, Finn MB, Stewart FR, Mahan TE, Cirrito JR, Heda A, Snider BJ, Li M, Yanagisawa M, de Lecea L, Holtzman DM. (2014) Potential role of orexin and sleep modulation in the pathogenesis of Alzheimer's disease. *J Exp Med,* 211(13):2487-96.

- Holmes BB, Furman JL, Mahan TE, Yamasaki TR, Mirbaha H, Eades WC, Belaygorod L, Cairns NJ, Holtzman DM, Diamond MI. (2014) Proteopathic tau seeding predicts tauopathy in vivo. *Proc Natl Acad Sci USA,* 111(14), E4376-85.

- Liao F, Zhang TJ, Mahan TE, Jiang H, Holtzman DM. (2014) Effects of growth hormone-releasing hormone on sleep and brain interstitial fluid amyloid-β in an APP transgenic mouse model. *Brain Behav Immun,* 47:163-71.

- Ulrich JD, Finn MB, Wang Y, Shen A, Mahan TE, Jiang H, Stewart FR, Piccio L, Colonna M, Holtzman DM. (2014) Altered microglial response to Aβ plaques in APPPS1-21 mice heterozygous for TREM2. *Mol Neurodegener,* 9:20

- Liao F, Hori Y, Hudry E, Bauer AQ, Jiang H, Mahan TE, Dearborn JT, Kim J, Culver JP, Wozniak DF, Hyman BT, Holtzman DM. (2014) Anti-Apolipoprotein E antibody given after plaque onset decreases Aβ accumulation and improves function in a mouse model of Aβ amyloidosis. *J Neurosci,* 34(21):7281-92.

- Yamada K, Holth JK, Liao F, Stewart FR, Mahan TE, Jiang H, Cirrito JR, Patel TK, Hochgräfe K, Mandelkow EM, Holtzman DM. (2014) Neuronal activity regulates extracellular tau in vivo. *J. Exp Med*, 211(3):387-93.

- Ulrich JD, Burchett JM, Restivo JL, Schuler DR, Verghese PB, Mahan TE, Landreth GE, Castellano JM, Jiang H, Cirrito JR, and Holtzman DM. (2013) In vivo measurement of apolipoprotein E from the brain interstitial fluid using microdialysis. *Mol Neurodegener,* 8:13.

- Yanamandra K, Kfoury N, Jiang H, Mahan TE, Ma S, Maloney SE, Wozniak DF, Diamond MI, Holtzman DM. (2013) Anti-Tau Antibodies that Block Tau Aggregate Seeding In Vitro Markedly Decrease Pathology and Improve Cognition In Vivo. *Neuron*, 80(2):402-414.

HONORS & VOLUNTEER SERVICE

- Keynote speaker for Hudson Falls Annual Science Symposium (2019)
- Mentor for Hudson Falls Science Research Program (2017-2019)
- Guest Speaker for McKendree University Biopsychology class (2017-2019)
- Lucille P. Markey Special Emphasis Pathway in Human Pathobiology (2017-19)
- Brain Discovery Neuroscience Outreach Program Volunteer (2017-2019)
- BP-ENDURE- Wire Together Fire Together Representative (2017)
- Amazing Brain Carnival Volunteer and Demo Presenter at St. Louis Science Center (2012-17)
- Camp Rainbow Volunteer Staff for Teen Camp and Summer Camp (2014-2016)
- USBC Men's Collegiate Bowling Academic All-American (2007)
- Sigma Zeta National Science and Mathematics Honor Society (2006-2007)
- Southeast Missouri Special Olympics Volunteer (2004-2012)
- McKendree University Honors Program (2003-2007)
- Board of Trustees Academic Scholarship (2003-2007)
- Dean's List, multiple semesters